COMPUTATIONAL NEUROIMAGING *of* visual field loss

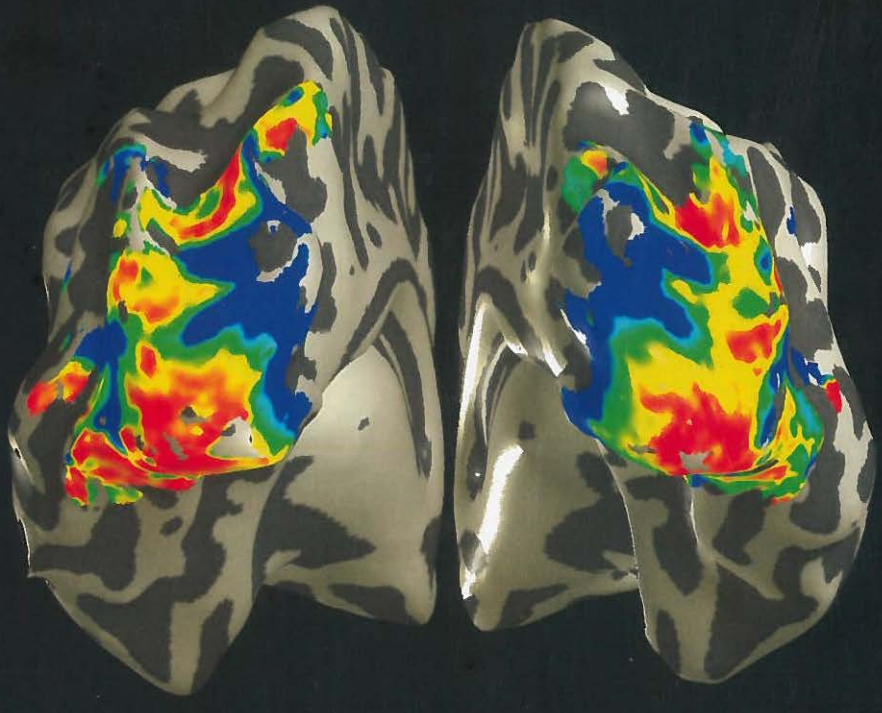

Koen Vincent Haak

COMPUTATIONAL NEUROIMAGING *of* visual field loss

The research in this thesis shows that the human brain areas responsible for vision do not reorganize themselves when the eye is damaged by disease. This finding opposes the prevailing opinion and is of great importance for developing treatments to overcome blindness.

Koen Vincent Haak was born on March 2, 1982 in Groningen, The Netherlands, where he studied Artificial Intelligence at the University of Groningen and received his Master's degree with distinction ('met veel genoegen') in 2007. Koen subsequently joined the Laboratory for Experimental Ophthalmology at the University Medical Center Groningen to obtain a Ph.D. degree in Visual Neuroscience. As part of his doctoral research, he also stayed at Stanford University (United States) and The University of York (United Kingdom). Koen is currently a postdoctoral researcher at the University of Minnesota in the United States of America.

ISBN 978-90-367-6053-9

cmb.

RIJKSUNIVERSITEIT GRONINGEN

Computational neuroimaging of visual field loss

Proefschrift

ter verkrijging van het doctoraat in de
Medische Wetenschappen
aan de Rijksuniversiteit Groningen
op gezag van de
Rector Magnificus, dr. E. Sterken,
in het openbaar te verdedigen op
maandag 25 februari 2013
om 12:45 uur

door

Koen Vincent Haak

geboren op 2 maart 1982
te Groningen

STELLINGEN

behorende bij het proefschrift:

COMPUTATIONAL NEUROIMAGING OF VISUAL FIELD LOSS

door

Koen Vincent Haak

1. The visual cortex of individuals with macular degeneration does not exhibit large-scale cortical reorganization (this thesis, chapter 2).

2. Ectopic receptive fields are not a decisive measure of cortical reorganization (this thesis, chapters 2 and 3).

3. Ectopic receptive fields may become apparent because the absence of visual input exposes feedback signals from the peripheral visual field (this thesis, chapter 3).

4. Assessing whether visual field maps are normal or abnormal can only reveal that cortical remapping did not occur (this thesis, chapter 4).

5. The retinotopic organization of visual areas V1-3 remains unaffected by the removal of an entire cerebral hemisphere (this thesis, chapter 4).

6. The stability of the human visual cortical circuitry is beneficial for treatments that aim to restore retinal function (this thesis, chapters 2 and 4).

7. It is possible to assess retinal sensitivity in ophthalmological disease with fMRI (this thesis, chapter 6).

8. Connective field modeling enables assessing how the spatial coupling between visual brain areas is influenced by changes in experimental context, ageing and disease (this thesis, chapter 5).

9. For the nonspecialist in statistics, it can be said that if a fairly complicated waveform is readily seen by visual inspection of the data, it is always highly significant (Bandettini et al. Magnetic Resonance in Medicine 30 (2), p169, 1993).

10. Onderzoek is één deel puur toeval, één deel inspiratie, en acht delen hard werk (vrij naar: René Fransen. Universiteitskrant 40 (29), p7, 2011).

Promotor	:	Prof. dr. J.M.M. Hooymans
Copromotores	:	Dr. F.W. Cornelissen Dr. R.J. Renken
Beoordelingscommissie	:	Prof. dr. A.V. van den Berg Prof. dr. P. van Dijk Prof. dr. S.A. Engel

With special thanks to:

my advisors:
Frans Cornelissen, Remco Renken & Anneke Hooymans,

my collaborators:
Antony Morland, Heidi Baseler & André Gouws,
Brian Wandell & Jonathan Winawer,
Serge Dumoulin, Ben Harvey & Dave Langers

my reading committee:
Stephen Engel, Albert van den Berg & Pim van Dijk,
Mark Greenlee & Rainer Goebel,

my fellow lab-members:
Richard Jacobs, Jan-Bernard Marsman Aditya Hernowo,
Ronald van den Berg & Marije van Beilen,

my administrators:
Wim Berghuis, Hedwig van Oosten, Diana Koopmans & Janine Wieringa,

my radiographers:
Anita Sibeijn-Kuiper & Judith Streurman

the financial support for performing my research:
European Union, Stichting Nederlands Oogheelkundig Onderzoek,
Research school of Behavioural and Cognitive Neurosciences &
Vereniging voor Biofysica & Biomedische Technologie

the financial support for printing this thesis:
Professor Mulderstichting,
University of Groningen
Research School of Behavioural and Cognitive Neurosciences.

my family:
Reinoud Haak, Frieda Groeneveld, Caroline Haak & Rinze Haak,

my other family:
Dick Faber, Hannah van der Feen,
Astrid Ranft, Arie van der Kooi &
Pleuni de Jong

my friends and colleagues

&

mijn liefste
Myrthe Faber

Contents

Chapter 1

Introduction

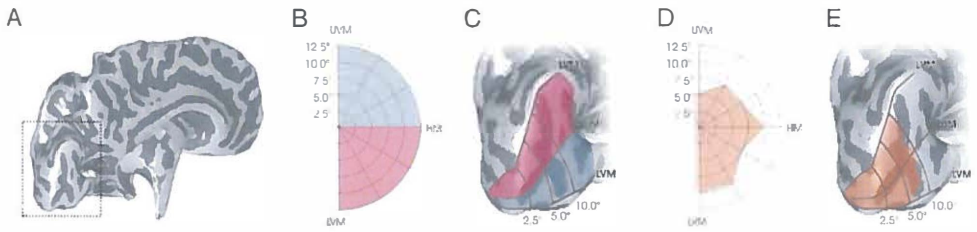

Figure 1. Schematics showing the visual field representation in primary visual cortex and the lesion projection zone (LPZ). An inflated three-dimensional reconstruction of the cortical surface of the left cerebral hemisphere is illustrated as if viewed from a posterior-medial position (a). The square depicted with a dashed line indicates the region of the brain that is shown magnified in panels c and e. A visual field coordinate map of the central 12.5 degrees of visual angle, with upper and lower quadrants colored blue and pink, respectively (b). The mapping of the visual field coordinate map onto the cortex in and surrounding the calcarine sulcus (c). The upper and lower visual quadrants are represented in the lower and upper banks of the calcarine sulcus. Also note the disproportionate area of cortex devoted to the central portion of the visual field. This feature is called cortical magnification. The visual field coordinate map with a shaded area indicating a central retinal lesion or scotoma (d). The transformation into cortical coordinates of the scotoma: the lesion projection zone (e). This figure and figure legend were adapted from: Baseler HA, Gouws A, Morland AB (2009) The organization of the visual cortex in patients with scotomata resulting from lesions of the central retina. Neuro-Ophthalmology 33(3): 149-157.

1.1. Background

Many eye diseases, such as macular degeneration, glaucoma and retinitis pigmentosa, cause visual field loss or otherwise reduce the visual abilities. It is also the case that, when a portion of the retina is damaged in both eyes, a certain part of the brain is no longer stimulated (figure 1). This raises the question of what happens to that part of the brain. Will it change its functional organization? The answer to this question determines the options available for treatment; especially when it comes to future treatments with stem cells and retinal prostheses, but also when it comes to rehabilitation (training) [1]. An important assumption in stem cell and prosthetic treatments is that the functional organization of the visual system remains unchanged, but whether this is actually the case is far from certain. For rehabilitation, and in particular for the very intensive training programs that are aimed at restoring vision, the assumption is that the visual system is able to adapt. That, however, is not entirely sure either: some claim that the adult human brain exhibits a large-scale reorganization of visual processing [2, 3], whereas others found no such reorganization [4]. It is thus important to establish the degree to which, and what parts of the visual system remain plastic throughout life.

A common way to map the functional organization of the human visual cortex is to systematically stimulate certain parts of the visual field, while at the same time monitoring the stimulus-evoked brain activity with functional magnetic resonance imaging (fMRI) [5-15]. Because the human visual cortex is organized in a retinotopic manner (i.e. nearby visual neurons in the brain respond to nearby locations in the visual field), it is then possible to identify a number of different visual field maps. The retinotopic mapping experiment is therefore also known as visual field mapping. Recently, it has been shown that it is also possible to use the visual field mapping data to estimate properties of the receptive fields of visual neurons [16]. The receptive field of a visual neuron refers to the stimulus positions that are most effective at driving the its response. The ability to estimate the receptive fields of visual neurons is important, because it allows us to determine precisely how the visual brain responds to a change or reduction in stimulation.

Estimating the receptive fields of visual neurons plays a very important role in the investigation of visual cortical reorganization. In animals, such as monkeys, cats and mice, it has been found that lesioning the retina alters the apparent position and/or size of the receptive fields [17-23]. Receptive field changes will have an impact on the overall functional organization of visual cortex, if they occur frequently; the receptive fields of visual brain cells together form the aforementioned topographical structure, which necessarily changes accordingly. Since recently, however, there is a debate about whether these 'ectopic' receptive fields should be

interpreted as evidence of cortical reorganization [24-27]. The argument is that the evidence of cortical reorganization does not derive from the observation that a single brain cell has been given another receptive field, but from the observation that the average receptive field of many visual brain cells has changed. This is because it was not possible for the same visual brain cells to be followed from before to after the application of the retinal damage. As such, there is a risk that the change of the average receptive field is actually caused by silencing a biased subset of visual neurons, which is not at all indicative to cortical reorganization.

In this thesis, we have aimed to determine whether and when the cortical representation of the visual field would be modified in the face of a visual field defect. Two additional aims of this thesis were to develop a new methodology that would be useful for assessing visual cortical plasticity in the future, and also to review the possibility of using fMRI as clinical tool for assessing visual field loss.

1.2. Outline

Using functional magnetic resonance imaging (fMRI), we measured the visual field maps in a large group of adult humans with central vision loss due to macular degeneration and compared them to the visual field maps in a group of healthy controls in whom we simulated a central visual field loss. We found that no significant remapping or reorganization was evident in the patients, although subtle changes in the visual field maps occurred in both the patients and the controls (**chapter 2**). Rather than cortical reorganization, these subtle changes appear to reflect a biased sampling of neuronal responses and feedback signals from higher order visual areas (**chapter 3**).

To determine the conditions under which the human visual field maps are plastic or stable, we also reviewed the literature on visual plasticity (**chapter 4**) and find that large-scale remapping of human visual cortex is limited to congenital disorders. In addition, we provide new data on the visual field maps in an individual who lost an entire cerebral hemisphere at age three. These data again indicate that the human visual field maps remain normal, even when an entire hemisphere is lost at preschool age. Thus, our findings challenge the contemporary view that the adult human visual cortex would be capable of large-scale reorganization.

As part of our research, we have also developed a new fMRI data-analysis method that we have called connective field modeling (**chapter 5**). Connective field modeling can be used to make inferences about how the spatial coupling among visual field maps is influenced by changes in experimental context (e.g., patient vs control). Connective field modeling opens up a wide

range of new research opportunities to study the visual system and may soon provide additional insights into the plasticity of the human visual brain.

The absence of cortical reorganization may prove to be beneficial for patients with retinal damage. New treatments, such as anti-angiogenic injections, retinal prostheses and stem-cell therapy, aim to restore the damaged retina and can only deliver maximum benefit if the brain remains correctly organized. That the human visual field maps are stable means that no large-scale cortical remapping would have to be undone. The absence of large-scale cortical reorganization also suggests that it is possible to determine, on the basis of fMRI measurements, whether the brain receives visual information from the eye. This would open up the possibility to use fMRI as a tool for detecting the presence and monitoring the progression of eye disease (**chapter 6**).

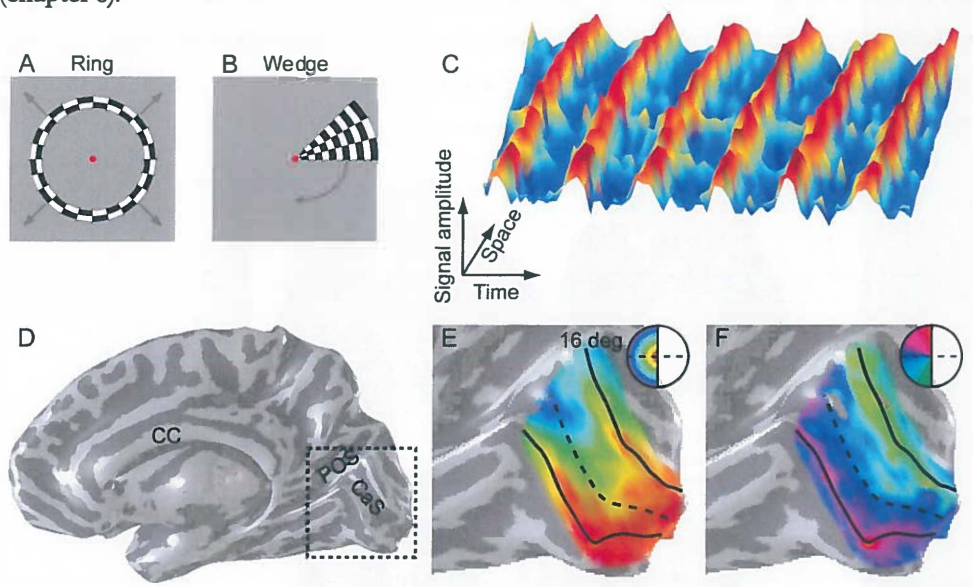

Figure 2. The phase-encoded visual field mapping method. The stimuli in a phase-encoded visual field mapping experiment typically consist of a set of high-contrast expanding/contracting rings (a) and (counter-)clockwise rotating wedges (b). These high-contrast rings and wedges typically elicit a BOLD signal modulation of 1-3% (c), which varies smoothly across the cortical surface (space, in this case along the calcarine sulcus, which is indicated by CaS in d and by the dashed lines in e). The phase delay of the BOLD signal modulation corresponds to the preferred stimulus location. To ease the visual examination of these data, the visual field maps are often viewed onto a inflated 3D reconstruction of the cortical surface (d). In this panel, the labels are as follows: corpus callosum, CC; parietal-occipital sulcus, POS; and calcarine sulcus, CaS. The dashed square indicates the portion of the image that is expanded in e and f. These panels display the cortical surface near the calcarine sulcus overlaid with the response phase at each cortical location (see color legends). These eccentricity (e) and polar-angle (f) maps define the hemifield map of the primary visual cortex (V1). This figure and figure legend were adapted from: Wandell BA, Dumoulin SO, and Brewer AA (2009) Visual field maps in human cortex. Neuron 56(2): 366-383, Figure 3.

1.2. Computational neuroimaging

The studies in thesis revolve around evaluating visual field maps in the human brain. These visual field maps emerge from the receptive field profiles of individual visual neurons (i.e., nearby visual neurons in cortex have receptive fields at nearby locations in the visual field). It is therefore unfortunate, that it is not yet possible to measure directly and non-invasively the receptive fields of single visual neurons. To measure the visual field maps in the living human brain, we have adopted the computational neuroimaging approaches that were developed to evaluate the average receptive field profile of many neurons. Computational neuroimaging is different from conventional neuroimaging because computational experiments "separate the question of localization from the measurements [and] are not organized around statistical classification methods – does the area light up? The experiments vary an independent parameter [...] and measure a range of cortical responses that are well above common statistical reliability criteria" [9]. The following paragraphs provide a short overview of these techniques.

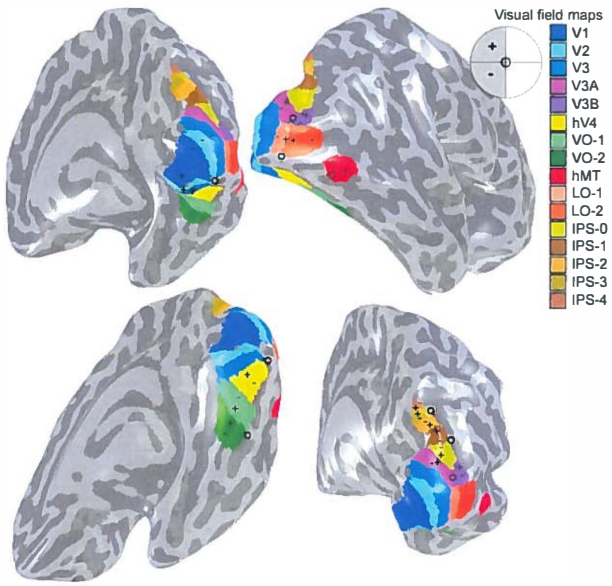

Figure 3. Visual field maps in the human brain. The positions of sixteen maps are shown on an inflated rendering of the cortical surface. Fovea and upper/lower visual fields are indicated by the "o", "+", and "–" symbols, respectively. The posterior visual maps in and around the calcarine sulcus are labeled V for visual, and a number, e.g., V1, V2, V3, V3A, following the naming of homologs in macaque monkey. The maps in the lateral occipital cortex are numbered as LO-x, the maps in the ventral occipital cortex are numbered as VO-x, and the maps in the intraparietal sulcus are numbered IPS-x. This figure and figure legend were adapted from: Wandell BA, Dumoulin SO, and Brewer AA (2009) Visual field maps in human cortex. Neuron 56(2): 366-383, Figure 2.

1.2.1. Functional MRI

Functional MRI is a widely used technique to make images of neural activity at certain points in time. To create these images, a very strong electromagnetic field (typically 3 Tesla) is used to detect changes in the concentration of deoxyhemoglobin (hemoglobin without bound oxygen molecules), an endogenous contrast agent indicative to neural activity (i.e., neurons need energy to function, which is provided by glucose and oxygen, and oxygen is bound to hemoglobin in red blood cells) [28-30]. The varying concentration of deoxyhemoglobin determines the image intensity, which is why the technique is sometimes also referred to as blood-oxygenation level-dependent (BOLD) imaging. BOLD imaging does not have a very high temporal resolution. The spatial resolution of BOLD imaging, however, is very good: with a typical 3 Tesla scanner it is possible to resolve signals that are 2-3 mm apart. Nevertheless, a standard voxel (volume-pixel) of 2.5^3 mm^3 will still capture the responses of ~1 million neurons [31, 32].

1.2.2. Phase-encoded visual field mapping

The BOLD images recorded during different experimental conditions can be compared to each other using t-tests and ANOVAs. However, while this approach is fine for localizing brain regions that are involved in some kind of cognitive task, it is less suitable for measuring the neural response to a continuously varying parameter such as visual field location [14-16]. It is therefore that the phase-encoded fMRI paradigm was developed (also called the traveling-wave method) [5]. This phase-encoded fMRI paradigm is based on a technique for analyzing a voxel's intensity in a sequence of BOLD images by correlation with a sinusoid to determine its statistical significance [33], but additionally infers the preferred stimulus position from the phase delay in the BOLD image intensity. The visual field mapping stimuli in the phase-encoded experiments typically consist of periodically expanding/contracting rings and (counter-)clockwise rotating wedges (figure 2). This is because the human visual pathways map the visual image from the Cartesian coordinates in the visual field to polar coordinates in cortex (i.e., eccentricity, which is the distance from the center of gaze, and polar-angle, which is the orientation with respect to the center of gaze). The ring stimulus is designed to measure eccentricity maps, while the wedge stimulus is designed to measure polar-angle maps.

1.2.3. Population receptive field modeling

The phase-encoded method has been very successful at uncovering visual field maps in the human brain. Using the phase-encoded method, at least sixteen visual field maps have been identified thus far (figure 3). The phase-encoded method has some limitations, however, particularly when measuring higher order visual field maps with large receptive fields [13]. To

overcome these limitations, another way of uncovering visual field maps has recently been introduced. Unlike the phase-encoded visual field mapping approach, the new method estimates explicitly the location and size parameters of the neuronal population receptive field (pRF) [16]. This is done by testing which of a wide range of receptive field models best predicts the BOLD signal (figure 4). The pRF approach has several advantages over the phase-encoded method. These include the freedom of using non-periodical drifting bar stimuli, as well as using mean-luminance periods for measuring the baseline activity [ref]. The pRF method does not require the standard ring and wedge stimuli because the eccentricity and polar-angle maps can be inferred from the pRF parameters. An important additional advantage of the pRF modeling method is that it provides a direct estimate of the pRF size. As will become clear in the following chapters, this feature is of particular importance in the context of visual cortical plasticity research. Finally, it is also of note that the connective field modeling methods in chapter 5 are based on the pRF analysis.

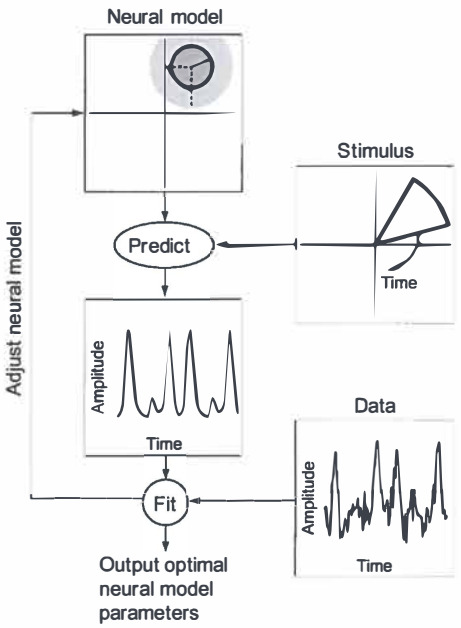

Figure 4. A flowchart describing the population receptive field (pRF) modeling procedure. The pRF model describes certain neuronal properties, such as receptive field center, size and scatter, along with non-neuronal nuisance factors, such as the hemodynamic response and eye movements. The pRF model is combined with the stimulus to generate a prediction of the BOLD data. The pRF model parameters are adjusted for each cortical location to minimize the difference between the prediction and the BOLD data. The best-fitting model parameters are the output of the analysis. This figure and figure legend were adapted from: Wandell BA, Dumoulin SO, and Brewer AA (2009) Visual field maps in human cortex. Neuron 56(2): 366-383, Figure 10.

References

[1] Baseler HA, Gouws A, Morland AB (2009) The organization of the visual cortex in patients with scotomata resulting from lesions of the central retina. Neuro-Ophthalmology 33(3): 149- 157.

[2] Baker CI, Peli E, Knouf N, Kanwisher NG (2005) Reorganization of visual processing in macular degeneration. Journal of Neuroscience 25: 614–618.

[3] Baseler HA, Brewer AA, Sharpe LT, Morland AB, Jagle H, Wandell BA (2002) Reorganization of human cortical maps caused by inherited photoreceptor abnormalities. Nature Neuroscience 5: 364–370.

[4] Sunness JS, Liu T, Yantis S(2004) Retinotopic mapping of the visual cortex using functional magnetic resonance imaging in a patient with central scotomas from atrophic macular degeneration. Ophthalmology 111: 1595–1598.

[5] Engel SA, Rumelhart DE, Wandell BA, Lee AT, Glover GH et al. (1994) fMRI of human visual cortex. Nature 369: 525.

[6] Sereno MI, Dale AM, Reppas JB, Kwong KK, Belliveau JW, et al. (1995) Borders of multiple visual areas in humans revealed by functional magnetic resonance imaging. Science 268: 889-893.

[7] DeYoe EA, Carman GJ, Bandettini P, Glickman S, Wieser J, et al. (1996) Mapping striate and extrastriate visual areas in human cerebral cortex. Proceedings of the National Academy of Science USA 93: 2382-2386.

[8] Engel SA, Glover GH, Wandell BA (1997) Retinotopic organization in human visual cortex and the spatial precision of functional MRI. Cerebral Cortex 7 (2): 181-192.

[9] Wandell BA (1999) Computational neuroimaging of human visual cortex. Annual Review of Neuroscience 22: 145-173.

[10] Dougherty RF et al. (2003) Visual field representations and locations of visual areas V1/2/3 in human visual cortex. Journal of Vision 3: 586–598.

[11] Brewer AA, Liu J, Wade AR, Wandell BA (2005) Visual field maps and stimulus selectivity in human ventral occipital cortex. Nature Neuroscience 8: 1102-1109.

[12] Wandell, B.A., Brewer, A.A. & Dougherty, R.F. (2005) Visual field map clusters in human cortex. Philosophical Transactions of the Royal Society London B 360, 693–707.

[13] Wandell BA, Dumoulin SO, and Brewer AA (2009) Visual field maps in human cortex. Neuron 56(2): 366-383.

[14] Wandell BA, Winawer J (2011) Imaging retinotopic maps in the human brain. Vision Research 51 (7): 718-737.

[15] Engel SA (2012) The development and use of phase-encoded functional MRI designs. Neuroimage 62(2): 1195-1200.

[16] Dumoulin SO, Wandell BA (2008) Population receptive field estimates in human visual cortex. Neuroimage 39: 647-660.

[17] Kaas JH *et al.* (1990) Reorganization of retinotopic cortical maps in adult mammals after lesions of the retina. Science 248, 229–231 (1990).

[18] Heinen SJ, Skavenski AA (1991) Recovery of visual responses in foveal V1 neurons following bilateral foveal lesions in adult monkey. Experimental Brain Research 83: 670–674.

[19] Chino YM, Kaas JH, Smith EL III, Langston AL, Cheng H (1992) Rapid reorganization of cortical maps in adult cats following restricted deafferentation in retina. Vision Research 32: 789–796.

[20] Gilbert CD, Wiesel TN (1992) Receptive field dynamics in adult primary visual cortex. Nature 356: 150–152.

[21] Darian-Smith C, Gilbert CD (1995) Topographic reorganization in the striate cortex of the adult cat and monkey is cortically mediated. Journal of Neuroscience 15: 1631–1647.

[22] Kaas JH (2002) Sensory loss and cortical reorganization in mature primates. Progress in Brain Research 138: 167–176.

[23] Giannikopoulos DV, Eysel UT (2006) Dynamics and specificity of cortical map reorganization after retinal lesions. Proceedings of the National Academy of Science USA 103: 10805–10810.

[24] Calford, MB, Chino YM, Das A, Eysel UT, Gilbert CD, Heinen SJ, Kaas JH, Ullman S (2005) Neuroscience: rewiring the adult brain. Nature 438: E3.

[25] Smirnakis SM, Brewer AA, Schmid MC, Tolias AS, Schuz A, Augath M, Inhoffen W, Wandell BA, Logothetis NK (2005) Neuroscience: rewiring the adult brain. Nature 438: E4.

[26] Smirnakis SM, Brewer AA, Schmid MC, Tolias AS, Schuz A, Augath M, Inhoffen W, Wandell BA, Logothetis NK (2005) Lack of long-term cortical reorganization after macaque retinal lesions. Nature 435: 300-307.

[27] Wandell BA and Smirnakis, SM (2009) Plasticity and stability of visual field maps in adult primary visual cortex. Nature Reviews Neuroscience 10: 873–884.

[28] Ogawa S, Lee TM, Nayak AS, Glynn P (1990) Oxygenation-sensitive contrast in magnetic resonance image of rodent brain at high magnetic fields. Magnetic Resonance in Medicine

14: 68–78.

[29] Ogawa S, Lee TM, Kay AR, Tank DW (1990) Brain magnetic resonance imaging with contrast dependent on blood oxygenation. Proceedings of the National Academy of Science USA 87: 9868–9872.

[30] Ogawa S, Tank DW, Menon R, Ellermann JM, Kim SG, Merkle H, Ugurbil K (1992) Intrinsic signal changes accompanying sensory stimulation: functional brain mapping with magnetic resonance imaging. Proceedings of the National Academy of Science USA 89: 5951–5955.

[31] Rockel AJ, Hiorns RW, Powell TP (1980) The basic uniformity in structure of the neocortex. Brain 103: 221-244.

[32] Leuba G, Garey LJ (1989) Comparison of neuronal and glial numerical density in primary and secondary visual cortex of man. Experimental Brain Research 77: 31-38.

[33] Bandettini PA, Jesmanowicz A, Wong EC, Hyde JS (1993) Processing strategies for time course data-sets in functional MRI of the human brain. Magnetic Resonance in Medicine 30: 161-173.

Large-scale remapping of visual cortex is absent in adult humans with macular degeneration

Based on: Baseler HA, Gouws A*, Haak KV *, Racey C, Crossland MD, Tufail A, Rubin GS, Cornelissen FW, Morland AB (2011) Large-scale remapping of visual cortex is absent in adult humans with macular degeneration. **Nature Neuroscience** 14 (5): 649-655.

* These second and third authors contributed equally to this work

Abstract

The occipital lobe contains retinotopic representations of the visual field. The representation of the central retina in early visual areas (V1–3) is found at the occipital pole. When the central retina is lesioned in both eyes by macular degeneration, this region of visual cortex at the occipital pole is accordingly deprived of input. However, even when such lesions occur in adulthood, some visually driven activity in and around the occipital pole can be observed. It has been suggested that this activity is a result of remapping of this area so that it now responds to inputs from intact, peripheral retina. We evaluated whether or not remapping of visual cortex underlies this activity. Our functional magnetic resonance imaging results provide no evidence of remapping, questioning the contemporary view that early visual areas of the adult human brain have the capacity to reorganize extensively.

2.1. Introduction

The human brain contains maps of the retina on the surface of the occipital lobes [1]. Abnormal visual development can modify these retinotopic maps [2-5]. Under circumstances in which individuals acquire early visual experience in the presence of a lesion to the center of the retina, reorganization of the visual representation occurs [6]. The visual brain in these individuals remaps by allocating a larger than normal area of cortex to intact, peripheral vision. Although brain plasticity is clearly possible when neural changes occur early in life, the adult brain also appears to be capable of plasticity. Experimentally induced retinal lesions in adult animals can lead to a remapping of primary visual cortex to respond to inputs from nearby intact retina [7-13]. We sought to determine whether cortical remapping generalizes to humans who acquire retinal lesions in adulthood.

Several groups have investigated reorganization in human adult cortex when retinal lesions were acquired as a result of disease (macular degeneration). These studies have produced variable results, generating some controversy. One group [14] found no evidence of activity in parts of visual cortex that normally receive input from lesioned retina (the lesion projection zone) in a single, elderly individual. Another study [15], on the other hand, reported widespread activation of the lesion projection zone in two adults with juvenile macular degeneration and suggested that this might reflect a cortical remapping via horizontal connections similar to, but larger than, those found in earlier animal studies. The remapping hypothesis is supported by another functional magnetic resonance imaging (fMRI) study claiming that activation of deprived cortex can be generated by eccentric fixation [16]. Stimulating the occipital cortex of an individual blinded in adulthood by trauma to the optic nerves resulted in abnormal phosphene maps, also suggesting cortical remapping [17]. Despite these reports, the implication that remapping is responsible for the large-scale spread of activation in the lesion projection zone of individuals with retinal lesions acquired in adulthood has been seriously questioned [18-20].

Using methods that explicitly evaluate visual cortical maps, we sought to determine whether humans with lesions acquired in adulthood exhibit reorganization in the form of cortical remapping of visual input over the large-scale seen in individuals with congenital foveal loss of vision [6]. In contrast with prior studies largely restricted to a few individuals with juvenile forms of macular degeneration (JMD), we compared responses in a large number of individuals in two different age groups: those with JMD and those with the more common age-related form (AMD), and their age-matched controls. We found no evidence of large-scale remapping in early visual areas in adults with acquired retinal lesions. Indeed, the area of activity in primary visual cortex measured in these individuals was no different from that predicted on the basis of normal

retinotopic maps. Furthermore, the absence of cortical remapping was not dependent on the age at which the individuals acquired retinal lesions in adulthood.

2.2. Results

Cortical responses were measured in 16 individuals with macular degeneration (see Table 1) and 12 age-matched controls with normal vision using fMRI. Individuals with macular degeneration had bilateral lesions for at least 1 year and had developed a stable preferred retinal locus that allows good fixation performance. We tested two age groups: young (mean age = 30) and elderly (mean age = 76). Participants passively viewed flickering checkerboard stimuli configured in a ring that expanded through increasing eccentricity or a wedge that rotated around a central point. Such stimuli reliably modulate blood oxygenation level–dependent signals and are used to map visual areas in occipital cortex [1, 21-24]. Response magnitude was first evaluated using coherence as an outcome measure, as in previous similar fMRI studies [18, 25] (Methods).

We made coherence maps for each of the individuals in the two groups, those with macular degeneration (the patient group) and the age-matched controls (the control group). Although control subjects showed substantial visually driven responses throughout visual cortex, both the young and elderly patient groups only displayed substantial responses in the anterior occipital lobe. Strong responses in these individuals are therefore limited to regions of the cortex that normally map peripheral (that is, intact) retina (Figure 1).

Responses in the lesion projection zone were compared quantitatively with those in regions that are normally driven by intact retina using regions of interest (ROIs) defined anatomically to avoid any bias toward activation patterns. In both hemispheres, one region was selected at the occipital pole, normally representing the central visual field, and another region in the fundus of the calcarine sulcus, normally representing more peripheral locations. The BOLD signal plotted as a function of time showed robust modulations in response to stimulus onset at both the occipital pole and calcarine sulcus in controls (Figure 1). Clear differences in the response latency of the signals measured at the occipital pole and calcarine sulcus reflect the normal retinotopic mapping of early visual areas. Fourier analysis was also applied to the average time series (Figure 1). The resultant spectra (and associated z scores) are consistent with the time series, showing robust signals at the stimulation frequency at both cortical locations in the control group, but only at the calcarine sulcus in the patient group.

Diagnosis	Sex	Age (yr)	Eye	Lesion diameter (°)	Acuity (logMAR)	BCEA (°)
AMD	F	90.9	OD	9	0.92	17.7
AMD	F	83.5	OD	8	0.98	12.43
AMD	F	81.8	OS	7	0.54	17.7
AMD	M	76.3	OS	6	0.36	8.26
AMD	M	80.2	OS	10	1.06	15.16
AMD	F	70.8	OS	4	0.9	12.37
AMD	M	83.8	OS	15	0.86	20.37
AMD	M	80.6	OD	13	0.76	5.33
Stargardt's	M	19.8	OS	5	0.74	11.71
Stargardt's	F	19.1	OS	3	1.02	2.24
Stargardt's	M	49.5	OD	6	0.56	14.47
Stargardt's	F	41.2	OD	10	0.9	1.69
Stargardt's	F	34.7	OD	8	1.08	13.54
Stargardt's	F	39.4	OD	9	0.98	18.11
Stargardt's	F	24.3	OS	3.5	0.66	9.33
Stargardt's	M	35.8	OS	17	1.12	13.26

Table 1. Summary of affected individuals in the study. BCEA, Bi-variate Contour Ellipse Area (a measure of fixation ability using microperimetry); logMAR, logarithm of the Minimum Angle of Resolution.

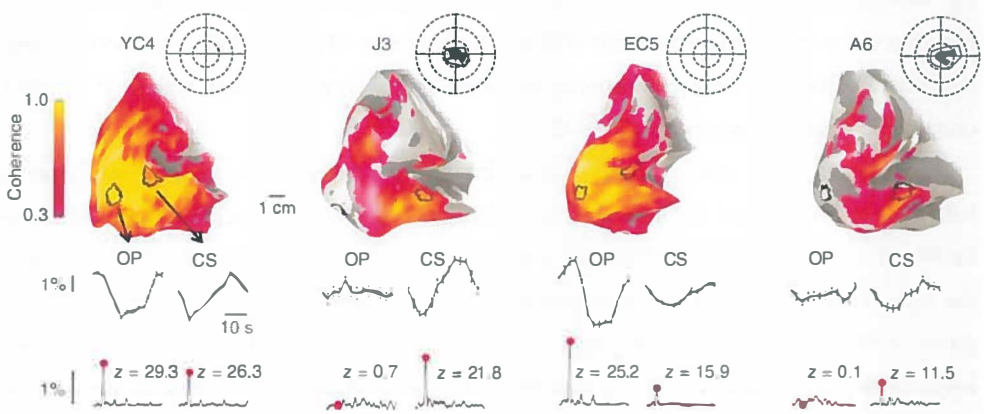

Figure 1. Cortical responses to visual stimulation. BOLD responses for four individuals (from left to right): a young control subject (YC4, age 30), a young patient (J3, age 49), an elderly control subject (EC5, age 66) and an elderly patient (A6, age 70). Visual field results from microperimetry for each subject are inset to the right of each brain image and indicate absolute (black) and partial (gray) scotoma. Dotted concentric circles represent 5, 10 and 15 deg eccentricity. BOLD response coherence is encoded in color and superimposed on smoothed, left occipital lobes. Single cycle time series averages are shown for the two occipital ROIs representing central (occipital pole, OP) and more peripheral retina (calcarine sulcus, CS). Fast Fourier transforms were performed on each full time series and amplitude spectra are also shown for each ROI; stimulus frequency (seven cycles per scan) is indicated by the red dot. z scores indicate the number of standard deviations the FFT amplitude at the stimulus frequency differs from the distribution of all of the other frequency amplitudes.

2.2.1. Group effects

Our data analysis (Figure 1) captured responses in individuals and conformed to the approach used in previous work on a limited number of cases [15, 18, 26]. Extending our analysis to the group level, we categorized participants according to age and visual status (young and elderly, patient and control). Responses were assessed at three cortical locations: the two mentioned above (calcarine sulcus and occipital pole; Figure 1), and a third control region located further anterior in the brain in non-visual cortex, chosen to serve as a baseline measure.

The results for the elderly group are shown in Figure 2a. We performed a two-way analysis of variance (ANOVA) with visual status (patient versus control group) and ROI (calcarine sulcus versus occipital pole versus control region) as main factors. A significant main effect was found for both visual status ($F = 8.62$, $P < 0.01$) and brain region ($F = 24.20$, $P < 10^{-6}$), with a significant interaction ($F = 3.30$, $P < 0.05$). Post hoc tests (corrected for multiple comparisons) revealed a significant difference between the patient and control groups at the occipital pole ($P < 0.01$), but none at the calcarine sulcus or at the control region. In the patient group, signals at the occipital pole were not significantly different from the baseline measure at the control region ($P > 0.05$), but were significantly different from signals from the intact retina at the calcarine sulcus ($P < 0.001$). Patient group responses at the calcarine sulcus were robust and well above baseline ($P < 0.001$). In the control group, signals at the occipital pole and calcarine sulcus were not significantly different from one another ($P > 0.05$), but both differed significantly from the baseline response (calcarine sulcus versus control region, $P < 0.001$; occipital pole versus control region, $P < 0.05$).

Previous work that revealed activity in the lesion projection zone primarily tested individuals who acquired lesions earlier in adulthood than the individuals with AMD that we examined. Comparing the young patient group with the young control group, however, yielded the same results as in the elderly patient group (Figure 2b), with significant main effects of visual status ($F = 52.32$, $P < 10^{-7}$) and ROI ($F = 95.72$, $P < 10^{-15}$) and a significant interaction between them ($F = 18.36$, $P < 10^{-5}$). Post hoc tests (corrected) also revealed the same pattern of results as in the elderly groups, but with all differences achieving significance at $P < 0.001$. Large-scale remapping appears to be absent independent of the age in adulthood at which the retinal lesions are acquired.

To test the reproducibility of our results, we acquired additional data on a separate day in most participants ($n = 20/28$) and found that the data conformed to the same pattern. Repeated-measures ANOVA revealed no main effect of session in all groups ($P > 0.05$). Combining data across sessions, we also tested explicitly for statistical differences associated with age across groups. A three-way ANOVA was performed on the elderly and young groups, with ROI, visual

status and age as factors. As in the individual age groups, significant main effects of visual status ($F = 23.40$, $P < 10^{-5}$) and ROI ($F = 60.00$, $P < 10^{-15}$) were found, as well as a significant interaction between them ($F = 7.18$, $P < 0.01$). There was also a main effect of age ($F = 8.82$, $P < 0.01$), a feature that we have noted previously [27]. However, there were no significant interactions between age and visual status ($F = 2.09$, $P = 0.15$) or age and ROI ($F = 2.31$, $P = 0.11$). Thus, although age affects the overall magnitude of fMRI responses, it does so similarly in both the patient and control groups and does not alter the pattern of differences found between them.

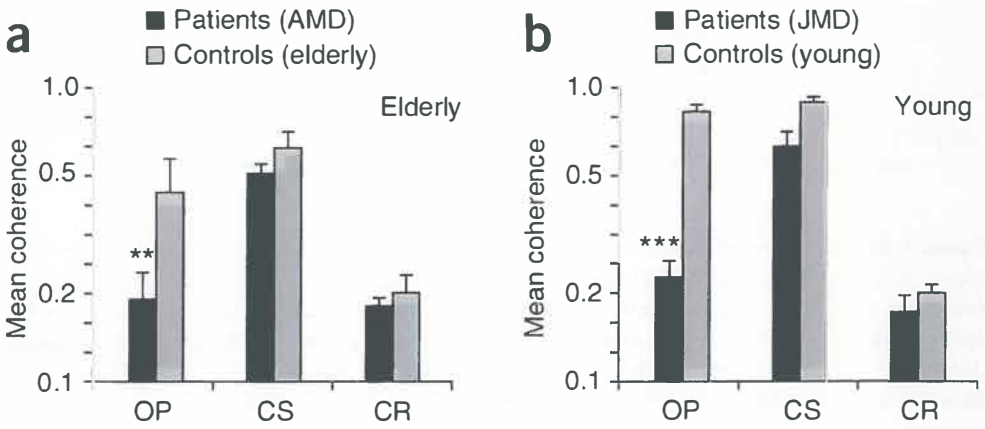

Figure 2. Mean coherences for each ROI, averaged across individuals for each group. CR, control region in non-visual cortex. Error bars indicate standard error. ***$P < 0.001$, **$P < 0.01$. (**a**) Elderly patients (AMD) versus elderly controls. (**b**) Young patients (JMD) versus young controls.

2.2.2. Simulating retinal lesion in controls

Using a control region in a non-visual brain area as a baseline measure comes with the danger that small, but genuine, occipital signals may escape detection, for example, if signal-to-noise ratios vary across the brain [28] or if the control region is in fact responsive to visual stimuli. To improve the specificity of our measurements, we compared signals in the same region of visual cortex (the occipital pole) in control subjects in the presence or absence of visual stimulation. We scanned 12 new control subjects (mean age = 27) while they passively viewed the expanding ring checkerboard stimulus either in full or with a central mask (gray disk radius = 7.5 degrees) simulating a macular lesion (Figure 3). The presence of the central mask in the stimulus largely removes significant responses from the occipital pole.

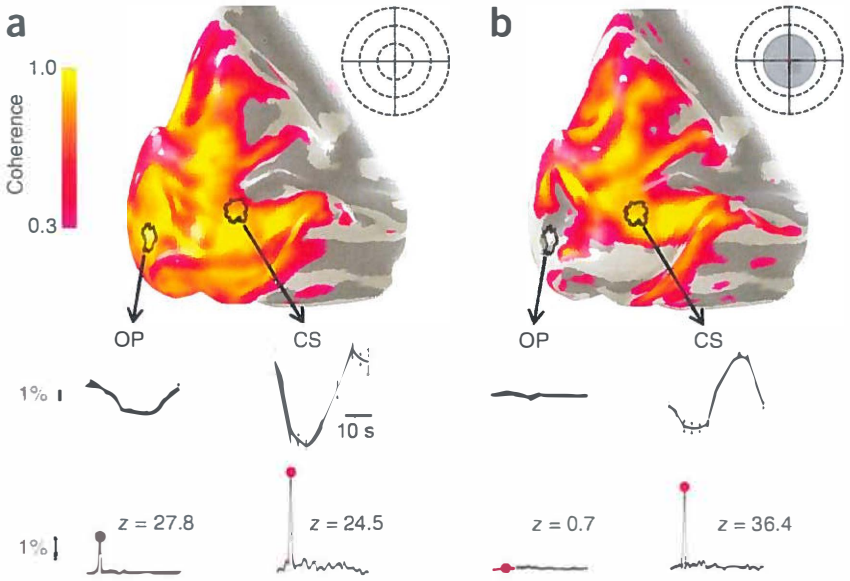

Figure 3. Simulating retinal lesions in a control subject. In both panels, the left occipital lobe of a control subject is shown with BOLD signal coherence superimposed on the surface. Below each panel time series (averaged to a single stimulus cycle) and amplitude spectra of the time series are given for circular regions of cortex at the occipital pole and calcarine sulcus. (**a**) Response to expanding checkerboard ring stimulus spanning full field. (**b**) Response to same stimulus as in a, but with central ±7.5 deg masked with a uniform, mean luminance gray disc. Data are presented as in Figure 1.

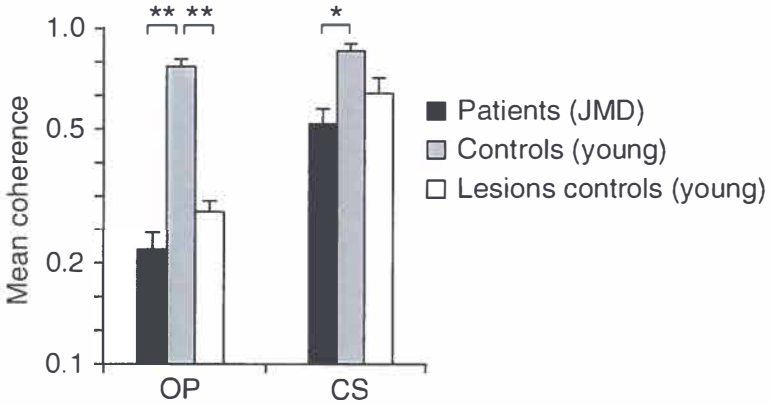

Figure 4. Occipital lobe responses compared across groups and ROIs. Mean coherences averaged across sessions and across individuals from three groups: young patient data from experiment 1, young control data from experiment 1 and lesion control group data from experiment 2 using new baseline measure at the occipital pole in response to stimulus with central ±7.5 deg masked with uniform gray. $^{**}P < 0.01$, $^{*}P < 0.05$. Error bars indicate the standard error of the mean.

Using the new baseline measure, we compared responses from the young control group with those from the young patient group and the control group from the first experiment, averaged across sessions (Figure 4). A two-way ANOVA revealed main effects of group (patient versus control versus new control groups, $F = 38.57$, $P < 10^{-9}$) and ROI (occipital pole versus calcarine sulcus, $F = 56.08$, $P < 10^{-8}$), as well as a significant interaction between them ($F = 8.50$, $P < 0.001$). Post hoc tests (corrected) showed that these effects were carried by important features at the occipital pole and calcarine sulcus. First, responses at the occipital pole did not differ significantly between the patient group and the new control group shown the simulated scotoma ($P > 0.05$), but both were significantly below those of the original control group shown the full stimulus ($P < 10^{-5}$ for both comparisons). Second, responses at the calcarine sulcus in all three groups were significantly above baseline, as expected ($P < 0.001$). The patient group responses at the calcarine sulcus fell significantly below those of the original age-matched controls ($P < 0.05$). In summary, our results using an improved baseline measure again support the absence of large-scale remapping in individuals with macular degeneration.

2.2.3. Partial volume effects

Even though stimulation of peripheral retina is expected to produce fMRI responses of equal magnitude in both patient and control groups, we noted that signals at the calcarine sulcus were relatively reduced in both the elderly and young patient groups (calcarine sulcus; Figure 2) and significantly so when data were combined across sessions ($P < 0.05$; Figure 4). Because lesion size was variable across the patient group, the anatomically defined ROI at the calcarine sulcus could include tissue in the lesion projection zone, effectively reducing the signal there. Such 'partial volume' effects are therefore predicted to be more likely when retinal lesions are large.

A multiple regression was performed with lesion size (mean lesion diameter; Table 1) and age as regressors, as age was shown previously to have a negative effect on fMRI responses (see above). The analysis revealed an overall significant relationship between lesion size, age and response (coherence) at the calcarine sulcus ($R^2 = 0.308$, $P < 0.05$). Consistent with the partial volume prediction, the effect was carried entirely by lesion size (t(one-tailed) $= -1.95$, $P = 0.036$) rather than age (t(one-tailed) $= -0.74$, $P = 0.238$). In contrast, no such relationship was found in regions where no response was predicted and partial volume effects were less likely, either well inside the lesion projection zone at the occipital pole ($R^2 = 0.059$, $P = 0.336$) or at the control region in non-visual cortex ($R^2 = 0.055$, $P = 0.346$).

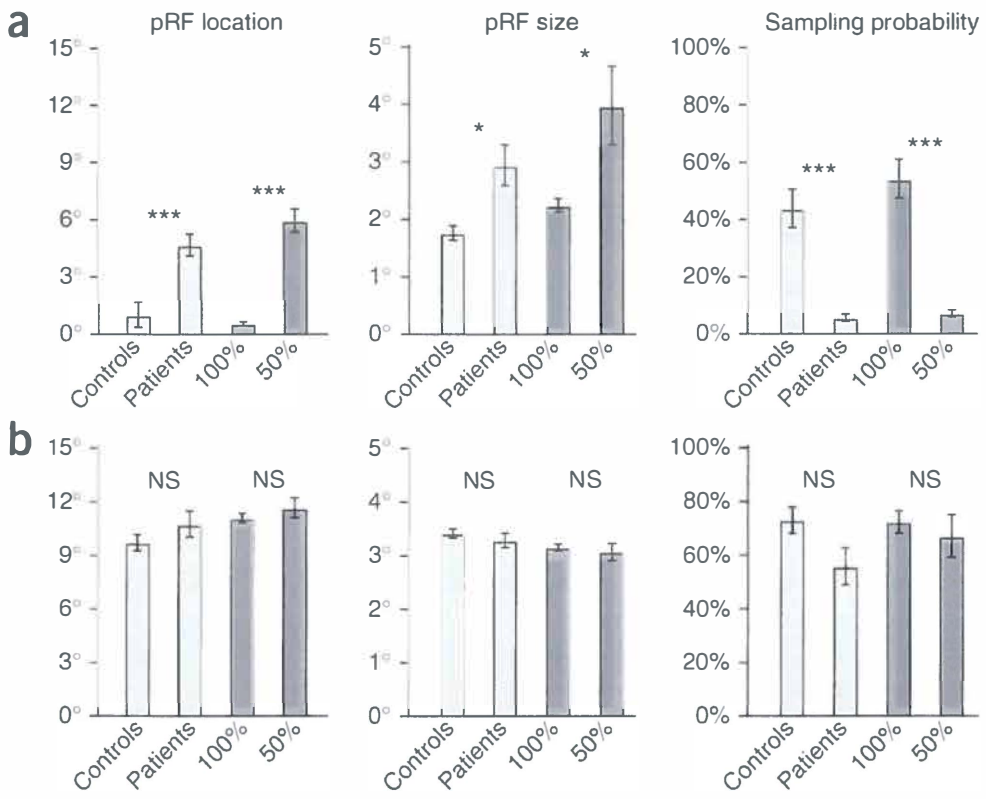

Figure 5. Receptive field characteristics. (**a**, **b**) Population receptive field (pRF) characteristics in the lesion projection zone (**a**) and the calcarine sulcus (**b**). Mean pRF locations and sizes and the sampling probability (percent voxels exceeding 15% variance explained) are shown. Light gray bars show data for individuals with macular degeneration and age-matched controls. Data are given for combined age groups, as none of the outcome measures showed group contrasts (patient group versus control group) that were specific to age (location, $F = 0.27$, $P = 0.603$; size, $F = 3.36$, $P = 0.074$; sampling probability, $F = 0.27$, $P = 0.603$). In two patients, we were unable to derive population receptive field estimates in the lesion projection zone. Dark gray bars show data for controls that were presented the unmasked (100%) stimulus or the stimulus simulating a central scotoma (50% masked). $*P < 0.05$, $***P < 0.001$. Error bars refer to the standard error of the mean.

2.2.4. Receptive field characteristics

Although there were no significant group differences in occipital pole signals between the patient group and the control group with simulated retinal lesions, there was a hint that occipital pole signals in both groups may exceed those found in the control region (Figure 2). It is possible that these signals are visually driven by a small proportion of neurons with large and/or eccentric receptive fields [19, 29] that extend into areas of stimulated retina.

To investigate the properties of potential visually driven signals, we modeled population

receptive fields [30] of responses in an enlarged region centered on the occipital pole region described above (Methods; Supplementary information). The mean population receptive field location and size around the occipital pole were abnormally large in both the patient group (location, $t = 3.81$, $P < 0.001$; size, $t = 2.90$, $P = 0.01$) and the control group when central retinal lesions are simulated (location, $t = 7.90$, $P < 0.001$; size, $t = 2.44$, $P = 0.032$) (Figure 5). The significant shift in population receptive field location (Figure 5a) implies an apparent shift in the representation of these voxels, that is, rendering them 'ectopic'. In contrast, population receptive fields in the calcarine sulcus region (Figure 5) did not differ significantly either between the patient and control groups (location, $t = 1.09$, $P = 0.285$; size, $t = 0.72$, $P = 0.481$) or between masked and unmasked conditions for the controls (location, $t = 0.84$, $P = 0.414$; size, $t = 0.44$, $P = 0.669$). Fixation instability in the patient group cannot account for the effects observed, as the patient and control groups with simulated lesions showed similar results and both the occipital pole and calcarine sulcus regions would be affected [5], which they clearly were not.

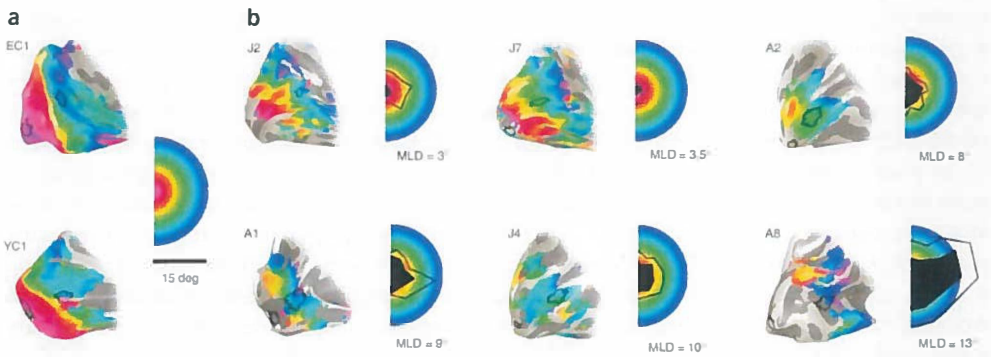

Figure 6. Individual eccentricity maps. (**a**,**b**) FMRI response maps of visual eccentricity superimposed on individual left, partially inflated, occipital lobes for control subjects (**a**) and six affected individuals (**b**). False color is used to indicate the position on the retina (see semi-circular key) to which the cortex is responsive. In **b**, filled black regions of the semicircular key indicate the absolute retinal lesion (scotoma), whereas outlined region exhibits significant, but not absolute, loss of vision. Patient group cortical maps are presented in ascending order (from left to right starting on the top row) of mean lesion diameter (MLD). The cortical representations closely corresponded to the spared retina. Indeed, even retinal locations with reduced sensitivity elicited activity. In all cases, however, the cortical activity did not spread to encompass the occipital pole. Note that this is a different subset of participants than those shown in Figure 1.

2.2.5. Cortical representation

Using phase encoded stimuli also allows the cortical mapping of retinal coordinates to be assessed at an individual level. Figure 6 shows fMRI response maps in the occipital lobes of several individuals in the elderly and young groups. Although subjects with normal vision showed

complete retinal representations throughout the occipital lobes (Figure 6a), individuals with macular degeneration showed response maps that were consistent with the projection from intact parts of retina only (Figure 6b). Furthermore, the extent of activation and its phase reflect the size of the spared retina. A large retinal lesion results in a smaller activation area on the brain (for example, A8) and vice versa (for example, J2).

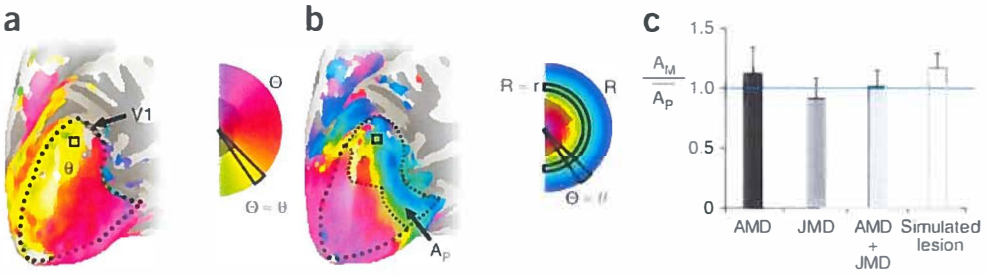

Figure 7. The cortical area representing intact visual field. (a,b) Schematic of the method by which the area of primary visual cortex representing a subject's intact visual field (measured by microperimetry) is predicted on the basis of normal retinotopic mapping. First, the primary visual cortex boundary was determined in each control participant by identifying the representations of the upper (purple) and lower (green) vertical meridians in calcarine cortex, as indicated by the dotted line on the surface reconstruction of the occipital lobe for one control participant (a). Second, we determined whether a voxel (as indicated by the small square in a and b) has a polar angle phase, θ, that is among the values of polar angle in the intact visual field, $\Theta\Theta$ (see inset false color map showing the location of the scotoma (shaded) and intact (unshaded) regions). If this is the case, as it is in the illustrated example, we then determined whether the eccentricity represented by the voxel, r, is among the eccentricities in the intact field, R, at the polar angle θ. If the voxel's polar coordinate (r,θ) is among the set of coordinates $(R,\Theta\Theta)$ of intact visual field locations, the voxel is retained. The predicted cortical area representing the patient's intact visual field, Ap, is then computed from all the retained voxels. For each patient, multiple values of Ap (one for each of the age-matched control retinotopic maps) were obtained and then averaged to compute the mean predicted area of activated V1, $\bar{A}p$. In each patient, the area of active primary visual cortex, Am, was also measured. (c) The ratio of Am to $\bar{A}p$ for the participant groups. No significant differences between groups or between group values and unity were found ($P > 0.05$). Non-significant differences from unity present in the AMD and simulated lesion groups are likely the results of the minority of ectopically responding voxels found in Figure 5, which could not be predicted from normal retinotopic maps. Error bars indicate the standard error of the mean.

To compare cortical maps quantitatively, we measured the area of activity in the primary visual cortex, Am, for each patient and control participant with simulated lesions and compared it with a mean predicted area, $\bar{A}p$, which was determined from the individual's scotoma and normal mappings of age-matched controls (Methods and Figure 7). The ratio $Am/\bar{A}p$ was compared across participant groups and we found no significant effect of group ($F = 0.81$, $P = 0.46$; Figure 7). Moreover, all groups exhibited ratios that were no different from unity (AMD, $t = 0.59$, $P =$

0.57; JMD, $t = -0.55$, $P = 0.60$; controls, $t = 1.93$, $P = 0.08$), an indication that the area of primary visual cortex activated in all participant groups can be predicted on the basis of normal retinotopic maps. Because each ratio was computed with age-matched control data, patient groups were combined to increase statistical power, but we still found no significant difference between the patient and control groups ($t = -0.81$, $P = 0.41$) or difference from unity in the ratio ($t = 0.14$, $P = 0.89$). Given the variance for patient and control groups in our ratio measure, a significant (at $P < 0.05$) difference in the ratio (of 0.23) would occur if the mean increase in cortical area compared with controls exceeded 160 mm² in each hemisphere. This is relatively small compared with the total area of primary visual cortex (~2,500 mm², see ref. 31). Our analysis provides strong, quantitative evidence that the extent of early visual cortical activity in the patient and control groups can be predicted on the basis of normal retinotopic maps.

2.3. Discussion

Seminal work on early visual deprivation in animals has shown that visual cortex can develop to devote more of its territory to intact visual input at the expense of its representation of impoverished input [32-35]. Such reallocation of cortical processing has also been demonstrated when early visual areas remap following congenital retinal lesions in human [6]. In adulthood, the cortex is less plastic, but even so, remapping of the visual cortical representation has been inferred on the basis of ectopic receptive fields in the lesion projection zone in animal models [7-13]. This effect is, however, rather modest and has been called into question recently [19]. Even so, recent studies of human adults [15, 26] suggest a large-scale extension of remapping of the type reported in animal models. We aimed to test explicitly whether or not visual cortical mapping changes following retinal lesions in adult humans. Our results indicate that it does not in three different ways.

First, we found that at the occipital pole, a cortical location that we are certain lies in the lesion projection zone, the signals observed in the patient group are no different than those found in the control group in whom we simulated a central scotoma. The spatially specific ROI analysis has been used extensively previously [15, 26] and has been shown to be highly sensitive to remapping [6]. Our result runs contrary to the view that the occipital pole in V1 takes on a new mapping to respond strongly to peripheral stimuli in a way that differs from normal. Previous work in this area has been limited to small numbers of affected individuals and control participants [15, 26]. Moreover, previous work has used task-stimulus combinations [15, 26] that produced widespread signals in the lesion projection zone in affected individuals, but less in

controls, most likely as a result of feedback from extrastriate cortex rather than remapping [18].

Second, our results indicate that throughout the lesion projection zone there are voxels with 'ectopic' receptive fields, but they are equally common and represent the same regions of visual field in both the patient and control group. This finding speaks more generally to the way in which ectopic receptive fields should be interpreted. Frequently, the existence of ectopic receptive fields has been taken as evidence for remapping [7-13]. That ectopic characteristics can be recorded from normally sighted controls challenges this notion, particularly in the context of fMRI research [15, 26]. Furthermore, we found that voxels with ectopic receptive fields were not restricted to the fringe of the lesion projection zone, where most electrophysiological measurements have been taken [7-13]. We propose, as have others [19, 30], that each cortical location (voxel) contains many neurons, the responses of which can be influenced by stimuli at a range of locations, but that the overall population response is heavily weighted to a modal location. If stimuli are presented only to locations that are a considerable distance from this modal location, the responses of the voxel will be weak, but could be driven by neurons with receptive fields that are large, displaced or large and displaced (see Supplementary information). We found that only 5–7% of voxels in the lesion projection zone could be classified as responsive, meaning that such signals could escape detection with conventional analyzes that average signals over the whole ROI. Notably, the probability of detecting a voxel with ectopic receptive fields is similar to the probability of detecting a neuron with ectopic receptive fields [13]. The ectopic signals in the lesion projection zone may originate from various sources, including feedback [36-38] and lateral connections [39, 40]. Task-specific feedback could elicit more activity in the lesion projections zone in the patient group than in the control group because of the absence of feedforward signals in the patient group [18]. Nevertheless, our results indicate that there is no need to invoke remapping as an explanation of responses in V1 of individuals with macular degeneration.

Third, our study performed for the first time, to the best of our knowledge, a quantitative assessment of the area of cortex driven by intact retina in individuals with retinal disease. The limited size of the patient and control groups coupled with the well-known large variance in visual cortical area across participants [31, 41] has prevented such an analysis in previous studies. Our results indicate that the representation of the visual field in V1 in affected individuals can be predicted accurately on the basis of normal retinotopic mapping and that no significant remapping or reorganization was evident. The measures that we derived are sensitive to relatively small changes in cortical maps (<6.5% of V1). This allows us to conclude that there is no remapping of visual cortex over the scale seen in those with congenital central retinal lesions [6]. If neural responses change over time in a very small strip of cortex on the edge of the lesion

projection zone, as some have proposed for animal models [7-13], this could escape detection with our analysis. However, we are principally concerned with a large-scale extension of this type of remapping, which we conclude does not exist in humans with central retinal lesions acquired in adulthood.

Consistent with our results, some previous studies on individuals have also found no evidence of remapping of primary visual cortex following retinal damage. A study using cytochrome oxidase to measure activity in an individual with macular degeneration and in macaque models of visual deafferentation found no long-term changes in primary visual cortical organization [42]. Using fMRI and retinotopic mapping methods similar to our own, no activation was found in the lesion projection zone in another individual with macular degeneration [14]. It has been proposed that this negative finding could be a result of the spared foveal vision that this individual exhibited [26]. With this in mind, we only included individuals with central lesions without foveal sparing. A combined fMRI and multi unit neurophysiological study in a carefully controlled animal model (homonymous retinal, but not macular, lesions induced in adult macaques) also showed no long-term changes that would indicate remapping of visual cortex [25]. A recent report of a case series of four individuals with age-related macular degeneration and four with the juvenile form also indicates limited reorganization, but explicit mapping experiments to assess group differences in cortical mapping quantitatively were not undertaken [43]. Having assessed retinotopic maps quantitatively in 16 affected individuals, we are confident that the absence of cortical remapping following retinal lesions in adulthood is a general finding.

The stability of visual organization that we observed may prove to be beneficial. Many of the most promising treatments aimed at restoring vision at the retinal level, such as anti-angiogenic injections, retinal prosthetics and stem-cell therapy, rely on the assumption that cortical circuitry remains largely unchanged. That we can detect no functional abnormality in the visual cortex of affected individuals is reassuring. However, the long-term removal of the principal input to visual cortex can give rise to a reduction in cortical volume [44]. It therefore remains to be seen if neurons in the lesion projection zone can process input normally once it is restored.

2.4. Methods

2.4.1. Participants

Eight individuals with stabilized AMD (ages 70–90) and a further eight with the JMD (Stargardt's

Disease) (ages 19–49) were recruited at the Moorfields Eye Hospital, London. All of the participants had established bilateral lesions for at least 1 year, with a central scotoma of less than 10-deg radius spanning the fovea and a stable preferred retinal locus. Visual field sensitivity and fixation ability for all participants were evaluated directly on the retina using an MP1 microperimeter (NIDEK). Location of the foveal center, preferred retinal locus coordinates and fixation stability (bi-variate contour ellipse area of fixation measurements) were determined using methods outlined in Timberlake *et al.* (2005). The mean diameter of the absolute retinal lesion was also computed from the microperimetry maps.

Five age-matched participants (ages 61–77) were recruited as controls for the AMD group and seven age-matched participants (ages 18–37) as controls for the JMD group. A further 12 control participants (ages 18–41) were recruited for a follow up experiment simulating retinal lesions. All control participants had normal or corrected-to-normal vision. Experimental protocols were approved by the London Multicenter Research Ethics Committee, Royal Holloway University of London Ethics Committee and the York Neuroimaging Center Science and Ethics Committee.

2.4.2. Scanning

fMRI and structural MRI data were acquired using 8-channel, phase-array head coils on either a Siemens Trio 3 Tesla at the Combined Universities Brain Imaging Center (Royal Holloway University of London), or on a GE 3-Tesla Signa HD Excite scanner at the York Neuroimaging Center (University of York).

For structural data, multi-average, whole-head T1-weighted anatomical volumes were acquired for each participant (1.0–1.13 mm^3 isotropic). Sequences used were 3D-MDEFT on the Siemens Trio or 3D-FSPGR on the GE Signa; imaging parameters in both sequences provide good gray-white contrast allowing the segmentation of anatomical data into gray and white matter, and subsequent visualization in volume and inflated cortical views. For functional data, gradient recalled echo pulse sequences were used to measure T2* BOLD data (repetition time = 3,000 ms, echo time = 30 ms, field of view = 28.8 cm, 128 × 128 matrix, 25 contiguous slices with 3-mm slice thickness). Images were read out using an EPI sequence. Magnetization was allowed to reach a steady state by discarding the first five volumes, an automated feature on both the scanners used.

2.4.3. Stimuli

Computer-generated visual stimuli were presented using a LCD projector (Sanyo PLC-XP40L at

Royal Holloway University of London, Dukane ImagePro 8942 at the University of York); stimuli were rear projected onto an acrylic screen situated in the bore of the MRI scanner, behind the participant's head. Participants viewed the stimuli via a mirror mounted on the head coil. Standard retinotopic mapping stimuli were used: a rotating wedge to map polar angle and an expanding annulus to map eccentricity [21-24]. Stimuli were generated with MATLAB (Mathworks) and controlled by MatVis (Neurometrics Institute). All stimuli were unmasked portions of a 100% contrast radial checkerboard with 8 rings and 24 radial segments on a mean gray background. Contrast reversal rate was 6 Hz. Each scan contained either the expanding annulus or rotating wedge. Projector throw was adjusted to stimulate the central 30 × 30 deg of visual angle (15-deg radius). The wedge stimulus was a 90-deg wedge of the flickering checkerboard, rotating about the center of the screen. The ring stimulus comprised three rings of the checkerboard that increased in angular extent (to a maximum of 15 deg). As it moved out from the center of the visual field; each ring was replaced by a new ring at the center as the existing ring approached the edge of the visual field. Both the wedge and ring stimuli had a period of 36 s and were repeated for seven full cycles.

2.4.4. Experiment 1

The standard expanding ring and rotating wedge stimuli described above were used. In addition, the position of a red fixation cross was manipulated to ensure that stimuli were centered on each individual participant's retina. For control participants, a red fixation cross was placed at the center of the stimulus. For the patient group, the cross was placed at each individual's stable preferred retinal locus, as measured by microperimetry. Four ring and four wedge datasets were typically collected for each participant during a single visit, except where participant discomfort or excessive movement required fewer scans. Only three scans were collected during the first session in two individuals with AMD and two individuals with JMD and only two scans were performed on one of the elderly controls. Scans were repeated in a second visit in most participants (20 out of 28). Four scans were again performed during the second session, except in two individuals with AMD (three scans) and four individuals with JMD (three had three scans, one had two scans).

2.4.5. Experiment 2

As in Experiment 1, standard retinotopic mapping stimuli were used. A red fixation cross was placed in the center of the stimulus. In separate scans, the 12 control participants were either shown the full stimulus (ring and wedge) or a masked version (of the rings) to simulate a central lesion. The mask consisted of a centrally placed static disk (7.5-deg radius) at mean luminance

gray such that the central portion of the visual field was constant throughout the scan (Figure 3). At least two scans were acquired for each condition. 10 of the 12 participants returned for a second scanning session on a separate date.

2.4.6. Data analysis

Data were analyzed using publicly available tools (http://white.stanford.edu/software/). Most data analysis was performed in Matlab using the mrVISTA toolbox. For anatomical data, the occipital cortices of acquired anatomical volumes were manually segmented into white and gray volumes (mrGray) [45]. The cortical surface (gray matter) of each subject was constructed and rendered in three dimensions from this segmentation using mrMesh/mrVista [46].

For function data, functional images were corrected for spatial inhomogeneity (mrInitRet). Motion correction was achieved using FSL's MCFLIRT [47]. Functional time series were high-pass filtered to remove baseline drifts. Percent signal change was computed for each voxel by dividing by and subtracting its mean amplitude value over time. The strength of stimulus-synchronized activity at each voxel was assessed using coherence. Coherence (C) is defined as the Fourier amplitude of the BOLD signal at the stimulus fundamental frequency (f_0 = 7) divided by the sum of amplitudes of frequency bins around the fundamental (refs. 18-25). The visual field representation of each voxel in cortex was derived by using the Fourier phase at the stimulus frequency, corresponding to the relative delay of the cyclical response [22, 48]. Functional data were averaged across scans for repeated scans (usually four) within a session for each individual. Functional data were manually aligned to the high-resolution anatomical volume and visualized in three dimensions.

ROIs were defined by an algorithm that gathered all contiguous gray matter in a circular patch 8 mm in diameter centered on a selected point in the high-resolution structural data. Three ROIs were chosen in each hemisphere of each participant based strictly on anatomical criteria: one at the occipital pole to represent activity from the fovea (the lesion projection zone in patients), one more anterior in the calcarine sulcus to represent activity from more peripheral retina (which is intact in patients) and one further anterior in the brain on the lateral aspect of the frontal lobes, serving as a control region in the first experiment. The mean coherence was calculated across voxels in an ROI for each individual and averaged across scans in each session. The fMRI noise distribution is not normal and may differ from one individual to the next or from one day to the next. To normalize the responses, the logarithm of the resulting coherence data was taken before averaging data across scanning sessions and across participants [49].

We assessed the degree to which the time series of any voxel in predefined regions of interest in the gray matter fitted a series of receptive field models as described previously [30].

Best fitting models were retained if they accounted for more than 15% of the variance of the time series of each voxel as in previous research [50]. The retained models were then averaged across voxels to give an overall measure of the population receptive field properties for each ROI. The data used for modeling were for the expanding ring stimuli only because it was for this presentation that we had a comparable number of runs across the participant groups, and it was the only stimulus that was masked to simulate retinal lesions. It is important to note that the candidate models were identical for all stimulus conditions and we did not restrict the receptive field models to any locations or sizes. The ROIs considered were calcarine sulcus, as specified above, and occipital pole, but in this case the diameter of occipital pole was 20 mm to gain increased sensitivity. Although the 20-mm diameter ROI might capture some signals from tissue receiving input from intact retina in patients with small retinal lesions, we ensured that for the control participants receiving full-field and simulated lesion stimulation, the occipital pole ROI only included voxels responding to eccentricities less than 7.5 deg when the full stimulus was presented.

We computed the area of primary visual cortex, Am, that exhibited activity above a coherence threshold of 0.30 for all participants in the patient and control groups in whom we simulated retinal lesions. Using responses to rotating wedge stimuli, we first identified the cortical representations of the upper and lower vertical meridians marking the boundaries of V1 in each participant (see Figure 7). We then defined a V1 ROI that was bounded by the extrapolation of the vertical meridians to the occipital pole and an anterior boundary that was just beyond the limit of activity in response to rotating wedges. This region was not restricted to those voxels that exceeded a specific threshold, but rather was a generously defined estimate of the extent of V1. Voxels in this V1 region that responded to rings at a coherence of greater than 0.30 were retained for the calculation of the area of significant activity in V1. The cortical area of activity was calculated using methods described previously [41]. We then computed a series of estimates of the predicted area of activation, Ap, based on the intact regions of visual field in patients (see Figure 7 for a schematic of the method). For each patient, we computed estimates from the corresponding group of age-matched controls (for example, for each individual with JMD we obtained seven estimates, one from each of the young control subjects). The mean predicted area, $\bar{A}p$, was then computed. We repeated these computations to obtain $\bar{A}p$ for controls with simulated central visual loss. Note that these computations were also based on the original data from the young control subjects. If remapping were to occur, Am will exceed $\bar{A}p$ and thus a ratio of the Am to $\bar{A}p$ will exceed unity. Using the ratio as our outcome measure is essential because it accounts for individual differences in retinal lesion size.

2.4.7. Statistical analyzes

Statistics were calculated using functions in the MATLAB Statistical Toolbox. A two-way analysis of variance was performed on the averaged expanding ring data (for each session) for the elderly group and for the young group. Visual status (patient versus control) and ROI (occipital pole versus calcarine sulcus versus control region) were the independent variables and log coherence (fMRI response magnitude) was the dependent variable. A repeated-measures ANOVA was performed on the data to test for significant differences within subjects across two sessions. To test for age effects, a three-way analysis of variance was performed on the combined data, with age, visual status and ROI as factors. All ANOVAs employed a Type III sum of squares calculation, and all subsequent multiple comparisons were corrected using the Tukey-Kramer criterion, as appropriate for an unbalanced design with unequal number of subjects across groups. A multiple regression analysis was performed on the patient data to determine the effects of lesion size and age on log coherence responses for each ROI. For the receptive field analysis, we used Student *t* tests to evaluate group differences in eccentricity and size of the receptive fields and sampling probability at each cortical location. Linear regression was used to assess the relationship between eccentricity and size of population receptive fields in the occipital pole ROI; 95% confidence intervals in the linear correlation parameters was estimated using jackknife resampling, taking into consideration the unequal number of points contributed by each participant. For the cortical area measures in Figure 7, group effects and deviations of the area ratio from unity were evaluated using *t* tests and ANOVAs, respectively.

2.5. Supplementary information

The population receptive field (pRF) method is a well-established technique for deriving the size and location of the region in the visual field that when stimulated elicits a BOLD response from a voxel [30]. The size and location of the pRF are derived by finding the best fitting Gaussian spatial response profile to explain the BOLD response to the visual stimuli presented. The term population is used to reflect the fact that each voxel will capture the responses of ~106 neurons. The neurons themselves exhibit a variety of receptive field properties [19, 51], which will contribute to the overall pRF estimate for a voxel. This variety of neural receptive field properties could lead to different pRF properties being recorded depending on the stimulus characteristics. We consider here the effect of our stimuli presented to controls on the pRF measurements.

First, consider a voxel that contains neurons with a variety of different receptive field properties (Supplementary Figure 1a). If a stimulus moves over a region of space that covers all

the neurons' receptive fields, all neurons should respond and contribute to the pRF estimate. This is true for the case when the stimulus is unmasked as indicated on the left of Supplementary Figure 1a. If, in contrast, a stimulus moves over a restricted region of space that covers a limited number of neurons' receptive fields, only a subset of neurons will respond and contribute to the pRF estimate. This is shown on the right of Supplementary Figure 1a for the masked condition we used. Therefore, the pRF estimates can change as a result of a stimulus change even when the underlying neural receptive field properties remain constant. In the case we illustrate, the pRF size will increase and the location will likely increase because only the most eccentric parts of a neuron's large receptive field will be stimulated. The results we report in the main body of our paper follow this qualitative pattern.

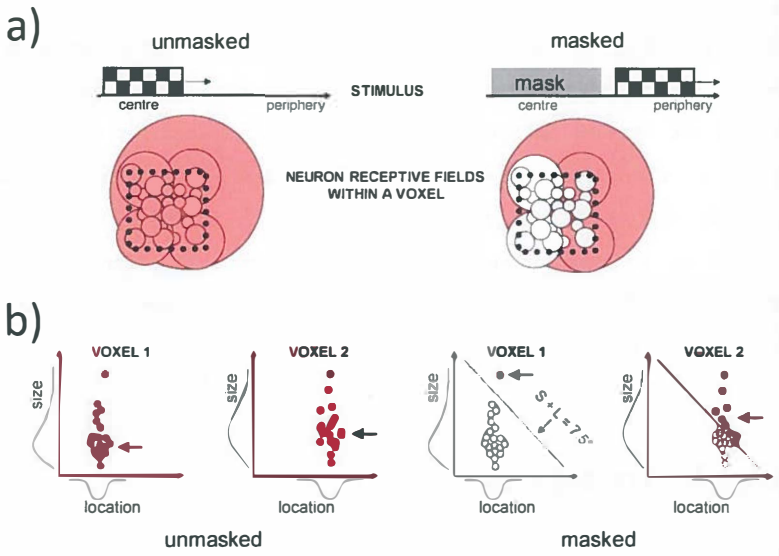

Supplementary Figure 1: A model of population receptive fields. **(a)** Top: A schematic of a visual stimulus (checkered block) moving through the visual field. On the left the stimulus moves through the whole visual field, whereas on the right a mask (shaded gray) occludes the central visual field simulating a central retinal lesion. **(a)** Bottom: A schematic showing the receptive fields of neurons within a voxel (the black dotted square illustrates the voxel boundary). The scale and alignment of the receptive fields match the positioning of the stimulus in the schematics above them. On the left the stimulus moves through the receptive field of all the neurons within the voxel (their activity indicated by red shading) and on the right it moves only through the receptive field of a few of the neurons (highlighted in red), because the stimulus is masked. **(b)** Plots of neuron receptive field location *vs.* size are presented for two voxels within the lesion projection zone. Voxel 1 captures neurons with more central receptive field locations than voxel 2. Active neurons are indicated in red. The pair of plots on the left and right illustrate the active neurons for the unmasked and masked conditions, respectively. In each plot the population receptive field size is indicated by the arrowheads and is based on the sum of all active neurons (red circles). The diagonal line in the two right hand plots is defined by the sum of size (S) and location (L) equating to 7.5° (the eccentricity of the mask).

We develop our framework further to assess quantitatively whether or not the pRF estimates we obtained are plausible, given the region of space that was stimulated in our control participants when the stimulus was masked. We now consider two voxels in the LPZ to show that it is the combination of neurons' receptive field size and location that will determine the pRF characteristics obtained under the masked condition. In Supplementary Figure 1b voxels 1 and 2 capture responses from neurons with central and more peripheral receptive field locations, respectively. These neural response properties would be accurately reflected by pRF measurements when the stimulus is unmasked (left pair of graphs). In the masked condition (right pair of plots), however, voxel 1 will only be driven by neurons with very large receptive fields (because the neurons' receptive field locations are central). A greater number of neurons with smaller receptive fields can contribute to the signal from voxel 2 due to their more eccentric receptive field locations. Two voxels are considered to emphasize that it is the sum of the size and location of the neurons' receptive fields that need to exceed the smallest stimulated eccentricity (7.5°) for any voxel to potentially exhibit visually driven activity. In the masked condition, the sum of the pRF sizes and locations exceeded 7.5° in 93% of responsive voxels in the LPZ. Based on a simple framework of neural properties we can explain the pRF characteristics in the LPZ of controls and patients without invoking reorganization of the retinotopic map in visual cortex.

Acknowledgments

We would like to thank all of our participants. We thank Edward Silson for constructive discussion of the manuscript. We are also grateful to the Medical Research Council for funding this study (G0401339). K.V.H. and F.W.C. were supported by a grant from Stichting Nederlands Oogheelkundig Onderzoek and by European Union grants #043157 (Syntex) and #043261 (Percept). A.T., G.S.R. and M.D.C. also received financial support from the Department of Health through an award made by the National Institute for Health Research to Moorfields Eye Hospital National Health Service (NHS) Foundation Trust and University College London Institute of Ophthalmology for a Specialist Biomedical Research Centre for Ophthalmology. The views expressed in this publication are those of the authors and not necessarily those of the NHS, the National Institute for Health Research, the Department of Health or the EU commission.

References

[1] Wandell, B.A., Dumoulin, S.O. & Brewer, A.A. Visual field maps in human cortex. Neuron 56, 366–383 (2007).

[2] Morland, A.B., Baseler, H.A., Hoffmann, M.B., Sharpe, L.T. & Wandell, B.A. Abnormal retinotopic representations in human visual cortex revealed by fMRI. Acta Psychol. (Amst.) 107, 229–247 (2001).

[3] Hoffmann, M.B., Tolhurst, D.J., Moore, A.T. & Morland, A.B. Organization of the visual cortex in human albinism. J. Neurosci. 23, 8921–8930 (2003).

[4] Muckli, L., Naumer, M.J. & Singer, W. Bilateral visual field maps in a patient with only one hemisphere. Proc. Natl. Acad. Sci. USA 106, 13034–13039 (2009).

[5] Levin, N., Dumoulin, S.O., Winawer, J., Dougherty, R.F. & Wandell, B.A. Cortical maps and white matter tracts following long period of visual deprivation and retinal image restoration. Neuron 65, 21–31 (2010).

[6] Baseler, H.A. *et al.* Reorganization of human cortical maps caused by inherited photoreceptor abnormalities. Nat. Neurosci. 5, 364–370 (2002).

[7] Kaas, J.H. *et al.* Reorganization of retinotopic cortical maps in adult mammals after lesions of the retina. Science 248, 229–231 (1990).

[8] Heinen, S.J. & Skavenski, A.A. Recovery of visual responses in foveal V1 neurons following bilateral foveal lesions in adult monkey. Exp. Brain Res. 83, 670–674 (1991).

[9] Chino, Y.M., Kaas, J.H., Smith, E.L. III, Langston, A.L. & Cheng, H. Rapid reorganization of cortical maps in adult cats following restricted deafferentation in retina. Vision Res. 32, 789–796 (1992).

[10] Gilbert, C.D. & Wiesel, T.N. Receptive field dynamics in adult primary visual cortex. Nature 356, 150–152 (1992).

[11] Darian-Smith, C. & Gilbert, C.D. Topographic reorganization in the striate cortex of the adult cat and monkey is cortically mediated. J. Neurosci. 15, 1631–1647 (1995).

[12] Kaas, J.H. Sensory loss and cortical reorganization in mature primates. Prog. Brain Res. 138, 167–176 (2002).

[13] Giannikopoulos, D.V. & Eysel, U.T. Dynamics and specificity of cortical map reorganization after retinal lesions. Proc. Natl. Acad. Sci. USA 103, 10805–10810 (2006).

[14] Sunness, J.S., Liu, T. & Yantis, S. Retinotopic mapping of the visual cortex using functional magnetic resonance imaging in a patient with central scotomas from atrophic

macular degeneration. Ophthalmology 111, 1595–1598 (2004).

[15] Baker, C.I., Peli, E., Knouf, N. & Kanwisher, N.G. Reorganization of visual processing in macular degeneration. J. Neurosci. 25, 614–618 (2005).

[16] Schumacher, E.H. *et al.* Reorganization of visual processing is related to eccentric viewing in patients with macular degeneration. Restor. Neurol. Neurosci. 26, 391–402 (2008).

[17] Cowey, A. & Walsh, V. Magnetically induced phosphenes in sighted, blind and blindsighted observers. Neuroreport 11, 3269–3273 (2000).

[18] Masuda, Y., Dumoulin, S.O., Nakadomari, S. & Wandell, B.A. V1 projection zone signals in human macular degeneration depend on task, not stimulus. Cereb. Cortex 18, 2483 2493 (2008).

[19] Wandell, B.A. & Smirnakis, S.M. Plasticity and stability of visual field maps in adult primary visual cortex. Nat. Rev. Neurosci. 10, 873–884 (2009).

[20] Masuda, Y. *et al.* Task-dependent V1 responses in human retinitis pigmentosa. Invest. Ophthalmol. Vis. Sci. 51, 5356–5364 (2010).

[21] DeYoe, E.A. *et al.* Mapping striate and extrastriate visual areas in human cerebral cortex. Proc. Natl. Acad. Sci. USA 93, 2382–2386 (1996).

[22] Engel, S.A., Glover, G.H. & Wandell, B.A. Retinotopic organization in human visual cortex and the spatial precision of functional MRI. Cereb. Cortex 7, 181–192 (1997).

[23] Engel, S.A. *et al.* fMRI of human visual cortex. Nature 369, 525 (1994).

[24] Sereno, M.I. *et al.* Borders of multiple visual areas in humans revealed by functional magnetic resonance imaging. Science 268, 889–893 (1995).

[25] Sereno, M.I. *et al.* Borders of multiple visual areas in humans revealed by functional magnetic resonance imaging. Science 268, 889–893 (1995).

[26] Baker, C.I., Dilks, D.D., Peli, E. & Kanwisher, N. Reorganization of visual processing in macular degeneration: replication and clues about the role of foveal loss. Vision Res. 48, 1910–1919 (2008).

[27] Crossland, M.D., Morland, A.B., Feely, M.P., von dem Hagen, E. & Rubin, G.S. The effect of age and fixation instability on retinotopic mapping of primary visual cortex. Invest. Ophthalmol. Vis. Sci. 49, 3734–3739 (2008).

[28] Parrish, T.B., Gitelman, D.R., LaBar, K.S. & Mesulam, M.M. Impact of signal-to-noise on functional MRI. Magn. Reson. Med. 44, 925–932 (2000).

[29] Cavanaugh, J.R., Bair, W. & Movshon, J.A. Nature and interaction of signals from the receptive field center and surround in macaque V1 neurons. J. Neurophysiol. 88, 2530 2546 (2002).

[30] Dumoulin, S.O. & Wandell, B.A. Population receptive field estimates in human visual

cortex. Neuroimage 39, 647–660 (2008).

[31] Andrews, T.J., Halpern, S.D. & Purves, D. Correlated size variations in human visual cortex, lateral geniculate nucleus, and optic tract. J. Neurosci. 17, 2859–2868 (1997).

[32] Hubel, D.H. & Wiesel, T.N. The period of susceptibility to the physiological effects of unilateral eye closure in kittens. J. Physiol. (Lond.) 206, 419–436 (1970).

[33] Hubel, D.H., Wiesel, T.N. & LeVay, S. Plasticity of ocular dominance columns in monkey striate cortex. Phil. Trans. R. Soc. Lond. B 278, 377–409 (1977).

[34] Le Vay, S., Wiesel, T.N. & Hubel, D.H. The development of ocular dominance columns in normal and visually deprived monkeys. J. Comp. Neurol. 191, 1–51 (1980).

[35] Horton, J.C. & Hocking, D.R. Timing of the critical period for plasticity of ocular dominance columns in macaque striate cortex. J. Neurosci. 17, 3684–3709 (1997).

[36] Williams, M.A. *et al.* Feedback of visual object information to foveal retinotopic cortex. Nat. Neurosci. 11, 1439–1445 (2008).

[37] Angelucci, A. & Bullier, J. Reaching beyond the classical receptive field of V1 neurons: horizontal or feedback axons? J. Physiol. (Paris) 97, 141–154 (2003).

[38] Angelucci, A. & Sainsbury, K. Contribution of feedforward thalamic afferents and corticogeniculate feedback to the spatial summation area of macaque V1 and LGN. J. Comp. Neurol. 498, 330–351 (2006).

[39] Lund, J.S. Anatomical organization of macaque monkey striate visual cortex. Annu. Rev. Neurosci. 11, 253–288 (1988).

[40] Gilbert, C.D. & Wiesel, T.N. Morphology and intracortical projections of functionally characterised neurones in the cat visual cortex. Nature 280, 120–125 (1979).

[41] Dougherty, R.F. *et al.* Visual field representations and locations of visual areas V1/2/3 in human visual cortex. J. Vis. 3, 586–598 (2003).

[42] Horton, J.C. & Hocking, D.R. Monocular core zones and binocular border strips in primate striate cortex revealed by the contrasting effects of enucleation, eyelid suture, and retinal laser lesions on cytochrome oxidase activity. J. Neurosci. 18, 5433–5455 (1998).

[43] Liu, T. *et al.* Incomplete cortical reorganization in macular degeneration. Invest. Ophthalmol. Vis. Sci. 51, 6826–6834 (2010).

[44] Boucard, C.C. *et al.* Changes in cortical grey matter density associated with long-standing retinal visual field defects. Brain 132, 1898–1906 (2009).

[45] Teo, P.C., Sapiro, G. & Wandell, B.A. Creating connected representations of cortical gray matter for functional MRI visualization. IEEE Trans. Med. Imaging 16, 852–863 (1997).

[46] Wandell, B.A., Chial, S. & Backus, B.T. Visualization and measurement of the cortical surface. J. Cogn. Neurosci. 12, 739–752 (2000).

[47] Jenkinson, M., Bannister, P., Brady, M. & Smith, S. Improved optimization for the robust and accurate linear registration and motion correction of brain images. Neuroimage 17, 825–841 (2002).

[48] Wandell, B.A., Brewer, A.A. & Dougherty, R.F. Visual field map clusters in human cortex Phil. Trans. R. Soc. Lond. B 360, 693–707 (2005).

[49] Lewis, S.M. *et al.* Logarithmic transformation for high-field BOLD fMRI data. Exp. Brain Res. 165, 447–453 (2005).

[50] Winawer, J., Horiguchi, H., Sayres, R.A., Amano, K. & Wandell, B.A. Mapping hV4 and ventral occipital cortex: the venous eclipse. J. Vis. 10, 1–22 (2010).

[51] Cavanaugh, J.R., Bair, W. & Movshon, J.A. Nature and interaction of signals from the receptive field center and surround in macaque V1 neurons. J Neurophysiol 88, 2530-46 (2002).

Chapter 3

Population receptive field dynamics in human visual cortex

Based on: Haak KV, Cornelissen FW, Morland AB (2012) Population receptive field dynamics in human visual cortex. **PLoS One** 7(5): e37686.

Abstract

Seminal work in the early nineties revealed that the visual receptive field of neurons in cat primary visual cortex can change in location and size when artificial scotomas are applied. Recent work now suggests that these single neuron receptive field dynamics also pertain to the neuronal population receptive field (pRF) that can be measured in humans with functional magnetic resonance imaging (fMRI). To examine this further, we estimated the pRF in twelve healthy participants while masking the central portion of the visual field. We found that the pRF changes in location and size for two differently sized artificial scotomas, and that these pRF dynamics are most likely due to a combination of the neuronal receptive field position and size scatter as well as modulatory feedback signals from extrastriate visual areas.

3.1. Introduction

Visual neurons respond to a limited part of the visual field. This portion of the visual field is known as the receptive field. To infer the distribution of receptive field location and size across human visual cortex, functional magnetic resonance imaging (fMRI) can be used [1-6]. Due to limited spatial resolution, however, fMRI can only capture the central tendency of many neuronal receptive fields. Hence, the region of visual space that stimulates a voxel is referred to as the population receptive field (pRF) [7].

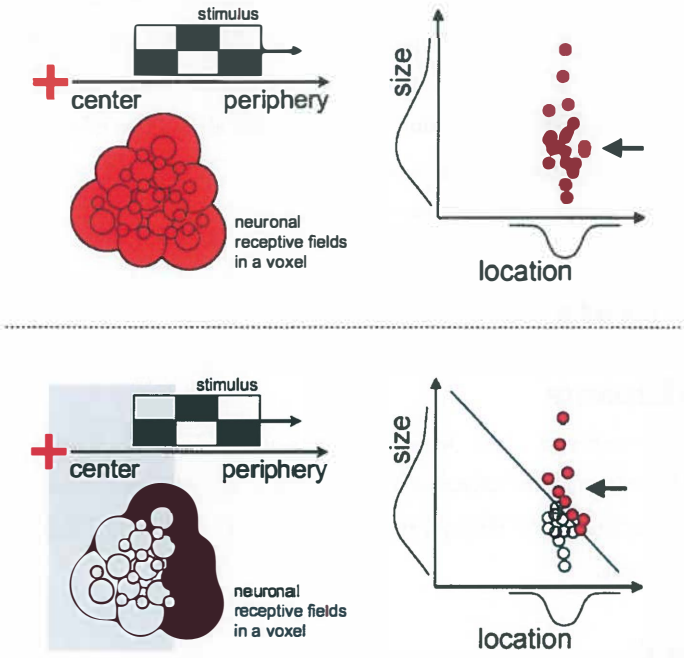

Figure 1. How changed population receptive fields may emerge from partially stimulating the visual field. See also [8, 14]. If a stimulus (the checkered block) moves over a region of visual space that covers all neurons' receptive fields (top row), all neurons should respond and contribute to the pRF estimate (as indicated by red shading). If, in contrast, a stimulus moves over a more restricted region of visual space that covers a more limited number of neurons', only a subset of neurons will respond and contribute to the pRF estimate. This is true in the masked conditions we used (bottom row). Therefore, the pRF estimates can change as a result of a stimulus change even when the underlying neuronal receptive field properties remain constant. When a central mask is applied, it is also true that neuronal receptive fields contributing to the pRF estimate have, on average, more eccentric locations in the visual field than those that were silenced by masking the stimulus. This is why more eccentric pRF estimates emerge. Finally, as illustrated by the pair of plots on the right, larger pRF estimates (indicated by the arrowheads) also emerge because the active neurons (red circles) during the masked conditions have receptive field that are more likely to be larger. The diagonal line in the lower right plot corresponds to the sum of the receptive field size and location equating to the size of the mask.

In previous work [8], we studied the mean pRF in the cortical lesion projection zone of patients with macular degeneration (MD). Compared with age-matched controls, we found that in MD patients the mean pRF was larger and also corresponded to a more peripheral location in the visual field. This result would have been taken as evidence for cortical reorganization, if it were not that the same changes occurred when the effect of an artificial scotoma was examined in a group of healthy participants. Rather, it seemed that central pRFs can be displaced and enlarged simply by silencing central visual field stimulation (Figure 1).

In the present study, we further examined these pRF dynamics for two differently sized artificial scotomas, asking whether the effect can be traced down to the level of single pRFs and what neuronal mechanisms could be causing it. For two differently sized artificial scotomas we found that some voxels in retinotopic representations of the center of the visual field also responded when more peripheral locations were stimulated alone. The effects we document are most likely due to a combination of the neuronal receptive field position and size scatter as well as modulatory feedback signals from extrastriate visual cortex.

3.2. Methods

3.2.1. Participants

We report on measurements from twelve subjects (ages 18-41) with normal or corrected-to-normal vision. All subjects gave informed written consent according to procedures that followed the tenets of the Declaration of Helsinki and were approved by the York Neuroimaging Research Governance committee.

3.2.2. Stimuli

The visual stimuli (Figure 2) consisted of expanding ring apertures in a mean luminance gray background that exposed a high contrast (100%) flickering radial checkerboard pattern. The expanding ring aperture comprised three rings of the checkerboard pattern that increased in angular extent to a maximum of 15°. A new ring at the center replaced each ring as it approached the outer border of the stimulated region of the visual field. During all experimental conditions, the expanding ring stimuli had a period of 36s and were repeated for seven full cycles. In separate scans, the subjects were either shown the full stimulus or masked versions. The masks consisted of a centrally placed static disk at mean luminance gray so that the central portion of the visual field was constant throughout the scan. Two masks were used such that the constant portion of the visual field subtended either a 5.0° or 7.5° radius. During all experimental conditions,

participants were asked to fixate a red fixation cross that was placed at the center of the screen. This fixation cross, which was visible throughout each scan, ensured that participants maintained fixation in each condition. The visual stimuli were generated with Matlab (Mathworks Inc.) and controlled by MatVis (Neurometrics Institute). The stimuli were presented using an ImagePro 8942 LCD projector and rear projected onto a translucent acrylic screen situated in the bore of the MRI scanner, behind the subject's head. Subjects viewed the stimuli via a mirror mounted on the head coil.

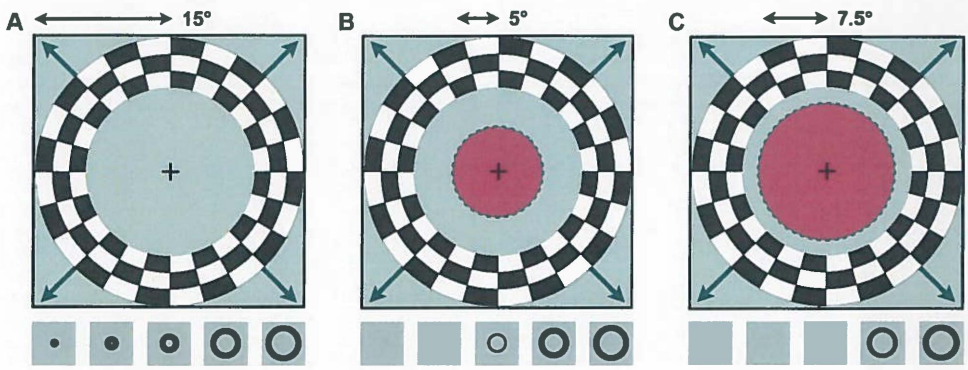

Figure 2. Illustration of the expanding ring stimuli in each experimental condition. (**a**) Stimulus schematic of the full-field condition. The maximum stimulus radius was 15°. The bottom panels show how the stimulus changes over time. (**b, c**) Stimulus schematic of the 5° and 7.5° masked conditions, respectively (masks are shown in opaque red). Bottom panels indicate the resulting stimulus sequence. For clarity, only 5 of the 12 ring positions are shown.

3.2.3. Magnetic resonance imaging

Functional and structural MRI data were acquired using an 8-channel, phase-array head coil on a GE 3-Tesla Signa HD Excite scanner. For structural data, multi average, whole-head T1 weighted anatomical volumes (1×1×1.13 mm^3) were acquired for each subject. For functional data, gradient-echo pulse sequences were used to measure the T2* BOLD signal (TR/TE = 3000/30ms, FOV = 28.8cm, 128×128 matrix, 25 contiguous slices with 3mm slice thickness). Images were read out using an EPI sequence. Magnetization was allowed to reach a steady state by discarding the first five volumes. For each of six scans (two for each condition), these first five volumes were followed by the acquisition of a further 84 volumes.

3.2.4. Data preprocessing

Data were analyzed using the mrVISTA toolbox (http://white.stanford.edu/software) and FSL (http://www.frmib.ox.ac.uk/fsl). For anatomical data, the occipital cortices in the acquired

anatomical volumes were manually segmented into white and gray volumes. For functional data, the images were corrected for spatial inhomogeneity. Motion correction was performed and functional time series were high-pass filtered to remove baseline drifts, after which they were converted to percent signal change (i.e., $\Delta\% = 100 \cdot [x / \text{mean}(x) - 1]$).

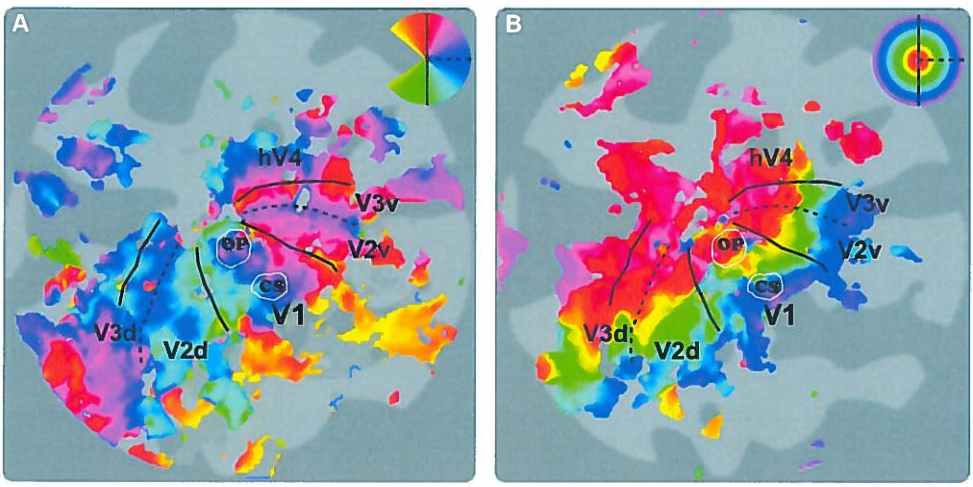

Figure 3. ROI locations on a flattened cortical surface of one of the participants. (**a**) The polar angle maps are indicative to the locations of the early visual areas. (**b**) The eccentricity maps are indicative to the centrals and peripheral visual field representations. The occipital pole (OP) ROIs are located in V1 at the border between the calcarine sulcus and the occipital pole, a region that responds to stimuli presented to the center of the visual field. The calcarine sulcus (CS) ROI is also located in V1, but more anteriorly in the calcarine sulcus, which responds to more peripherally presented stimuli. Insets indicate the color maps that define the visual field representation. Solid black lines indicate the representation of the vertical meridian, and dashed black lines indicate the representation of the horizontal meridian. Solid white lines indicate the borders of the ROIs.

3.2.5. Regions-of-interest (ROI) definition

ROIs were defined using an algorithm that gathered all contiguous gray matter in a circular patch centered on a selected point in the high-resolution anatomical data. Based on anatomical criteria, two ROIs were chosen in each hemisphere of each subject: the OP ROI at the border between the calcarine sulcus and the occipital pole, a region in the primary visual cortex (V1) that represents activity from central retina, and the CS ROI located more anteriorly in the calcarine sulcus that represents V1 activity from more peripheral retina (Figure 3). Both ROIs were 20 mm diameter in all participants. To exclude the possibility that the OP ROIs included extrastriate cortex, V1 was defined in both hemispheres from separate scans that included (unmasked) rotating wedge-stimuli (note that the wedge data were not included in any other analyzes; see ref

[8] for a description of the wedge-stimuli). All voxels that did not fall within V1 were excluded from the ROIs.

3.2.6. Population receptive field modeling

Population receptive field (pRF) modeling was performed to assess the degree to which the time series of the voxels in the ROIs fitted a series of circular symmetric two-dimensional Gaussian receptive field models [6]. Crucially, all experimental conditions were analyzed based on model predictions that assumed full-field stimulation. That is, we did not constrain the potential pRFs to respond only to stimulated parts of the visual field. This is essential if we wish to compare voxel response properties under different conditions; we can change only one thing – the stimulus – while keeping the analysis procedure constant. As in previous work [6,8,9], best fitting models were retained if they accounted for more than 15% of the variance of the time series. Given that the time-series consisted of 84 time-frames, this threshold corresponded to a significance level of $p < 0.001$ (uncorrected) [10]. This procedure was carried out for each condition separately. Importantly, we ensured that for the occipital pole ROIs our subsequent analyzes only included voxels for which the pRF center eccentricity was less than 5.0° and 7.5° when the full stimulus was presented, respectively.

3.2.7. Estimating temporal phase and duty-cycle

To verify the pRF modeling approach, a one-dimensional variant of the two-dimensional pRF modeling method was also performed [4]. In this analysis the temporal phase of the time-series was computed for each individual voxel whose best-fitting 2D pRF model explained more than 15% of the time-series variance by finding the phase of their fundamental Fourier components. Furthermore, in the case of ring-stimuli, the spread of the circular symmetric Gaussian pRF model is proportional to the duty-cycle of the time-series. This duty-cycle was estimated by generating a number of time-series predictions from a set of square waves with 100 different phase delays (equally spaced between 0-2π) and 100 different duty-cycles (equally spaced between 0-100%). As in the pRF modeling approach, the time-series predictions were convolved with a two-gamma hemodynamic response function. The best-fitting duty-cycle was then found by minimizing the residual sum of squares between the fMRI and the predicted time-series.

3.2.8. Statistical analyzes

Statistics were calculated using functions of the Matlab Statistical Toolbox. Taking into consideration the unequal number of points contributed by each subject, all reported ranges correspond to the 95% confidence intervals of the jackknifed (leave one subject out) mean. This

procedure allowed us to capture the between-subject variance without completely disregarding the between voxel variance within subjects.

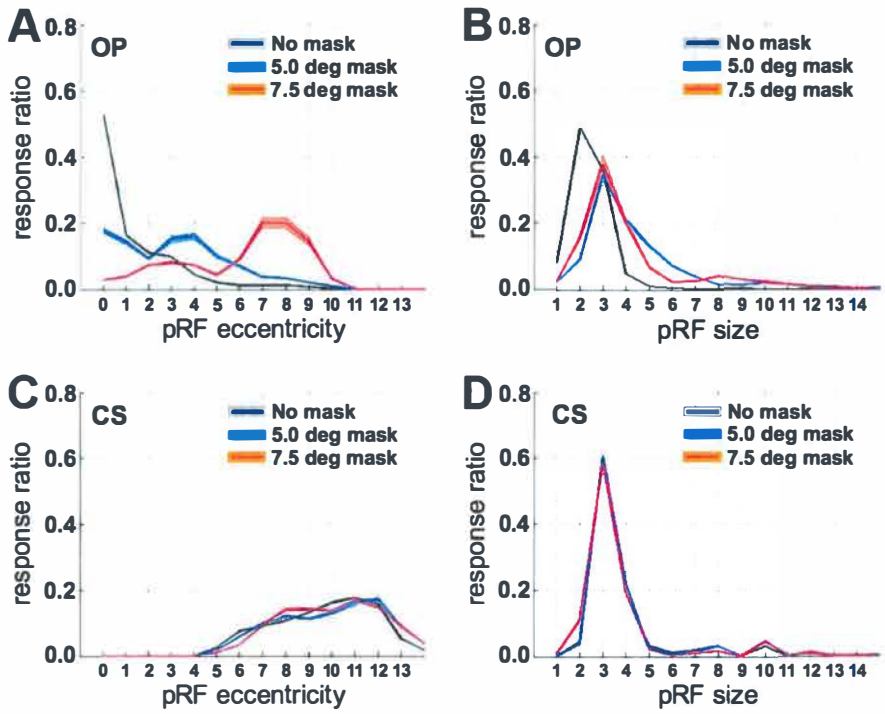

Figure 4 Response distributions for the unmasked and masked conditions. A. Response ratio (i.e., the number of responsive voxels per bin divided by the total number of responsive voxels) versus pRF eccentricity for the unmasked and masked conditions for the OP region-of interest. **B.** Response ratio versus pRF size for the unmasked and masked conditions in the OP region-of interest. **C.** Response ratio versus pRF location for the unmasked and masked conditions in the CS region-of interest. **D.** Response ratio versus pRF size for the unmasked and masked conditions in the CS region-of interest. Note that in the masked conditions the pRFs shift away from their original location in the OP regions (**A**) but not in the CS region (**C**). The pRFs in the OP regions are also larger for the masked conditions in the OP regions (**B**), but not in the CS region (**D**). Gray, blue and orange shadings indicate the jackknifed 95% confidence interval for the unmasked and the two masked conditions, respectively.

3.3. Results

We first evaluated the response distributions of the pRF location and size for the unmasked and masked conditions (Figure 4). In the OP region, the full stimulus resulted in central pRFs that were small. In the CS region, the full stimulus led to peripheral pRFs that were large. When the stimulus was masked, however, the response distributions of pRF location and size in the OP region shifted towards greater eccentricities and larger sizes, respectively. These shifts and

increases occurred for both masks, but not for the CS region. Of note is also the pRF size in the OP region for the full stimulus, which is rather large compared to some of the previous studies using the same pRF modeling method [5,6]. This feature has also been observed by Winawer et al. [9] and may be due to B_0 field distortions related to the presence of several dural sinuses, voxel size differences, or the fact that the ring apertures were large relative to the receptive field sizes in V1. In the following, we assume that these limitations apply equally to all experimental conditions.

In the OP region, far fewer voxels had a reliable pRF when the stimulus was masked compared to when it was not (no mask: 56%, 5° mask: 27%, 7.5° mask: 8 %). Therefore, it is possible that the distribution shifts in Figure 4 resulted from sampling, in the masked conditions, only those voxels that had large and eccentric pRFs in the first place. To avoid such sampling bias, we restricted all further analyzes to voxels that responded above threshold (more than 15% variance explained) in both the unmasked and at least one of the two masked conditions. For these 'matched' voxels we found that there were significant shifts in pRF location of 1.45° ± 0.08° and 4.13° ± 0.2° for the 5.0° and 7.5° masks, respectively. Significant increases in pRF size were also found; 1.43° ± 0.05° and 0.92° ± 0.1° for the 5.0° and 7.5°masks, respectively. Similar results were also obtained using a higher threshold for the variance explained by the model. For all voxels that responded in both masked and unmasked conditions explaining more than 20% of time-series variance, the location changes were 1.44° ± 0.07° (5.0° mask) and 4.19° ± 0.2° (7.5° mask), and the size changes were 1.13° ± 0.03° (5.0° mask) and 0.39° ± 0.1° (7.5° mask). Therefore, our results do not appear to be crucially dependent on a specific statistical threshold.

Given the pRF changes observed, differences should be clearly visible in the individual time-series and their model fits. That is, a shift in pRF position should be visible as a phase-shift in the individual time-series, and an increased pRF size should be visible as broader peaks corresponding to longer activation. Figure 5 shows two examples of the time-series and model fits during the masked and unmasked conditions for the same voxel. The predicted time-series generated by the best-fitting models in this example explained 63% for the unmasked condition, and 50% and 43% for the masked conditions. As expected, compared with the time-series for the unmasked condition, the peaks in the masked conditions were shifted in time and corresponded to longer activation durations.

That the voxel time-series in Figure 5 exhibited a phase-shift and broader peaks when the stimulus was masked also suggests that the observed pRF changes did not emerge from the particulars of the pRF modeling approach. In the present experiment we basically fitted a two-dimensional pRF model to a one-dimensional data set (eccentricity only). It could therefore be argued that the pRF changes reflect unstable model fits due to over-fitting. Hence, we also

assessed whether the pRF changes could be derived using a one-dimensional variant of the pRF modeling method that estimates the phase and duty-cycle of the voxel time-series [4]. Indeed, for all voxels that responded above threshold in both the unmasked condition and at least one of the two masked conditions, we found that the phase of the time-series shifted from 0.67 to 1.51 radians for the 5.0° mask, and from 1.08 to 2.82 radians for the 7.5° mask. Converted to eccentricity these values corresponded to 1.59°, 3.61°, 2.57° and 6.72°, respectively. With regard to verifying the observed pRF size change, the estimated duty-cycle also showed a substantial increase as a result of the two masks: for the 5° mask the duty-cycle increased from 42% to 45%, and for the 7.5° mask the duty-cycle increased from 44% to 49%. Of note is also that these one-dimensional duty-cycle estimates are very similar to those reported previously. For example, based on a similar ring-only stimulus prescription, Smith et al. [4] found that the duty-cycle in V1 ranged between 40% and 60% for eccentricities spanning the central 10 degrees of visual angle.

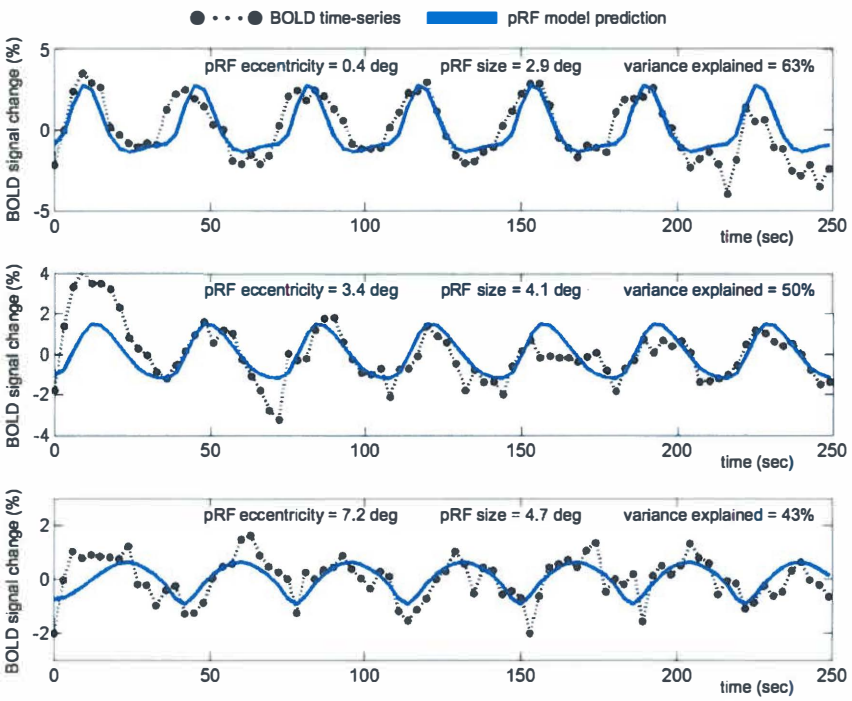

Figure 5. Examples of the model fits. Model fits to BOLD time-series are shown for a voxel in the OP region that explained more than 15% of the time-series variance in the unmasked (top) and both of the two masked conditions (middle and bottom). The BOLD time-series show increasingly broader peaks and more pronounced phase-shifts corresponding to an increased estimate of the pRF size and location, respectively. Note that the y-axes in the three panels have different scales.

Figure 6 illustrates further the relationship between the pRF location estimates obtained from the occipital pole in the unmasked and both masked conditions. For most voxels the pRF locations fall above the black dotted line of unit slope, indicating a shift to more eccentric locations as a result of the mask. However, there are also voxels that exhibit pRF locations that lie well within the masked zone and it is not clear whether these voxels are genuinely driven by peripheral stimuli. To examine this, we tested the prediction that the sum of pRF location and size exceeded the radius of the masks. The gray dots in Figures 6 indicate that the vast majority of voxels (81% for the 5.0° mask and 94% for the 7.5° mask) responded to stimulus positions beyond the masked region, given each voxel's combination of the pRF location and size. Importantly then, the pRF estimates for the voxels in the occipital pole indicate that voxels are genuinely visually driven by eccentric stimuli. In the unmasked condition only 37% of the pRFs of the matched voxels extended beyond 5° and 32% beyond 7.5°, indicating again that it was the mask that caused the peripheral responses in the occipital pole regions.

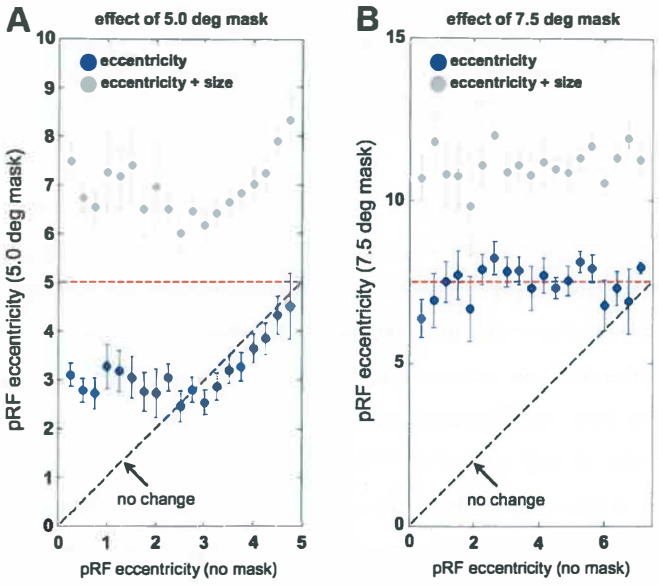

Figure 6. The effect of masking the central portion of the visual field on pRF eccentricity. A. The population receptive field (pRF) eccentricity within the OP ROI derived for the 5.0° masked condition as function of the same measure derived from the unmasked condition is plotted on blue. The sum of pRF location and size for the 5.0° masked condition are also plotted as a function of pRF location for the unmasked condition (gray). **B.** The same plot as in **A** but for the 7.5° masked condition. The dashed black lines indicate the predicted result if voxels that responded in the same way in both conditions. The dashed red lines in each plot show the borders of the masks. Error-bars indicate the standard error. Note that the axes in the two panels have different scales.

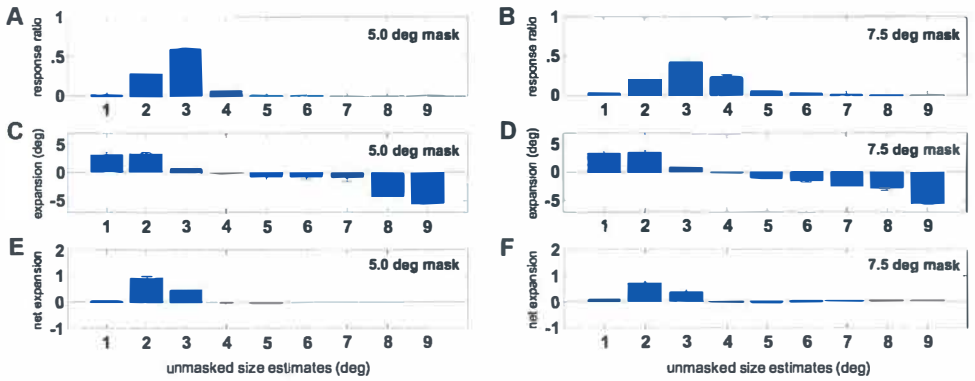

Figure 7. Response and expansion distributions across the different pRF sizes. A. Response distribution of pRF sizes estimated for the unmasked conditions for voxels that responded in the 5.0° masked condition as well as the full-field condition. **B.** Response distribution of pRF sizes estimated for the unmasked conditions for voxels that responded in the 7.5° masked condition as well as the full-field condition. **C.** Mean pRF expansion for voxels that responded in the 5.0° masked condition as well as the full-field condition. **D.** Mean pRF expansion for voxels that responded in the 7.5° masked condition as well as the full-field condition. **E.** The net effect of the change in pRF size, as measured by the product of the mean change and the number of voxels per bin induced by the 5.0° mask. **F.** The net effect of the change in pRF size, as measured by the product of the mean change and the number of voxels per bin induced by the 7.5° mask. The error-bars for each bin are jackknife estimates of the 95% confidence interval.

There are two relationships between pRF size and location that should emerge if the pRF parameters are capturing information about neural responses. The first simply reflects what has already been demonstrated in previous pRF analyzes and is well known from electrophysiological measurements, namely, that in the unmasked condition there should be a positive relationship between the receptive field size and location. The second captures the feature that if a region of cortex normally encodes a small eccentricity, it would require a large receptive field to be driven by an eccentric stimulus and vice versa. This should lead to a negative relationship between receptive field size and location in the occipital pole region of interest under masked conditions. Indeed, for both the 5° mask and 7.5° the correlation coefficient between the pRF eccentricity and size changed from positive (r = 0.248 ± 0.01; r = 0.421 ± 0.02) to negative (r = -0.006 ± 0.02; r = -0.416 ± 0.02).

While we report an overall increase in pRF size in masked conditions, our data also revealed decreases in size for some voxels. In order to establish the source of such decreases, we examined the change in sizes of pRFs for all voxels binned by the receptive field size estimates for the unmasked condition (Figure 7). First, the pRF size frequency (response ratio) distributions are given for the unmasked condition (Figures 7A and 7B). The bar graphs in Figures 7C and 7D clearly show that increases in pRF size are observed for voxels that recorded

small (under 4°) receptive field sizes in the unmasked condition. However, the voxels that had large pRFs (over 4°) in the unmasked condition exhibited decreases in pRF size. It is also clear that large (over 4°) pRFs are rather uncommon (Figures 7A and 7B). Because the number of voxels with large pRFs is small, the net change (frequency × change) is an expansion (Figures 7E and 7F).

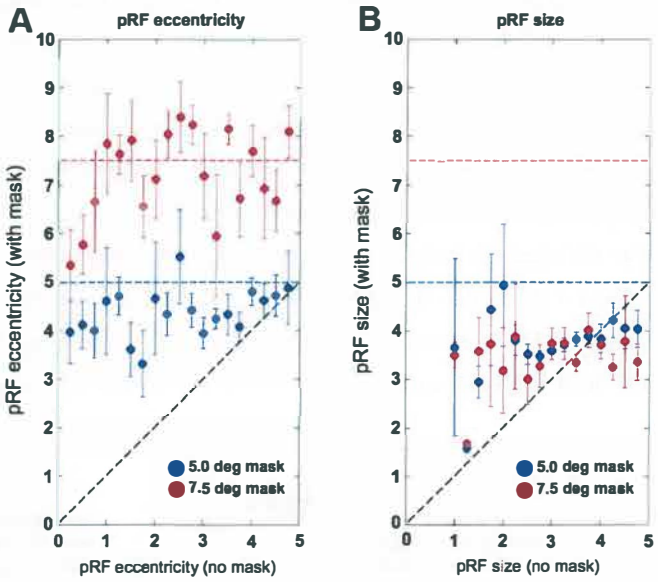

Figure 8. Effect of masking the central visual field for voxels that responded in all three conditions. A. The pRF eccentricity within the OP ROI derived for the 5.0° (blue) and 7.5° (red) masked conditions as function of the same measure derived from the unmasked condition. **B.** The pRF size within the OP ROI derived for the 5.0° (blue) and 7.5° (red) masked conditions as function of the pRF size derived from the unmasked condition. The dashed black lines indicate the predicted result if voxels that responded in the same way in both conditions. The dashed blue and red lines represent the borders of the 5.0° and 7.5° masks, respectively. Error-bars indicate the standard error.

The results presented thus far concerned voxels that responded above threshold during the unmasked condition and one of the two masked conditions, but not necessarily during all three conditions. This was done because the fraction of voxels responding during all three conditions is much smaller than the fraction of voxels responding in the unmasked and one of the two masked conditions. In addition, it should be noted that there is a genuine effect if the pRF eccentricity moved from 5.5 to 7 degrees of visual angle for the condition with the 7.5° mask, but not for the 5° mask, and excluding all voxels beyond the extent of the smaller mask would bias the results for the condition with the larger mask. However, with this in mind, to analyze directly the relationship between two mask sizes, we nevertheless compared the effect of

applying an increasingly larger mask (from 0° to 5° to 7.5°) in all voxels that responded above threshold during all three conditions for which the pRF eccentricity in the unmasked condition did not exceed 5°. Figure 8A shows that the pRFs for these voxels shifted away lawfully from their original location towards the fringe of mask. Figure 8B further shows that the pRF size increases to roughly 3.5° in the masked conditions (see also Figure 4B).

Finally, as indicated in the methods section, the above results were obtained from model predictions that assumed full-field stimulation. This was done so to avoid changing both the stimulus and the modeling procedure. It is, however, possible that this choice made the fitting procedure more unstable during the masked conditions. We therefore repeated the model fitting procedure for the masked conditions with the mask included to generate the model predictions. Being conscious of the fact that any pRF changes found could now be due to changing the modeling rather than the stimulus, it should still be possible to detect the above-mentioned pRF changes. Indeed, Figure 9 shows that the pRFs in the OP ROIs shift towards ~4° when the 5° mask was applied, and to ~7° when masking the central 7.5° of the visual field. Furthermore, the pRF size in the OP ROI increased with ~1° and ~2° in the 5° and 7.5° masked conditions, respectively.

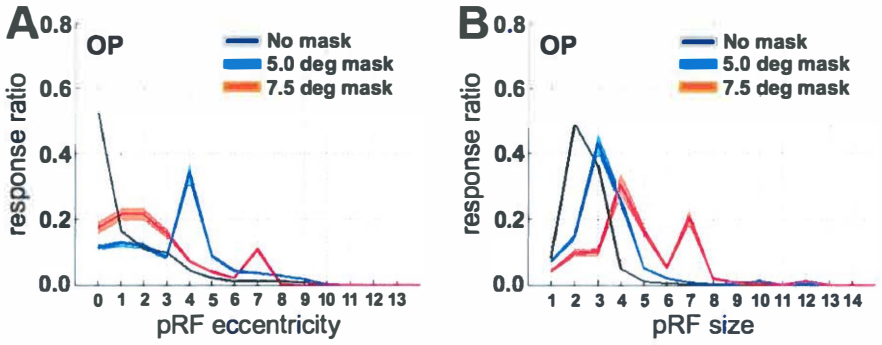

Figure 9. The effect of modeling the presence of a central mask. A. Response ratio (i.e, the number of responsive voxels per bin divided by the total number of responsive voxels) versus pRF eccentricity for the unmasked and masked conditions for the OP region-of interest. **B.** Response ratio versus pRF size for the unmasked and masked conditions in the OP region-of interest. Gray, blue and orange shadings indicate the jackknifed 95% confidence interval for the unmasked and the two masked conditions, respectively.

3.4. Discussion

The results show that some voxels in the cortical representations of the central visual field also respond when more peripheral locations are stimulated alone. These responses give rise to larger and more eccentric pRF estimates. Standard 2.5×2.5×2.5 mm^3 fMRI voxels capture of the order of 10^6 neurons [11,12] that will have a variety of receptive field properties, and the pRF estimate only captures their central tendency. This central tendency measure will necessarily change if only a biased subset of the neural population is activated. This scenario would occur if the masked stimuli primarily activated neurons with large or eccentric receptive fields. Under such circumstances, the pRF estimates would register only the larger and more eccentric values of the subset of neurons activated by the peripheral stimulation (Figure 1). Similar arguments have been put forward in a review on adult V1 plasticity to explain receptive field changes following retinal lesions [13]. However, the key question is whether some of the neural receptive fields and the position scatter are indeed sufficiently large to be driven by stimulation beyond 5° or 7.5° eccentricity. From Figure 1 it seems that a rather large amount of RF variation would be required to cover the position shifts that we report, and the primate classical receptive field at low eccentricities does not extent sufficiently far into the periphery to cover the observed expansions [14]. The model presented in Figure 1 may therefore not be telling the full story.

Other work has also revealed BOLD signals in the central representations of the visual field as a result of peripheral visual stimulation in normally sighted individuals [15] and patients [16]. In these studies, the patterns of activity were dependent on task/stimulus combinations, and the results were therefore interpreted in terms of feedback signaling from higher order visual areas. Indeed, the wide-spread BOLD signals that give rise to the larger and more eccentric pRF estimates are consistent with the distant BOLD modulation found in the macaque [17], and may well reflect the anatomical substrate of the very long spatial interactions in single V1 neurons [18] and of human contrast perception [19]. These very long-range spatial interactions are thought to arise from very rapidly conducting feed-forward-feedback loops [20-23] between V1 and higher order visual regions. Therefore, it could be that feed-back signals from the far periphery, which facilitate the neuronal response at low levels of excitation [18,20,21,24], are visible as a change in the BOLD signal when the center of the visual field is masked. Figure 10 illustrates the effect of these interactions for a single neuron in V1. While the models in Figures 1 and 10 both give rise to displaced and enlarged pRF estimates when the neuronal population is partially stimulated, it appears that only the model in Figure 10 can explain the extent of the pRF displacements and expansions.

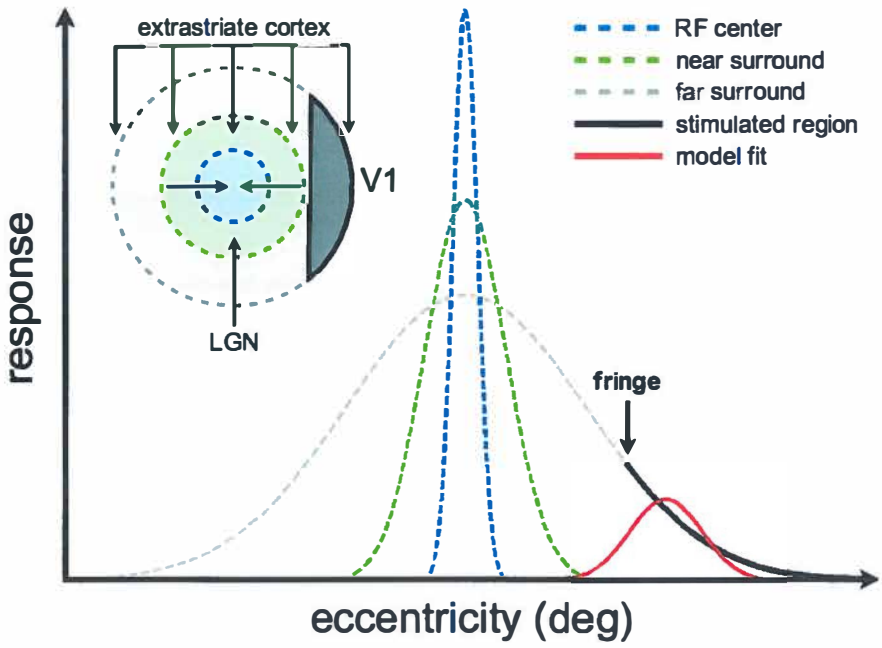

Figure 10. An explanation of the pRF dynamics in terms of feedback signals from extrastriate cortex. V1 neurons are presumed to have a receptive field (RF) center (dashed blue) that is measured by presenting high-contrast stimuli and commensurate with feed-forward connections from the lateral geniculate nucleus (LGN), a near surround (dashed green) that is measured by presenting low-contrast stimuli and commensurate with intra-areal V1 horizontal connections, and a far surround (dashed gray) that is commensurate with extrastriate feed-back connections [18, 20, 21]. We further assume that the pRF, which is measured by presenting high-contrast checkerboard stimuli, is an estimate of the RF center (dashed blue) when there is no mask. Normally, the response to stimulating the RF center is modulated by suppressive feed-back signals from the far periphery of the visual field [20-23]. However, when there is little or no stimulus contrast on the receptive field center, these feedback signals can also be excitatory [18, 20, 21, 24]. Under such circumstances, the far surround will be partially stimulated, which results in the skewed response indicated by the thick black curve. Fitting a Gaussian receptive field model to these responses will necessarily be shifted towards the fringe of the mask. It will also be larger than the RF center if the far surround extents sufficiently far into the periphery. Interestingly, this model also predicts that increasing the size of the mask (shifting the fringe to the right) results in a decrease of the pRF expansion. This is indeed what appears to happen when the mask size increases from 5.0° to 7.5° (see Figure 4B and corresponding text).

Regardless of explanation, the results indicate broad spatial tuning at the population level. This may underlie perceptual phenomena such as color, brightness, texture, and motion filling-in [25-31]. When the pRF expands or shifts away from its original to a more eccentric visual field location, the neuronal population will erroneously signal the presence of central stimuli to afferent neuronal populations [32,33]. A similar mechanism might also account for the Delboeuf illusion [34] or perceptual distortions seen in patients with damage to the afferent visual pathways

following stroke [35]. It could be interesting, therefore, to examine whether the pRF changes are also present under conditions in which these illusions and perceptual distortions occur. Furthermore, it has been observed that the receptive fields that were initially displaced and enlarged due to retinal lesions in animals, subsequently reduce in size towards the completion of the reorganization process (e.g., [36]). In adult human patients with macular lesions, only pRF expansions and displacements can be seen [8]. The most parsimonious explanation for these two observations is that the enlarged and displaced receptive fields provide a basis for long-term structural changes, but that these long-term structural changes do not necessarily follow through in human adulthood. To test this hypothesis, it would be worth studying the pRF characteristics in individuals with congenital loss of foveal vision, who do appear to exhibit cortical reorganization in the form of remapping [37].

Acknowledgments

We thank Heidi Baseler, Andre Gouws, and Christopher Racey for their contributions to the acquisition and pre-processing of the data, and two anonymous reviewers for their helpful comments and suggestions.

References

[1] Engel SA, Rumelhart DE, Wandell BA, Lee AT, Glover GH et al. (1994) fMRI of human visual cortex. Nature 369: 525.

[2] Sereno MI, Dale AM, Reppas JB, Kwong KK, Belliveau JW, et al. (1995) Borders of multiple visual areas in humans revealed by functional magnetic resonance imaging. Science 268: 889-893.

[3] DeYoe EA, Carman GJ, Bandettini P., Glickman S, Wieser J, et al. (1996) Mapping striate and extrastriate visual areas in human cerebral cortex. Proceedings of the National Academy of Science USA 93: 2382-2386.

[4] Smith AT, Singh KD, Williams AL, Greenlee MW (2001) Estimating receptive field size from fMRI data in human striate and extrastriate visual cortex. Cerebral Cortex 11: 1182 1190.

[5] Larsson J, Heeger DJ (2006) Two retinotopic visual areas in human lateral occipital cortex. Journal of Neuroscience 26: 13128-13142.

[6] Dumoulin SO, Wandell BA (2008) Population receptive field estimates in human visual cortex. Neuroimage 39: 647-660.

[7] Victor JD, Purpura K, Katz E, Mao B (1994) Population encoding of spatial frequency, orientation, and color in macaque V1. Journal of Neurophysiology 72: 2151-2166.

[8] Baseler HA, Gouws A, Haak KV, Racey C, Crossland MD, et al. (2011) Large-scale remapping of visual cortex is absent in adult humans with macular degeneration. Nature Neuroscience 14: 649-655.

[9] Winawer J, Horiguchi H, Sayres RA, Amano K, Wandell BA (2010) Mapping hV4 and ventral occipital cortex: the venous eclipse. Journal of Vision 10(5):1, 1-22.

[10] Bandettini PA, Jesmanowicz A, Wong EC, Hyde JS (1993) Processing strategies for time course data-sets in functional MRI of the human brain. Magnetic Resonance in Medicine 30: 161-173.

[11] Rockel AJ, Hiorns RW, Powell TP (1980) The basic uniformity in structure of the neocortex. Brain 103: 221-244.

[12] Leuba G, Garey LJ (1989) Comparison of neuronal and glial numerical density in primary and secondary visual cortex of man. Experimental Brain Research 77: 31-38.

[13] Wandell BA, Smirnakis SM (2009) Plasticity and stability of visual field maps in adult primary visual cortex. Nature Reviews Neuroscience 10: 873-884.

[14] Cavanaugh JR, Bair W, Movshon JA (2002) Nature and interaction of signals from the receptive field center and surround in macaque V1 neurons. Journal of Neurophysiology 88: 2530-2546.

[15] Williams MA, Baker CI, Op de Beeck HP, Mok Shim W, Dang S, et al. (2008) Feedback of visual object information to foveal retinotopic cortex. Nature Neuroscience 11: 1439-1445.

[16] Masuda Y, Dumoulin SO, Nakadomari S, Wandell BA (2008) V1 projection zone signals in human macular degeneration depend on task, not stimulus. Cerebral Cortex 18: 2483-2493.

[17] Shmuel A, Augath M, Oeltermann A, Logothetis NK (2006) Negative functional MRI response correlates with decreases in neuronal activity in monkey visual area V1. Nature Neuroscience 9: 569-577.

[18] Ichida JM, Schwabe L, Bressloff PC, Angelucci A (2007) Response facilitation from the "suppressive" receptive field surround of macaque V1 neurons. Journal of Neurophysiology 98: 2168-2181.

[20] Nurminen L, Peromaa T, Laurinen P (2010) Surround suppression and facilitation in the fovea: very long spatial interactions in contrast perception. Journal of Vision 10(13):9, 1-13.

[21] Schwabe L, Obermayer K, Angelucci A, Bressloff PC (2006) The role of feedback in shaping the extra-classical receptive field of cortical neurons: a recurrent network model. Journal of Neuroscience 26: 9117-9129.

[22] Schwabe L, Ichida JM, Shushruth S, Mangapathy P, Angelucci A (2010) Contrast dependence of surround suppression in macaque V1: experimental testing of a recurrent network model. Neuroimage 52: 777-792.

[23] Bullier J (2001) Integrated model of visual processing. Brain Research Reviews 36: 96-107.

[24] Girard P, Hupé JM, Bullier J (2001) Feedforward and feedback connections between areas V1 and V2 of the monkey have similar rapid conduction velocities. Journal of Neurophysiology 85: 1328-1331.

[25] Vanni S (2012) Local model for contextual modulation in the cerebral cortex. Neural Networks 25: 30-40.

[26] Zipser K, Lamme VA, Schiller PH (1996) Contextual modulation in primary visual cortex. Journal of Neuroscience 16: 7376-7389.

[27] Lamme VA, Super H, Spekreijse H (1998) Feedforward, horizontal, and feedback processing in the visual cortex. Current Opinion in Neurobiology 8: 529-535.

[28] Lamme VA, Zipser K, Spekreijse H (2002) Masking interrupts Figure-ground signals in V1. Journal of Cognitive Neuroscience 14: 1044-1053.

[29] Kinoshita M, Komatsu H (2001) Neural representations of the luminance and brightness of a uniform surface in the macaque primary visual cortex. Journal of Neurophysiology 86: 2559-2570.

[30] Wachtler T, Albright TD, Sejnowski TJ (2001) Nonlocal interactions in color perception: nonlinear processing of chromatic signals from remote inducers. Vision Research 41: 1535-1546.

[31] Roe AW, Lu HD, Hung CP (2005) Cortical processing of a brightness illusion. Proceedings of the National Academy of Sciences USA 102: 3869-3874.

[32] Cornelissen FW, Wade AR, Vladusich T, Dougherty RF, Wandell BA (2006) No functional magnetic resonance imaging evidence for brightness and color filling-in in early human visual cortex. Journal of Neuroscience 26: 3634-3641.

[33] Pettet M, Gilbert CD (1992) Dynamic changes in receptive-field size in cat primary visual cortex. Proceedings of the National Academy of Sciences USA 89: 8366-8370.

[34] Gilbert CD, Das A, Ito M, Kapadia M, Westheimer G (1996) Spatial integration and cortical dynamics. Proceedings of the National Academy of Sciences USA 93: 615- 622.

[35] Delboeuf JLR (1892) Sur une nouvelle illusion d'optique. Academie Royale des Sciences, des Lettres et des Beaux Arts de Belgique. Bulletins 24: 545-558.

[36] Dilks DD, Serences JT, Rosenau BJ, Yantis S, McCloskey M (2007) Human adult cortical reorganization and consequent visual distortion. Journal of Neuroscience 27: 9585-9594.

[37] Gilbert CD, Wiesel TN (1992) Receptive field dynamics in adult primary visual cortex. Nature 356: 150-152.

[38] Baseler HA, Brewer AA, Sharpe LT, Morland AB, Jägle H, et al. (2002) Reorganization of human cortical maps caused by inherited photoreceptor abnormalities. Nature Neuroscience 5: 364-370.

Abnormal visual field maps in human cortex: a mini-review and case report

Based on: Haak KV, Langers RM, Renken, R, van Dijk P, Borgstein J, Cornelissen FW (2013). Abnormal maps in human visual cortex: a mini-review and a case report. **Cortex**, in press.

Abstract

Human visual cortex contains maps of the visual field. Much research has been dedicated to answering whether and when these visual field maps change if critical components of the visual circuitry are damaged. Here, we first provide a focused mini-review of the functional magnetic resonance imaging (fMRI) studies that have evaluated the human cortical visual field maps in the face of retinal lesions, brain injury, and atypical retinocortical projections. We find that there is a fair body of research that has found abnormal fMRI activity, but also that this abnormal activity does not necessarily stem from cortical remapping. The abnormal fMRI activity can often be explained in terms of task effects and/or the uncovering of normally hidden system dynamics. We then present the case of a sixteen-year-old patient who lost the entire left cerebral hemisphere at age three for treatment of chronic focal encephalitis (Rasmussen syndrome) and intractable epilepsy. Using an fMRI retinotopic mapping procedure and population receptive field (pRF) modeling, we found that (1) despite the long period since the hemispherectomy, the retinotopic organization of early visual cortex remained unaffected by the removal of an entire cerebral hemisphere, and (2) the intact lateral occipital cortex contained an exceptionally large representation of the center of the visual field. The same method also indicates that the neuronal receptive fields in these lateral occipital brain regions are extraordinarily small. These features are clearly abnormal, but again they do not necessarily stem from cortical remapping. For example, the abnormal features can also be explained by the notion that the hemispherectomy took place during a critical period in the development of the lateral occipital cortex and therefore arrested its normal development. Thus, caution should be exercised when interpreting abnormal fMRI activity as a marker of cortical remapping; there are often other explanations.

4.1. Introduction

Human visual cortex contains several maps of the visual field (Wandell et al., 2005, 2007). Within each of these visual field maps, cortical neurons respond to stimuli in a limited region of the visual field, the neuronal receptive field, and neighboring neurons respond to neighboring regions of visual space. If critical components of the visual system are damaged, some visual neurons may change their receptive field profile (Kaas et al., 1990; Heinen and Skavenski, 1991; Chino et al., 1992; Gilbert and Wiesel, 1992; Darian-Smith and Gilbert, 1992; Kaas et al., 2002; Calford et al., 2005; Giannikopoulos and Eysel, 2006). These neuronal receptive field changes result in abnormal visual field maps. A method that has gained increased popularity over the past decade to infer the presence or absence of an abnormal visual field map is functional magnetic resonance imaging (fMRI). This review therefore concentrates on the fMRI studies of abnormal visual field maps in humans. By stimulating specific parts of the visual field one can evaluate whether stimulus-locked fMRI activity is present or absent at an expected cortical location. For example, when the center of the retina is damaged, a normal visual field map should no longer respond to stimuli presented at the center of the visual field. Such a silent zone is usually referred to as the lesion projection zone or LPZ. Another way to infer the presence or absence of an abnormal visual field map is by explicitly evaluating the layout of the map using an experimental paradigm called retinotopic mapping (Engel et al., 1994; DeYoe et al., 1994, 1996; Engel et al., 1997; Sereno et al., 1995; Wandell and Winawer, 2011; Engel, 2011).

4.2. Abnormal maps following retinal lesions

Let us start with the abnormal visual field maps that were found in patients with retinal lesions due to inherited photoreceptor abnormalities (Baseler et al., 2002). In a condition called rod-monochromacy, a genetic deficit causes the malfunctioning of the cone photoreceptor cells in the retina. Because the most central portion of the human retina contains only these cone cells, the patient is left with a small but permanent scotoma (blind spot) at the center of his or her visual field. In addition, the cortical regions that would normally be driven by this central portion of the retina, the LPZ, are now deprived from inputs. Interestingly, however, the LPZ was not entirely unresponsive, as would be expected if the visual field maps in these rod-monochromats were normal. Instead, it was found that the LPZ was now driven by those parts of the visual field directly surrounding the scotoma, suggesting that the receptive fields of the cortical neurons inside the LPZ had shifted away from their original location. Importantly, these abnormal responses could not be detected in normal control subjects in whom the retinal lesions were

simulated by performing the same experiment but stimulating only their rod photoreceptor cells. It is therefore, that the abnormal visual field maps in rod-monochromats are taken as evidence for cortical reorganization.

Abnormal LPZ responses can also be recorded in patients who acquired bilateral scotomas later in life, for example as a result of the eye-disease macular degeneration (MD). However, there is substantial controversy as to whether these responses can also be taken as evidence for cortical reorganization. Abnormal responses in MD patients were first presented by Baker et al. (2005). In this study, the authors presented a series of face, object and scene images to the intact, peripheral portions of the patients' visual field while requiring them to indicate whether the current image was the same as the one presented immediately before (one-back task). Interestingly, Baker et al. found that the activity in response to these peripherally presented stimuli was not only located in the expected regions of cortex that normally represent the periphery of the visual field, but also inside the patients' LPZ. Like the abnormal responses found in rod-monochromats, these abnormal responses were not present in normal controls, which is why the abnormal responses in the LPZ were taken to "demonstrate large-scale reorganization of visual processing in humans with MD" (Baker et al., 2005, p614).

Given their experimental paradigm, however, there are also mechanisms other than reorganization that could potentially explain the abnormal LPZ responses reported by Baker et al. (2005). For example, it could not be ruled out that the abnormal LPZ activations were caused by the task rather than the stimulus. This in turn opened up the possibility that the differences between patients and controls were due to differences in the strength of the top-down feedback signals from higher order visual cortex. To address this issue, Masuda et al. (2008) examined the abnormal LPZ responses in more detail, testing whether these responses were also present when MD patients performed a task that was not directed to the face stimuli, or when there was no task at all. In addition, the authors asked whether the abnormal responses could be due to the fact that the stimuli were meaningful by repeating the experiment using a simple checkerboard pattern instead of faces. The authors found that the abnormal responses observed by Baker et al. (2005) were indeed a consequence of the task rather than the stimulus or how meaningful they were. Similar task-dependent LPZ responses were also found some years later, in patients with another eye-disease, retinis pigmentosa (Masuda et al., 2008).

Because the Masuda studies seriously questioned the idea that cortical reorganization is responsible for the abnormal activations in the LPZ reported by Baker et al (2005), Baseler et al. (2011a) had also sought to determine whether the visual cortex of MD patients exhibits abnormal visual field maps. In contrast to the previous studies that were largely restricted to only a few individuals and did not explicitly evaluate the visual field maps, however, Baseler et al.

(2011a) performed retinotopic mapping measurements in two relatively large groups of different MD patients: those with the juvenile form of macular degeneration (JMD) and those with the more common, age-related form of macular degeneration (AMD). The authors compared the results of these measurements with the measurements in an age-matched group of healthy control subjects, and additionally, another group of healthy control subjects in whom we simulated the effect of macular degeneration by masking out the central portions of the retinotopic mapping stimuli. The results were threefold. First, we found that the signals inside the LPZ of both JMD and AMD patients were no different than those in the control group in whom we simulated the retinal lesion. Second, there were voxels with changed receptive field profiles throughout the patients' LPZ, but these were equally common and represented the same regions of the visual field as those in our control group. Third, a quantitative assessment of the area of cortex driven by the intact portions of the retina revealed that any differences in this respect were within the bounds of the large variance of visual cortical area of normal health participants. Hence, Baseler et al. (2011a) concluded that there is as of yet no evidence of cortical remapping in patients with retinal lesion acquired in adulthood.

4.3. Abnormal maps following brain injury

In addition to retinal lesions, visual cortex can also be deprived from input as a result of brain injury. There are numerous examples of patients who lost parts of their sight after an stroke had damaged their optic radiations. In many cases, however, these patients demonstrate a process of recovering the visual field which continues over months after the stroke occurred (e.g., Poppelreuter, 1917; Holmes, 1918; Bodian, 1964; Barnet et al., 1970; Zihl and von Cramon, 1980, 1985, 1986; Flodmark et al., 1990; Kasten and Sabel, 1995; Potthoff, 1995; Poggel et al., 2001; Hoyt, 2003; Julkunen et al., 2003; Werth and Seelos, 2005; Zhang et al., 2006; Schmielau and Wong, 2007), which suggests that their brains are changing in response to the permanent optic radiation damage. There is little data on the functional organization of visual cortex following stroke, but one case study suggests the presence of an abnormal visual field map within primary visual cortex (V1) following cortical deafferentiation by optic radiation damage (Dilks et al., 2007). In this patient, a stroke destroyed the optic radiation fibers that normally relay the visual information from the upper left visual hemifield (LVF) to V1 and as a consequence the patient was blinded in the upper quadrant of the LVF. Interestingly, however, the patient also exhibited a distorted perception of the intact, lower quadrant of the LVF, such that the patient perceived a square as a rectangle extending upward. Retinotopic mapping with fMRI revealed that this perceptual distortion was accompanied by a distorted visual field map in V1. That is, the authors

found that the V1 regions that normally represent the lower quadrant of the LVF near the edge of visual field defect in the upper LVF were expanded such that more cortical space was dedicated to representing the left horizontal meridian. The authors concluded that "the behavioral and fMRI data show that loss of input to V1 after stroke leads to cortical reorganization in the adult human visual system, and provide the first evidence that reorganization of the adult visual system affects visual perception" (Dilks et al., 2007, p9585).

However, just as Masuda et al (2008) argued that the term "reorganization" should not be used in reference to the activity observed by Baker et al. (2005) in the LPZ of MD patients, we would argue that the term "reorganization" should not be used with regard to the visual field map distortions observed by Dilks et al. (2007). The reason is that the term "reorganization" implies the presence of long-term anatomical changes, which cannot be inferred from the data. Moreover, we would suggest that the abnormal activity observed by Dilks et al. (2007) can be explained on the basis of intrinsic neuronal properties that surface only when the normal input signal is absent. Let us explain this in more detail. Neurons in V1 have receptive fields that consist of a excitatory center and a modulatory surround. The latter is usually suppressive but can also facilitate the neuronal response under conditions in which the center is hardly stimulated (Schwabe et al., 2006; Ichida et al., 2007; Schwabe et al., 2010). The receptive field surround can extent across very large distances in visual space. These very long-range spatial interactions are thought to arise from very rapidly conducting feed-forward-feed-backward loops between V1 and higher-order visual areas (Bullier, 2001; Girard et al., 2001; Schwabe et al., 2006; Schwabe et al., 2010). It is quite possible that, when neurons are deprived from their original input, the feedback signals from the far periphery of the visual field become visible as a distortion of the visual field map, and consequently affect perception (Haak et al., 2012). Of note is that the same explanation also applies to the abnormal responses recorded by Baker et al. (2005) and that this notion correctly predicts that ectopic population receptive fields can be recorded in both MD patients and controls with simulated lesions (Baseler et al., 2011a; Haak et al., 2011; Haak et al., 2012).

Brain injuries may not only occur in the vicinity of the optic radiations, but can also destroy parts of the visual cortex itself. Damage to different parts of the visual cortex will have different effects. For example, when damage is done to the ventral occipital surface near visual area V4 at the posterior part of the fusiform gyrus, chances are that the patient will become colorblind (Meadows, 1974). When damage is done to a more anterior portion of the fusiform gyrus, the patient may become unable to recognize faces (e.g., Bodamer, 1947; Hecaen and Angelerques, 1962; Gloning et al., 1966; Benton and van Allen, 1972; Kanwisher et al, 1997). The most detrimental effect of damage to the occipital lobes, however, is seen when the brain damage occurred within the primary visual (striate) cortex, V1. Because V1 provides the main source of

the inputs to the higher-order visual areas, patients with unilateral V1 lesions become completely unaware of the visual information from the contralateral visual hemifield. Baseler et al. (1999) therefore asked to what extent the extrastriate, higher-order visual field maps reorganize following V1 damage. Using the retinotopic mapping technique, the authors examined the visual field maps in patient G.Y. who had a large lesion which included most of the peripheral visual field representation in the left V1, but spared the representation of the most central (foveal) portions of the right visual field. When the retinotopic mapping stimuli were presented across the full visual field (full wedge condition), the authors could easily identify several visual areas. However, when the stimuli were restricted to the blind, peripheral portion of the visual field (annular wedge condition), the experiment revealed abnormal maps for the visual areas located dorsally to V1. The maps "that had shown normal organization when the fovea was also stimulated now responded primarily to positions near the lower vertical meridian" (Baseler et al., 1999, p2625). Importantly, such abnormal visual field maps were not observed in a healthy control subject in the same stimulus conditions. These results also corroborate earlier work which has shown that visual functions can be represented by extrastriate areas in humans, even if the early visual areas are missing in one or both hemispheres of the brain (Werth, 2006).

How can these extrastriate visual field maps be both normal and abnormal? Baseler et al. (1999) provide a framework for understanding this: "In the full wedge condition, neurons representing the fovea drive the nearby peripheral representations and generate a normal representation of angular visual field position. In the annular wedge condition, neurons representing the fovea are not stimulated. Instead, nearby neurons that represent the peripheral portion of the lower vertical meridian generate an abnormal representation of the visual field position" (Baseler et al., 1999, p2626). The authors based this argument on the assumption that when extrastriate regions are deprived of their normal V1 input, "they are colonized by other neurons in neighboring cortex". Furthermore, they argued, that they "do not see the same colonization [...] in normal controls suggests that the activity in G.Y. is mediated by connections that have been strengthened or added through plastic reorganization" (Baseler et al., 1999, p2626). This latter statement, however, should be treated with caution as it is still possible that the relative contribution of these 'new' connections was modulated by the difference between *no* input and *zero-contrast* input, which also seems to be the case in the MD and stroke patients.

4.4. Abnormal retinocortical projections

In human albinism, there is an abnormal projection of the retinal fibers from the eye to cortex. Normally, fibers from the nasal retina project to the contralateral cerebral hemisphere and fibers

from the temporal retina project to the ipsilateral hemisphere of the brain. This crossing of fibers splits the two visual hemifields between the two hemispheres such that the primary visual area in the left cerebral hemisphere of the brain is driven by the visual field right to the vertical meridian and vice versa. With albinism this projection of visual fibers is very different: there are many visual fibers that project from the temporal retina to the contralateral hemisphere, which would normally stay on the ipsilateral side of the brain (Hedera et al., 1994). Therefore, humans with albinism are expected to exhibit abnormal visual field maps. Indeed, using retinotopic mapping Hoffmann et al. (2003) found that the abnormal fiber crossings in human albinism give rise to abnormal visual field maps. These maps area abnormal in the sense that "the abnormally crossing fibers from the temporal retina of the albino form a mirror-image map in striate cortex that is superimposed on the normal retinotopic map of the nasal retina. Voxels in V1, therefore, represent two visual field locations that are mirrored about the vertical meridian" (Hoffmann et al., 2003, p8928). This superposition suggests that the neurons contained by these voxels are ordered in a 'hemifield dominance column' arrangement (von dem Hagen et al., 2005).

Uncrossed optic nerve fibers were also observed in a recent case study of a patient born without the entire right cerebral hemisphere (Muckli et al., 2009). As a consequence, this patient's remaining left hemisphere has not only developed maps of the contralateral visual hemifield, but also maps of the ipsilateral visual hemifield, which caused the patient to develop a normal visual sensitivity across the entire visual field. To explain this, the authors suggested that the absence of the right cerebral hemisphere resulted in an absence of molecular repressors that normally prevent axons from the nasal retina to enter the ipsilateral hemispheres. Unlike the abnormal visual field maps seen in human albinism, the maps of the temporal visual hemifield in this patient were not superimposed on the normal retinotopic maps of the nasal retina. Instead, "islands of ipsilateral visual field representations were located along the representations of the vertical meridian. In V1, smooth and continuous maps from contra- and ipsilateral hemifield overlap each other, whereas in ventral V2 and V3 ipsilateral quarter field representations invaded small distinct cortical patches" (Muckli et al., 2009, p13034).

4.5. Case study

The study by Muckli et al. (2009) describes the outcome of loosing an entire cerebral hemisphere before the retinocortical pathways are in place, but what happens to the functional organization of human visual cortex when half the brain is removed after? What effect will the removal of an entire cerebral hemisphere have on visual field maps that used to receive input from the opposite hemisphere of the brain? It is clear that in some cases, hemispherectomized patients exhibit a

regained sensitivity across the full extent of the visual field, suggesting that the intact cerebral hemisphere developed visual field maps of the ipsilateral visual hemifield (Werth, 2006), just like those described by Muckli et al. (2009). However, there are also many patients that have never recovered. Are the visual field maps in these patients also abnormal as a consequence of the missing inter-hemispheric inputs? There are many visual areas of which it is now known that they contain neurons with very large receptive fields that overlap substantially with the vertical meridian. These neurons are expected to malfunction when they are deprived from half their normal input. This presents an opportunity for abnormal visual field maps to manifest. Therefore, using a functional magnetic resonance imaging (fMRI) retinotopic mapping procedure and population receptive field modeling, we examined the topographic organization of the intact visual cortex of a patient who lost an entire hemisphere at the age of three. Importantly, the patient was hemianopic which allowed us to examine exclusively the effects of commissural deafferentiation without the potential confound of potentially rerouted afferent visual pathways.

4.5.1. Methods

4.5.1.1 Participants

Visual responses were measured in the right occipital lobe of a 16-year-old girl who had a complete hemispherectomy at the age of three for treatment of Rasmussen syndrome (chronic focal encephalitis) and intractable epilepsy (figure 1a). Annual Goldman perimetry exams indicate a permanent right homogeneous hemianopia with no macular sparing (figure 1b). Nevertheless, the patient can fixate reliably. The first author of this paper served as a representative control subject. Both subjects gave informed written consent according to procedures approved by the Medical Ethics Committee of the University Medical Center Groningen, The Netherlands.

4.5.1.2 Stimuli

Stimuli were created and presented with the Psychtoolbox (Brainard, 1997; Pelli, 1997) extensions for Matlab (Mathworks, Natick, MA), using an Apple Macbook Pro 2.2 (Apple, Cupertino, CA). The stimuli were back-projected on a translucent display (44x34 cm) using a Barco LCD Projector G300 (Barco, Kortrijk, Belgium) set at a resolution of 800x600 pixels. Both subjects viewed the translucent display via a mirror placed 11 cm from the eyes. The distance between the mirror and the translucent display was 64 cm. In this configuration, the maximum stimulus radius was approximately 12 degrees of visual angle. The stimulus was a black and white chequered bar on a grey background. The luminance of the black checks was 155 cd/m^2 and the luminance of the white checks was 2800 cd/m^2. The grey background's luminance was 990 cd/m^2. Cortical

responses were measured to drifting bar apertures at various orientations that exposed a checkerboard pattern (figure 2). The moving bar width subtended $1/4^{th}$ of the stimulus radius and moved at a speed of $1/8^{th}$ of the stimulus radius per time frame. Four bar orientations and two different motion directions for each bar were used, giving a total of 8 different bar configurations within a given scan. Periods in which the subjects saw only a mean luminance (zero contrast) field were also included. The mean luminance block are important because they avoid systematic underestimation of the pRF size. The mean luminance periods were inserted at a rate of 4 cycles/scan during the last 12 seconds of the diagonal bars. During each scan, both subjects fixated on a small disc at the center of the screen (~1/4 degrees radius). The task was to press a button each time the fixation disc changed color. The color of the disc alternated between red and green at random intervals unrelated to the stimulus sequence.

4.5.1.3 Magnetic resonance imaging

Magnetic resonance images were acquired with a 3 Tesla Philips Achieva MR-scanner, equipped with a standard 8-channel phased-array (SENSE) head volume coil. Foam padding was used to minimize head motion. Functional MR images (TR/TE 1500/30 msec) were acquired using T_2*-sensitive multi slice gradient/field echo-planar imaging (EPI) with 24 slices oriented parallel to the Calcerine sulcus without slice gap. The effective voxel size was 2.3x2.3x3 mm^3 (FOV = 194x72x224 mm; flip-angle 80°). The functional scans were acquired during 136 time frames (scan duration of 204 sec). Four scans were performed for each subject. In the same session, a high resolution whole-brain T1-weighted anatomical MRI data set was also acquired. In addition, a T1-weighted anatomical data set with the same orientation and in-plane resolution as the functional images was acquired for co-registration purposes. The T1-weighted anatomical scans were re-sampled to a 1 mm isotropic resolution. Gray and white matter was segmented from the whole-brain anatomical MRI using FSL (http://fmrib.ox.ac.uk/fsl) routines (Smith et al., 2004) and hand-edited to minimize segmentation errors (Teo et al., 1997). The cortical surface was reconstructed at the gray/white-matter border and rendered as a smoothed three-dimensional surface (Wandell et al., 2000). The in-plane anatomical MRI was aligned with the whole-brain anatomical data (Nestares and Heeger, 2000) and the functional scans interpolated to the anatomical resolution.

4.5.1.4 Functional image processing

Functional MRI data were analyzed using the mrVISTA toolbox for Matlab (http://vistalab.stanford.edu/software). The first 8 time frames of each functional scan were discarded to avoid start-up magnetization transients. Head movements within and between scans

were measured and corrected for (Nestares and Heeger, 2000), although most scans had less than 1 mm head motion. The four clipped motion corrected time-series from a scans were then averaged and baseline drifts were subtracted from the averaged time-series by high-pass temporal filtering. All subsequent analyzes were based on the resulting averaged time-series.

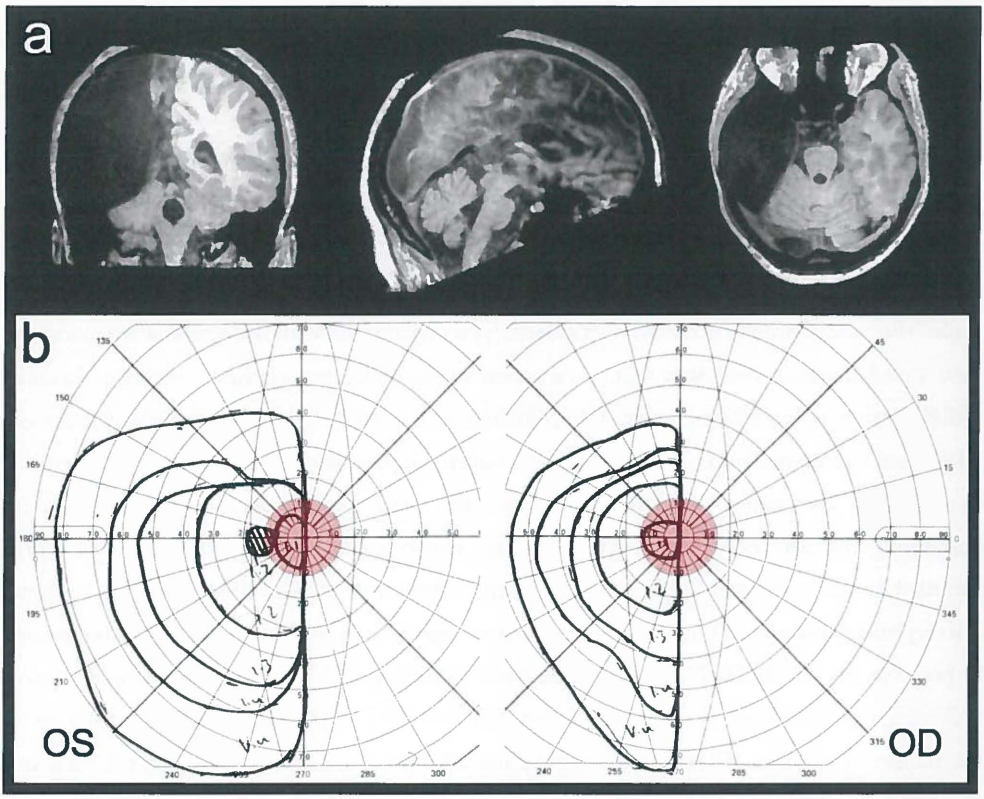

Figure 1. MRI and Goldmann perimetry of the hemispherectomized patient. (**a**) A high-resolution anatomical MRI scan of the 16-year-old hemispherectomized patient indicates the absence of the entire left (dominant) cerebral hemisphere (left = coronal, middle = sagittal, right = axial view). The left hemisphere was removed for treatment of Rasmussen syndrome at age 3. Remarkably, the patient is fully bilingual and has a partially recovered right-sided hemiplegia, despite the absence of the left hemisphere's language centers and motor control for the right side of the body. (**b**) Goldmann perimetry of the hemispherectomized patient's left (OS) and right (OD) eyes demonstrates a complete right hemianopia without macular sparing (the black contours represent the visual field sensitivity boundaries for 5 different target sizes). The hatched region in the left panel indicates the position of the patient's physiological blind spot, which lies between 10 and 20 deg eccentricity. The opaque red disks in the center of each panel indicate the location and size of the stimulated visual field region during the fMRI experiment.

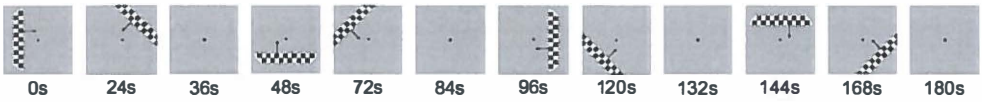

Figure 2. Stimulus schematic. For each functional MRI scan, bar apertures at four different orientations in two opposing directions (eight configurations in total) revealed a 100% contrast checkerboard pattern whose rows drifted in opposite directions along the orientation of the aperture. Four mean luminance periods were inserted during the last 12s of every diagonal bar aperture. Note that these mean luminance periods are necessary to accurately estimate large pRFs (Dumoulin and Wandell, 2008). The arrows indicate the aperture's motion direction and were not present during the experiment.

4.5.1.5 Population receptive field modeling

In accordance to procedures described Dumoulin and Wandell (2008), the population receptive fields (pRFs) that together define the retinotopic organization in occipital cortex were estimated using a model-based analysis in which the blood oxygen-level dependent (BOLD) response was predicted for each voxel using a circular symmetric two-dimensional Gaussian population receptive field model. The parameters of this model are its center eccentricity (r), polar angle (θ), and size (σ), the standard deviation of the Gaussian, and are all expressed in degrees of visual angle. The predicted time series were calculated by a convolution with the stimulus sequence and then an additional convolution with a canonical two-gamma hemodynamic response function (HRF; Friston et al., 1998; Glover, 1999; Worsley et al., 2002). Best fitting model parameters minimized the residual sum of squares (RSS) between the predicted and observed time series.

After estimating the pRF parameters, the HRF parameters were determined by minimizing the RSS between the predicted and observed BOLD responses over the entire recorded surface where the pRF model explained more than 10% of the time-series variance (Harvey and Dumoulin, 2011). During this iterative search, the HRF parameters were constrained to preserve the overall HRF profile of one initial peak followed by a late negative undershoot. Following this procedure, the pRF parameters were refined to optimize the pRF estimates given the subjects' individual HRFs and best fitting models were retained if they accounted for more than 15% of the variance of the time series of each voxel.

4.5.2. Results

The pRF estimates were very reliable in many parts of the patient's preserved right visual cortex, explaining on average 39% of the fMRI time-series variance in visual areas V1-3 and 50% of the time-series variance in lateral occipital regions (figure 3). Figure 4 shows the pRF estimates on an inflated three-dimensional reconstruction of the patient's cortical surface. As in previous work

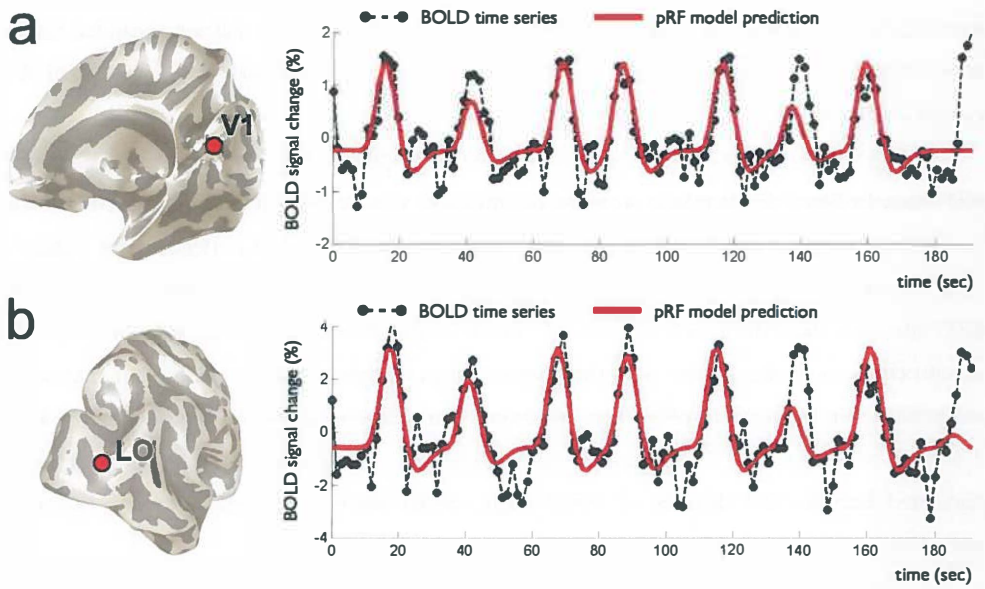

Figure 3. Examples of model predictions (the solid red curves) fit to the patient's BOLD time series (the black dot-dashed lines) for a voxel in visual area V1 (**a**) and another voxel in visual area LO-1 (**b**). The red disks on the inflated cortical surfaces indicate the approximate locations of the two voxels. The pRF model predictions for these voxels explained 53% and 57% of the BOLD time series variance and the pRF size corresponded to 0.5 and 1.0 degrees of visual angle, respectively.

(Baseler et al., 2011a), this was done for all voxels for which the pRF explained at least 15% of the time-series variance (corresponding to $p < .0001$ uncorrected; cf. Bandettini et al., 1993). Figure 4b indicates that the hemispherectomized patient's polar angle map is largely normal. The ipsilateral responses at the occipital pole are most likely caused by a slight left fixation offset, given that the patient is hemianopic without macular sparing (as verified with Goldmann perimetry, figure 1). The patient's eccentricity map (figure 4c), by contrast, suggests that an unusually large portion of the lateral occipital cortex responds to central visual stimulation.

To quantify the expanded foveal representation in the patient's lateral occipital regions, we measured the pRF eccentricity as a function of the cortical distance to the most foveal representation of visual area LO-1 (Larsson and Heeger, 2006; Amano et al., 2009). Figure 5a compares these measurements to the averaged LO-1 cortical magnification function from 14 normal hemispheres (Amano et al., 2009). Within the range of 0 to 20 mm from the most foveal representation of LO-1, the patient's cortical magnification factor amounts to ~16 mm/deg, while this would normally be ~7 mm/deg. This increase in cortical magnification factor indicates that a substantially larger portion of the cortical surface is dedicated to the center of the visual field in the patient. From 20-25 mm cortical distance the cortical magnification factor was ~1.5

mm/deg for the patient and ~3 mm/deg for the controls. This suggests that the expanded foveal representation came together with a stronger compression of the visual field just beyond the central 2 degrees.

Figure 4 also shows that the patient's lateral occipital cortex registered unusually small pRF sizes. In figure 5b, therefore, we show the pRF size as a function of pRF eccentricity for the hemispherectomized patient and the control subject in visual area LO-1. Because the patient's responses in this region were largely restricted to the central visual field, we only compared the pRF size for the central 2.5 degrees of visual angle. Within the 0-2.5 degrees range of eccentricities, both the patient and the control subject exhibited larger pRFs with increasing eccentricity, but the patient's pRFs were consistently smaller. For the patient, the pRF size in LO-1 ranged between 0 and 1.5 degrees of visual angle. For the control subject the LO-1 regions registered between 2-4 degrees of visual angle, which corresponds well to values reported previously (Amano et al., 2009).

The pRF estimates that we report were refined using the subjects' individual HRF parameters. This was done because the HRF could be abnormal following hemispherectomy; assuming a canonical HRF may therefore be inappropriate. However, because there is a weak negative correlation between the HRF width and the pRF size (Dumoulin and Wandell, 2008), it is also important to ask whether the refinement of the pRF estimates using the subjects' individual HRF could have caused the abnormal pRF estimates in LO-1. Hence, we also computed the pRF maps without the refinement and compared the results from both approaches. We first assessed whether the refinement increased the quality of the pRF estimates. This was indeed the case. The best-fitting pRF model predictions that were generated using the patient's individual HRF explained on average 39% and 50% of the time-series variance in V1-3 and LO-1, respectively. Without this refinement these values registered at 27% and 29%. We also computed a correlation coefficient to measure the agreement between the pRF position and size estimates from the same data using the two methods (Dumoulin et al., 2003). The pRF position and size estimates with and without refinement were highly correlated in all visual areas (table 1; all $p < .0001$). However, the refinement had some effect on the pRF size. Therefore, we also assessed explicitly whether the refinement resulted in systematically smaller pRFs in the LO-1 region by performing a paired *t*-test. Rather than smaller, this test revealed that the pRF size was in fact significantly bigger following the refinement ($t = 4.8$, $p = 3{\cdot}10^{-6}$). Together, these results indicate that the HRF refinement increased the overall quality of the pRF estimates, that it did not affect the pRF position estimates, and that it did not bias the pRF size estimates towards smaller values.

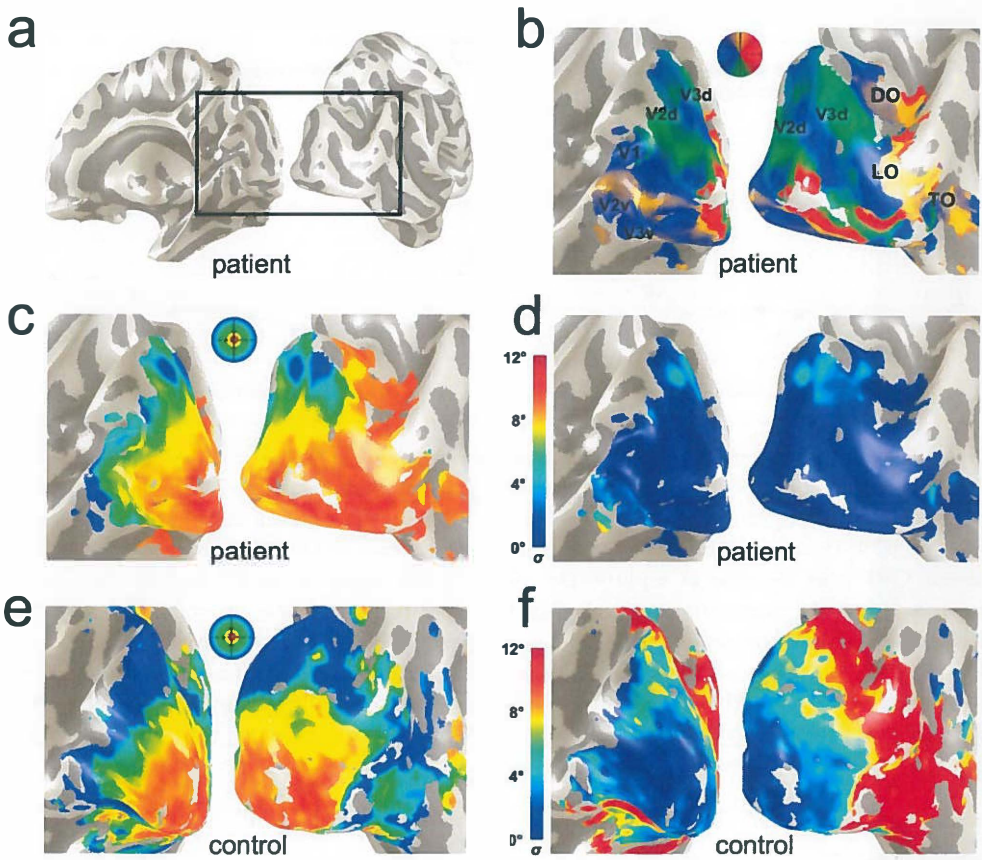

Figure 4. Population receptive field (pRF) maps for the hemispherectomized patient (**a-d**) and the control participant (**e, f**). (**a**) Medial (left) and lateral (right) views of an inflated three-dimensional reconstruction of the patient's cortical surface. The black rectangle indicates the occipital region enlarged in panels **b-d**. (**b**) The pRF polar angle maps for the patient (DO = Dorsal Occipital, LO = Lateral Occipital, and TO = Temporal Occipital). (**c**) The pRF eccentricity maps for the patient. (**d**) The pRF size maps for the patient. (**e**) The pRF eccentricity maps for the control subject. (**f**) The pRF size maps for the control participant.

Correlation coefficient (r)	pRF eccentricity	pRF polar-angle	pRF size
V1	0.99	0.99	0.76
V2	0.99	0.99	0.88
V3	0.99	0.99	0.94
LO-1	0.94	0.93	0.68

Table 1. Effect of refining the pRF estimates using individual hemodynamic response functions. The correlation coefficient (r) compares the pRF estimates with and without the refinement using the patient's / control's individual HRF parameters. The correlation coefficient was computed for all voxels in the regions-of-interest for which the best-fitting pRF models explained more than 15% of the variance in their time-series.

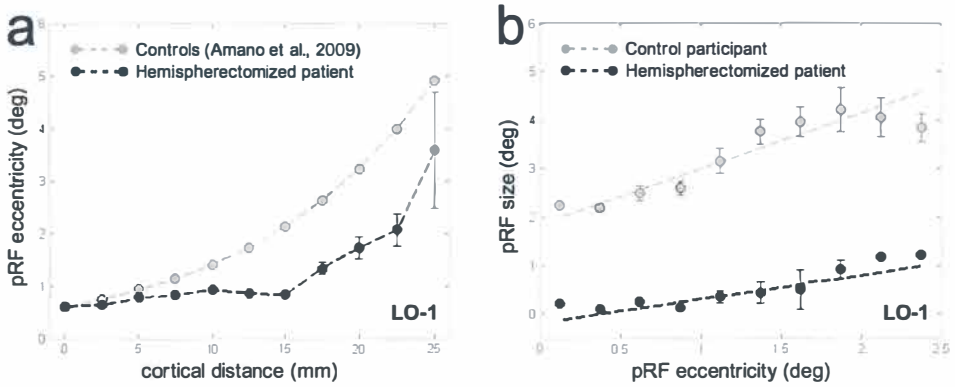

Figure 5. Quantitative comparison between the hemispherectomized patient and healthy control subjects. (a) Population receptive field (pRF) eccentricities as a function of cortical distance from the most foveal representation in the patient's LO-1 ROI (~0.7 deg). The gray dots represent the cortical magnification function (CMF) averaged across 14 normal cerebral hemispheres in LO-1 (Amano et al., 2009). This normal CMF takes the form of exp[0.084D+ln(10)] and was aligned at the 0.7 deg point in order to compare it with the current measurements. The black data points represent the cortical magnification function of the hemispherectomized patient in visual area LO-1. (b) Population receptive field (pRF) size as a function of pRF eccentricity in the patient's LO-1 ROI. The gray data points represent the relationship between pRF size and eccentricity in the right LO-1 region of the control subject. The black data points represent the same relationship for the hemispherectomized patient in visual area LO-1. Error bars indicate the standard error.

4.5.3. Discussion

Here, we evaluated the pRF maps in the intact visual cortex of a patient who lost the entire left cerebral hemisphere at the age of three. Since the surgery, the patient has suffered from a complete right hemianopia, and consistent with this, no reliable responses to the ipsilateral visual hemifield were detected. The patient's polar-angle maps were normal, as were the eccentricity maps in the early visual areas V1-3. However, the eccentricity maps in the patient's lateral occipital cortex showed a marked expansion of the representation of the very central visual field. The same regions of cortex also exhibited unusually small pRF size estimates. The abnormal pRF estimates cannot be explained by the omission of mean luminance periods or abnormal hemodynamics (Dumoulin and Wandell, 2008). Furthermore, the possibility that fixation instability would be the source of the abnormal pRF eccentricity and size maps can also be ruled out. First, the patient's fixation stability has been annually evaluated, and has always been found good. Second, fixation instability adds noise but no bias to the pRF eccentricity estimates (Levin et al., 2010). Third, fixation instability would cause an increase in the pRF size, rather than a

decrease (Levin et al., 2010). Hence, it appears that the pRF maps in the patient's lateral occipital cortex are genuinely abnormal.

4.6. Arrested development

One explanation for the abnormal pRF estimates in our case study is that large-scale reorganization of the lateral occipital cortex has occurred. Indeed, the patient was very young at the time of the hemispherectomy, and strikingly, the patient also showed a remarkable recovery from the right-sided hemiplegia after the surgery. What is more, despite the removal of the language centers in the left hemisphere of the brain (the left hemisphere of the patient's brain was also the language dominant hemisphere), the patient is now fully bilingual. Hence, this patient's brain is clearly capable of adapting to the severe brain injury that occurred when the patient was younger. However, it should also be noted that these remarkable recoveries all occurred in non-visual domains and that the complete right hemianopia was not relieved. In addition there is no obvious behavioral advantage to expand the foveal representation and decrease the neuronal receptive field size in the lateral occipital cortex. Nevertheless, it could still be speculated that the removal of the contralateral hemisphere caused the visual neurons in the lateral occipital cortex to malfunction, which in turn resulted in a redistribution of these neuronal resources among other visual functions requiring a very detailed processing of the central visual field.

The finding that the pRF sizes in the patient's lateral occipital cortex are unusually small can also be explained based on the idea that the normally very large neuronal receptive fields in these regions were deprived from inputs from the opposite cerebral hemisphere. Indeed, that this effect occurs mainly in the lateral occipital cortex is consistent with previous work that found the same regions of cortex to respond to stimuli presented in the ipsilateral visual hemifield (Tootell et al., 1998). The absence of inter-hemispheric signaling does not, however, directly explain the exceptionally large foveal representation in these regions. Nevertheless, it should be noted that the patient's left cerebral hemisphere was removed at the age of three, an age at which lateral occipital cortex is still developing (Connor et al., 2004). In recent work, Levin et al (2010) also found an unusually large foveal representation in the lateral occipital cortex of a patient who was blinded at the age of three but regained the retinal image at the age of 46. In addition, this patient had an unusually small splenium of the corpus callosum, suggesting that this patient too had impoverished inter-hemispheric connectivity between the occipital lobes. Even though our patient's visual cortex received visual inputs during subsequent development, and the patient described by Levin and colleagues did not, the most parsimonious explanation for both findings

would be that the retinotopic map development of the lateral occipital cortex has been disrupted. In this regard it is also worth mentioning that the epileptic seizures pre-hemispherectomy may have affected the development of the lateral occipital cortex of the remaining hemisphere.

In our case study, we have shown that the lateral occipital cortex of a 16-year-old hemispherectomized girl exhibits an unusually large representation of the central visual field and also exceptionally small receptive fields. Rather than explaining these results in terms of cortical reorganization, we propose that the abnormal features of the patient's lateral occipital cortex are due the fact that the hemispherectomy took place during the critical period in development of neurons in these regions. If so, the present case not only increases our understanding of the consequences of a childhood hemispherectomy on the remaining cortical circuitry, but also provides an important example of a patient whose visual cortex did not undergo an extensive remapping despite the young age at which the brain injury occurred.

4.6. Conclusion

In this chapter, we have provided a focused mini-review of the fMRI studies that have evaluated the human visual field maps in the face of retinal lesions, brain injury, and atypical retinocortical projections. In addition, we have presented new data on the retinotopic organization of human visual cortex following childhood hemispherectomy. Many studies have claimed evidence of cortical reorganization based the reasoning that the presence of abnormal visual field maps suffices to demonstrate it, but there are often other explanations. Assessing whether visual field maps are normal or abnormal can only reveal that reorganization did not occur (modus tollens). Unless cortical reorganization can be asserted as the only sufficient condition for an abnormal visual field map to arise, it is a deductive fallacy to conclude reorganization on the sole basis that the maps are abnormal. Our review and case study suggest that the data thus far only provide evidence for cortical reorganization in the presence of a congenital condition and atypical retinocortical projections. In all other cases it is as likely that the abnormal maps can be explained on the basis of a total or partial absence of the normal input signal. This is not to say, however, that it is not worth studying the human visual field maps under atypical conditions, because studying the functional organization of visual cortex in the context of different perturbations is a very fruitful way to understanding it in normal development and aging. In the case of retinal lesions it is also important to establish that the visual cortex does not undergo reorganization. This is because "any plastic changes that result in a remapping of inputs could cause a disruption or distortion of visual processing if retinal function is later restored" (Baseler et al., 2011b, p1255-1256). In addition, there is evidence that long-standing retinal lesions are associated with a

decreased cortical gray matter density in the early visual areas (Boucard et al., 2009, Plank et al., 2011). These gray-matter changes might adversely affect the visual field maps. Finally, it is also important to study the human visual field maps under atypical conditions because assessing visual field maps might helpfully determine visual sensitivity in patients who find it hard to fixate for perimetry measurements (Haak et al., 2011).

Acknowledgments

This research was supported by the foundation for Dutch ophthalmology research (SNOO), the Netherlands organization for scientific research (NWO), and the Netherlands organization for health research and development (ZonMw). We thank Jan Bernard Marsman for assistence during scanning.

References

Albert ML, Reches A, and Silverberg R. Hemianopic colour blindness. Journal of neurology, neurosurgery, and psychiatry, 38 (6):546-549, 1975.

Amano K, Wandell BA, and Dumoulin SO. Visual field maps, population receptive field sizes, and visual field coverage in the human MT+ complex. J.Neurophysiol., 102 (5):2704-2718, 2009.

Baker CI, Peli E, Knouf N, and Kanwisher NG. Reorganization of visual processing in macular degeneration. J.Neurosci., 25 (3):614-618, 2005.

Bandettini PA, Jesmanowicz A, Wong EC, and Hyde JS. Processing strategies for time-course data sets in functional MRI of the human brain. Magn.Reson.Med., 30 (2):161-173, 1993.

Barnet AB, Manson JI, and Wilner E. Acute cerebral blindness in childhood. Six cases studied clinically and electrophysiologically. Neurology, 20 (12):1147-1156, 1970.

Baseler HA, Brewer AA, Sharpe LT, Morland AB, Jagle H, and Wandell BA. Reorganization of human cortical maps caused by inherited photoreceptor abnormalities. Nat.Neurosci., 5 (4):364-370, 2002.

Baseler HA, Gouws A, Crossland MD, Leung C, Tufail A, Rubin GS, and Morland AB. Objective visual assessment of antiangiogenic treatment for wet age-related macular degeneration. Optom.Vis.Sci., 88 (10):1255-1261, 2011.

Baseler HA, Gouws A, Haak KV, Racey C, Crossland MD, Tufail A, Rubin GS, Cornelissen FW, and Morland AB. Large-scale remapping of visual cortex is absent in adult humans with macular degeneration. Nat.Neurosci., 14 (5):649-655, 2011.

Baseler HA, Morland AB, and Wandell BA. Topographic organization of human visual areas in the absence of input from primary cortex. J.Neurosci., 19 (7):2619-2627, 1999.

Behr C. Die komplizierte, hereditair-familiaire Optikusatrophie des Kindesalters: ein bisher nicht beschriebener Symptomkompleks. Klinische Monatsblatter fur Augenheilkunde, 47:138-160, 1909.

Benton AL and Van Allen MW. Prosopagnosia and facial discrimination. J.Neurol.Sci., 15 (2):167-172, 1972.

Bodamer J. Die Prosop-Agnosie. Archiv fur Psychiatrie und Nervenkrankheiten, 179:6-53, 1947.

Bodian M. Transient Loss of Vision Following Head Trauma. N.Y.State J.Med., 64:916-920,

1964.

Boucard CC, Hernowo AT, Maguire RP, Jansonius NM, Roerdink JB, Hooymans JM, and Cornelissen FW. Changes in cortical grey matter density associated with long-standing retinal visual field defects. Brain, 132 (Pt 7):1898-1906, 2009.

Brainard DH. The Psychophysics Toolbox. Spat.Vis., 10 (4):433-436, 1997.

Bullier J. Integrated model of visual processing. Brain Res.Brain Res.Rev., 36 (2-3):96-107, 2001.

Calford MB, Chino YM, Das A, Eysel UT, Gilbert CD, Heinen SJ, Kaas JH, and Ullman S. Neuroscience: rewiring the adult brain. Nature, 438 (7065):E3; discussion E3-4, 2005.

Chino YM, Kaas JH, Smith EL,3rd, Langston AL, and Cheng H. Rapid reorganization of cortical maps in adult cats following restricted deafferentation in retina. Vision Res., 32 (5):789-796, 1992.

Conner IP, Sharma S, Lemieux SK, and Mendola JD. Retinotopic organization in children measured with fMRI. J.Vis., 4 (6):509-523, 2004.

Damasio A, Yamada T, Damasio H, Corbett J, and McKee J. Central achromatopsia: behavioral, anatomic, and physiologic aspects. Neurology, 30 (10):1064-1071, 1980.

Darian-Smith C and Gilbert CD. Topographic reorganization in the striate cortex of the adult cat and monkey is cortically mediated. J.Neurosci., 15 (3 Pt 1):1631-1647, 1995.

DeYoe EA, Bandettini P, Neitz J, Miller D, and Winans P. Functional magnetic resonance imaging (FMRI) of the human brain. J.Neurosci.Methods, 54 (2):171-187, 1994.

DeYoe EA, Carman GJ, Bandettini P, Glickman S, Wieser J, Cox R, Miller D, and Neitz J. Mapping striate and extrastriate visual areas in human cerebral cortex. Proc.Natl.Acad.Sci.U.S.A., 93 (6):2382-2386, 1996.

Dilks DD, Serences JT, Rosenau BJ, Yantis S, and McCloskey M. Human adult cortical reorganization and consequent visual distortion. J.Neurosci., 27 (36):9585-9594, 2007.

Dumoulin SO, Hoge RD, Baker CL,Jr, Hess RF, Achtman RL, and Evans AC. Automatic volumetric segmentation of human visual retinotopic cortex. Neuroimage, 18 (3):576-587, 2003.

Dumoulin SO and Wandell BA. Population receptive field estimates in human visual cortex. Neuroimage, 39 (2):647-660, 2008.

Engel SA. The development and use of phase-encoded functional MRI designs. Neuroimage, 2011.

Engel SA, Glover GH, and Wandell BA. Retinotopic organization in human visual cortex and the spatial precision of functional MRI. Cereb.Cortex, 7 (2):181-192, 1997.

Engel SA, Rumelhart DE, Wandell BA, Lee AT, Glover GH, Chichilnisky EJ, and Shadlen MN. fMRI of human visual cortex. Nature, 369 (6481):525, 1994.

Flodmark O, Jan JE, and Wong PK. Computed tomography of the brains of children with cortical visual impairment. Dev.Med.Child Neurol., 32 (7):611-620, 1990.

Friston KJ, Fletcher P, Josephs O, Holmes A, Rugg MD, and Turner R. Event-related fMRI: characterizing differential responses. Neuroimage, 7 (1):30-40, 1998.

Giannikopoulos DV and Eysel UT. Dynamics and specificity of cortical map reorganization after retinal lesions. Proc.Natl.Acad.Sci.U.S.A., 103 (28):10805-10810, 2006.

Gilbert CD and Wiesel TN. Receptive field dynamics in adult primary visual cortex. Nature, 356 (6365):150-152, 1992.

Girard P, Hupe JM, and Bullier J. Feedforward and feedback connections between areas V1 and V2 of the monkey have similar rapid conduction velocities. J.Neurophysiol., 85 (3):1328-1331, 2001.

Gloning I, Gloning K, Hoff H, and Tschabitscher H. Zur prosopagnosie. Neuropsychologia, 4:113-132, 1966.

Glover GH. Deconvolution of impulse response in event-related BOLD fMRI. Neuroimage, 9 (4):416-429, 1999.

Haak KV and Clatworthy P, Morland A.B. Assessing visual dysfunction with fMRI. Advances in Clinical Neuroscience and Rehabilitation, 11 (3):20-21, 2011.

Haak KV, Cornelissen FW, and Morland AB. Population receptive field dynamics in human visual cortex. PLoS One, 7 (5):e37686, 2012.

Harvey BM and Dumoulin SO. The relationship between cortical magnification factor and population receptive field size in human visual cortex: constancies in cortical architecture. J.Neurosci., 31 (38):13604-13612, 2011.

Hecaen H and Angelergues R. Agnosia for faces (prosopagnosia). Arch.Neurol., 7:92-100, 1962.

Hedera P, Lai S, Haacke EM, Lerner AJ, Hopkins AL, Lewin JS, and Friedland RP. Abnormal connectivity of the visual pathways in human albinos demonstrated by susceptibility-sensitized MRI. Neurology, 44 (10):1921-1926, 1994.

Heinen SJ and Skavenski AA. Recovery of visual responses in foveal V1 neurons following bilateral foveal lesions in adult monkey. Exp.Brain Res., 83 (3):670-674, 1991.

Hoffmann MB, Tolhurst DJ, Moore AT, and Morland AB. Organization of the visual cortex in human albinism. J.Neurosci., 23 (26):8921-8930, 2003.

Holmes G. Disturbances of vision by cerebral lesions. Britisch Journal of Ophthalmology, 2:353-384, 1918.

Hoyt CS. Visual function in the brain-damaged child. Eye (Lond), 17 (3):369-384, 2003.

Ichida JM, Schwabe L, Bressloff PC, and Angelucci A. Response facilitation from the "suppressive" receptive field surround of macaque V1 neurons. J.Neurophysiol., 98 (4):2168-2181, 2007.

Julkunen L, Tenovuo O, Jaaskelainen S, and Hamalainen H. Rehabilitation of chronic post-stroke visual field defect with computer-assisted training: a clinical and neurophysiological study. Restor.Neurol.Neurosci., 21 (1-2):19-28, 2003.

Kaas JH. Sensory loss and cortical reorganization in mature primates. Prog.Brain Res., 138:167-176, 2002.

Kaas JH, Krubitzer LA, Chino YM, Langston AL, Polley EH, and Blair N. Reorganization of retinotopic cortical maps in adult mammals after lesions of the retina. Science, 248 (4952):229-231, 1990.

Kanwisher N, McDermott J, and Chun MM. The fusiform face area: a module in human extrastriate cortex specialized for face perception. J.Neurosci., 17 (11):4302-4311, 1997.

Kasten E and Sabel BA. Visual field enlargement after computer training in brain-damaged patients with homonymous deficits: an open pilot trial. Restor.Neurol.Neurosci., 8 (3):113-127, 1995.

Larsson J and Heeger DJ. Two retinotopic visual areas in human lateral occipital cortex. J.Neurosci., 26 (51):13128-13142, 2006.

Levin N, Dumoulin SO, Winawer J, Dougherty RF, and Wandell BA. Cortical maps and white matter tracts following long period of visual deprivation and retinal image restoration. Neuron, 65 (1):21-31, 2010.

Masuda Y, Dumoulin SO, Nakadomari S, and Wandell BA. V1 projection zone signals in human macular degeneration depend on task, not stimulus. Cereb.Cortex, 18 (11):2483-2493, 2008.

Masuda Y, Horiguchi H, Dumoulin SO, Furuta A, Miyauchi S, Nakadomari S, and Wandell BA.

Task-dependent V1 responses in human retinitis pigmentosa. Invest.Ophthalmol.Vis.Sci., 51 (10):5356-5364, 2010.

Meadows JC. Disturbed perception of colours associated with localized cerebral lesions. Brain, 97 (4):615-632, 1974.

Muckli L, Naumer MJ, and Singer W. Bilateral visual field maps in a patient with only one hemisphere. Proc.Natl.Acad.Sci.U.S.A., 106 (31):13034-13039, 2009.

Nestares O and Heeger DJ. Robust multiresolution alignment of MRI brain volumes. Magn.Reson.Med., 43 (5):705-715, 2000.

Pelli DG. The VideoToolbox software for visual psychophysics: transforming numbers into movies. Spat.Vis., 10 (4):437-442, 1997.

Plank T, Frolo J, Brandl-Ruhle S, Renner AB, Hufendiek K, Helbig H, and Greenlee MW. Gray matter alterations in visual cortex of patients with loss of central vision due to hereditary retinal dystrophies. Neuroimage, 56 (3):1556-1565, 2011.

Poggel DA, Kasten E, Muller-Oehring EM, Sabel BA, and Brandt SA. Unusual spontaneous and training induced visual field recovery in a patient with a gunshot lesion. J.Neurol.Neurosurg.Psychiatry., 70 (2):236-239, 2001.

Poppelreuter W. Die Psychischen Schadigungen Durch Kopfschuss Im Kriege 1914-1916. Bd. I. Die Storungen Der Niederen Und Hoheren Sehleistungen Durch Verletzungen Des Okzipitalhirns. L. Voss., 1917.

Potthoff RD. Regeneration of specific nerve cells in lesioned visual cortex of the human brain: an indirect evidence after constant stimulation with different spots of light. J.Neurosci.Res., 40 (6):787-796, 1995.

Schmielau F and Wong EK. Recovery of visual fields in brain lesioned patients by reaction perimetry treatment. Journal of NeuroEngineering and Rehabilitation, 16:4-31, 2007.

Schwabe L, Ichida JM, Shushruth S, Mangapathy P, and Angelucci A. Contrast-dependence of surround suppression in Macaque V1: experimental testing of a recurrent network model. Neuroimage, 52 (3):777-792, 2010.

Schwabe L, Obermayer K, Angelucci A, and Bressloff PC. The role of feedback in shaping the extra-classical receptive field of cortical neurons: a recurrent network model. J.Neurosci., 26 (36):9117-9129, 2006.

Sereno MI, Dale AM, Reppas JB, Kwong KK, Belliveau JW, Brady TJ, Rosen BR, and Tootell RB.

Borders of multiple visual areas in humans revealed by functional magnetic resonance imaging. Science, 268 (5212):889-893, 1995.

Smith SM, Jenkinson M, Woolrich MW, Beckmann CF, Behrens TE, Johansen-Berg H, Bannister PR, De

Luca M, Drobnjak I, Flitney DE, Niazy RK, Saunders J, Vickers J, Zhang Y, De Stefano N, Brady JM, and Matthews PM. Advances in functional and structural MR image analysis and implementation as FSL. Neuroimage, 23 Suppl 1:S208-19, 2004.

Teo PC, Sapiro G, and Wandell BA. Creating connected representations of cortical gray matter for functional MRI visualization. IEEE Trans.Med.Imaging, 16 (6):852-863, 1997.

Tootell RB, Mendola JD, Hadjikhani NK, Liu AK, and Dale AM. The representation of the ipsilateral visual field in human cerebral cortex. Proc.Natl.Acad.Sci.U.S.A., 95 (3):818-824, 1998.

von dem Hagen EA, Houston GC, Hoffmann MB, Jeffery G, and Morland AB. Retinal abnormalities in human albinism translate into a reduction of grey matter in the occipital cortex. Eur.J.Neurosci., 22 (10):2475-2480, 2005.

Wandell BA, Brewer AA, and Dougherty RF. Visual field map clusters in human cortex. Philos.Trans.R.Soc.Lond.B.Biol.Sci., 360 (1456):693-707, 2005.

Wandell BA, Chial S, and Backus BT. Visualization and measurement of the cortical surface. J.Cogn.Neurosci., 12 (5):739-752, 2000.

Wandell BA, Dumoulin SO, and Brewer AA. Visual field maps in human cortex. Neuron, 56 (2):366-383, 2007.

Wandell BA and Winawer J. Imaging retinotopic maps in the human brain. Vision Res., 51 (7):718-737, 2011.

Werth R. Visual functions without the occipital lobe or after cerebral hemispherectomy in infancy. Eur.J.Neurosci., 24 (10):2932-2944, 2006.

Werth R and Seelos K. Restitution of visual functions in cerebrally blind children. Neuropsychologia, 43 (14):2011-2023, 2005.

Worsley KJ, Liao CH, Aston J, Petre V, Duncan GH, Morales F, and Evans AC. A general statistical analysis for fMRI data. Neuroimage, 15 (1):1-15, 2002.

Zhang X, Kedar S, Lynn MJ, Newman NJ, and Biousse V. Natural history of homonymous hemianopia. Neurology, 66 (6):901-905, 2006.

Zihl J and Mayer JC. Colour perimetry: method and diagnostic value (author's transl). Nervenarzt, 52 (10):574-580, 1981.

Zihl J and von Cramon D. Recovery of visual field in patients with postgeniculate damage. Neurology:188-194, 1986.

Zihl J and von Cramon D. Visual field recovery from scotoma in patients with postgeniculate damage. Brain, 108:335-365, 1985.

Zihl J and von Cramon D. Registration of light stimuli in the cortically blind hemifield and its effect on localization. Behavioural Brain Research, 1:287-298, 1980.

Chapter 5

Connective field modeling

Based on: Haak KV, Winawer J, Harvey BM, Renken R, Dumoulin SO, Wandell BA, Cornelissen FW (2013) Connective field modeling. **NeuroImage** 66: 376-384.

Abstract

The traditional way to study the properties of visual neurons is to measure their responses to visually presented stimuli. A second way to understand visual neurons is to characterize their responses in terms of activity elsewhere in the brain. Understanding the relationships between responses in distinct locations in the visual system is essential to clarify this network of cortical signaling pathways. Here, we describe and validate connective field modeling, a model-based analysis for estimating the dependence between signals in distinct cortical regions using functional magnetic resonance imaging (fMRI). Just as the receptive field of a visual neuron predicts its response as a function of stimulus position, the connective field of a neuron predicts its response as a function of activity in another part of the brain. Connective field modeling opens up a wide range of research opportunities to study information processing in the visual system and other topographically organized cortices.

5.1. Introduction

The interpretation of visual neuroscience measurements made in different parts of the brain is unified by the receptive field concept. A measurement at any point in the visual pathway is usually summarized by referring to the stimulus properties (location, contrast, color, motion) that are most effective at driving a neural response. Stimulus-referred receptive fields provide a common framework for understanding the sequence of visual signal processing. The classic receptive field construct summarizes the entire set of signal processing steps from the stimulus to the point of measurement. This sequence of signal processing can be made explicit by modeling how the activity of one set of neurons predicts the responses in a distinct set of neurons. Characterizing the responses of a cortical neuron in terms of the activity of neurons in other parts of cortex can provide insights into the computational architecture of visual cortex. Such measurements are exceptionally difficult to achieve with single-unit recordings. The relatively large field of view in functional magnetic resonance imaging (fMRI) offers an opportunity to measure responses in multiple brain regions simultaneously, and thus to derive neural-referred properties of the cortical responses. These cortical response properties provide important information about how neuronal signals are transformed along the visual processing pathways. For example, stimulus-referred measurements in cortex show that visual space is sampled according to a compressive function (i.e., the V1 cortical magnification factor corresponds to a logarithmic compression of cortical space with eccentricity). Neural-referred measurements show that this compression is established at the earliest stages of vision; later visual field maps sample early maps uniformly and inherit the early compressive representation (Harvey and Dumoulin, 2011, Kumano and Uka, 2010 and Motter, 2009).

A limitation in developing models of how fMRI responses in two parts of cortex relate to each other is that the problem is under-constrained. For example, there are many voxels in visual area V1, and there are many ways in which these responses could be combined to predict the response in a voxel in V2. Hence, any estimate requires imposing some kind of prior constraint on the set of possible solutions. Heinzle and colleagues (Heinzle et al., 2011), for example, used a support vector machine approach to reduce the dimensionality of the solution of V1 signals and predict responses in extrastriate cortex. Here, we take a different approach based on the idea that in retinotopic cortex connections are generally spatially localized. We build on a model-based population receptive field (pRF) analysis that was developed to estimate the stimulus-referred visual receptive field of a voxel (Dumoulin and Wandell, 2008). In the pRF analysis, the receptive field is modeled and fit to the fMRI signals elicited by visual field mapping

stimuli. This is done by generating fMRI signal predictions from a combination of the receptive field model and the experimental stimuli. In the present analysis, fMRI signal predictions are generated from fMRI signals originating from the regions of cortex covered by a model of the inter-areal connective field (Angelucci et al., 2002, Lehky and Sejnowski, 1988 and Sholl, 1953). Conceptually, this means that the localized activity in one cortical region acts as a stimulus for voxels in another region. We model the connective field as a two-dimensional, circular symmetric Gaussian that is folded to follow the cortical surface (figure 1). The assumption of a Gaussian connective field model is motivated by findings that the receptive fields of two extrastriate areas in the macaque, V4 and MT, can be described as two-dimensional, circularly symmetric, Gaussian sampling from the V1 map (Kumano and Uka, 2010 and Motter, 2009). The Gaussian width parameter provides crucial information about the connective field, namely its size. Because the inter-areal connective field size is a measure of spatial integration, the analysis can be used to trace the extent of spatial integration as information moves from the primary visual cortex to higher visual areas.

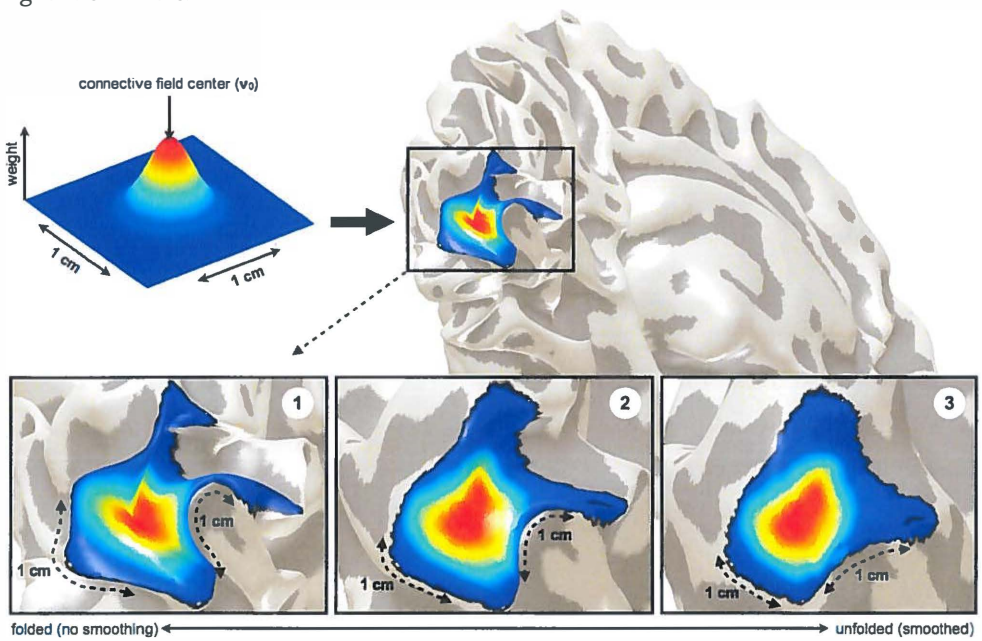

Figure 1. Connective field models follow the curvature of the cortex. A two-dimensional, Gaussian connective field model (top-left) is defined as a function of Dijkstra's shortest path distance between pairs of vertices in a three-dimensional mesh representation of the original, folded cortical surface (top-right). The advantage of this approach is that the measurement of cortical distance avoids the distortions introduced if the Gaussian were projected onto a flattened, two-dimensional cortical surface representation. Panels 1, 2 and 3 (bottom) further illustrate the connective field model projection when the surface mesh is unfolded (smoothed).

5.2. Methods

5.2.1. Participants

Cortical responses were measured using 7 Tesla fMRI in subjects S1 and S2 with 1.6, 2.0 as well as 2.5 mm isotropic voxel sizes. S1 also participated in a 3 Tesla fMRI experiment with a 2.5 mm isotropic resolution. During all experimental sessions, the participants viewed high-contrast drifting bar stimuli interposed with mean luminance periods. Both subjects had normal visual acuity. All experiments were performed with the informed written consent of the subjects and approved by the UMCU Medical Ethics Board.

5.2.2. Stimulus presentation

The visual stimuli were generated in the Matlab programming environment using the Psychtoolbox extensions (Brainard, 1997 and Pelli, 1997). Stimuli were displayed in one of two configurations. In both configurations, the participants viewed the display through an angled mirror. The first display configuration consisted of an LCD projecting the stimuli on a translucent display at the back of the magnet bore with a maximum stimulus radius of 5.5 degrees of visual angle. This configuration was used during the 7T experiments. The second display configuration consisted of an LCD with a maximum stimulus radius of 6.25 degrees of visual angle. This configuration was used during the 3T experiment.

5.2.3. Stimulus description

In both the 7T and 3T experiments, we measured responses to drifting bar apertures at various orientations that exposed a high-contrast checkerboard pattern (Dumoulin and Wandell, 2008, Harvey and Dumoulin, 2011 and Zuiderbaan et al., 2012). Parallel to the bar orientation, alternating rows of checks moved on opposite directions. This motion reversed at random intervals of at least 4 s. The bar width subtended 1/4th of the maximum stimulus radius. The bar moved across the stimulus window in 20 equally spaced steps. Four bar orientations and two different motion directions for each bar were used, giving a total of 8 different bar configurations within a given scan (up, down, left, right, and the four diagonals). After each horizontal and vertical pass, a 30 s zero contrast, mean luminance stimulus was presented.

5.2.4. Magnetic resonance imaging

Magnetic resonance images were acquired with 3T and 7T Philips MRI scanners equipped with sixteen-channel SENSE head coils. Foam padding was used to minimize head motion. Functional T2* weighted echo-planar images were acquired at both field-strengths. For the 3T runs, images

were acquired at an isotropic resolution of 2.5 mm, 24 slices. The TR was 1500 ms, the TE was 30 ms, and the flip-angle was 70°. For the 7T runs, images were acquired at isotropic resolutions of 1.6 mm, 2.0 mm, and 2.5 mm. The TR was 1500 ms, the TE was 25 ms, and the flip-angle was 80°. The functional runs each were 248 time frames (372 s). The first eight time-frames (12 s) were discarded. At 7T, eight functional runs were performed using 1.6 mm isotropic voxels, 5 functional runs were performed using 2.0 mm isotropic voxels, and 5 functional runs were performed using 2.5 mm isotropic voxels. At 3T, 9 functional runs were performed. In addition to the functional runs, high-resolution T1-weighted whole-brain anatomical MR images were acquired at 3T for both subjects.

5.2.5. Preprocessing of MR images

The T1-weighted anatomical MRI data sets were re-sampled to a 1 mm isotropic resolution. Gray and white matter were automatically segmented from the whole-brain anatomical data set using FSL (Smith et al., 2004) and subsequently hand-edited to minimize segmentation errors (Teo et al., 1997). The cortical surface was reconstructed at the white/gray matter border and rendered as a smoothed 3D surface (Wandell et al., 2000). Motion correction within and between scans was applied (Nestares and Heeger, 2000). Finally, functional images were aligned with the whole-brain anatomical segmentation.

5.2.6. Population receptive field analysis

Population receptive field (pRF) parameters were estimated according to procedures described by Dumoulin and Wandell (Dumoulin and Wandell, 2008). Briefly, fMRI time-series predictions were generated by varying the parameters (x, y and σ) of a circular symmetric Gaussian pRF model across a wide range of plausible values. The optimal pRF parameters were found by minimizing the residual sum of squares (RSS) using a coarse-to-fine search. First, the fMRI data were re-sampled to an 1 mm isotropic resolution within the identified gray matter. The fMRI data were then smoothed along the cortical surface using a diffusion smoothing process that approximated a 5 mm full-width at half-maximum Gaussian kernel, after which the pRF parameters were estimated for a sub-sample of the voxels and interpolated for the remaining voxels. Subsequently, an optimization algorithm (Fletcher and Powell, 1963) was applied for every voxel whose initial estimates exceeded 10% of the variance explained, so that the pRF model predictions were fitted to fMRI time courses without any spatial smoothing. As in previous work, eccentricity, polar angle, and pRF size maps were derived from the best pRF fits that exceeded 15% of the variance explained (Baseler et al., 2011, Haak et al., 2012 and Winawer et al., 2010).

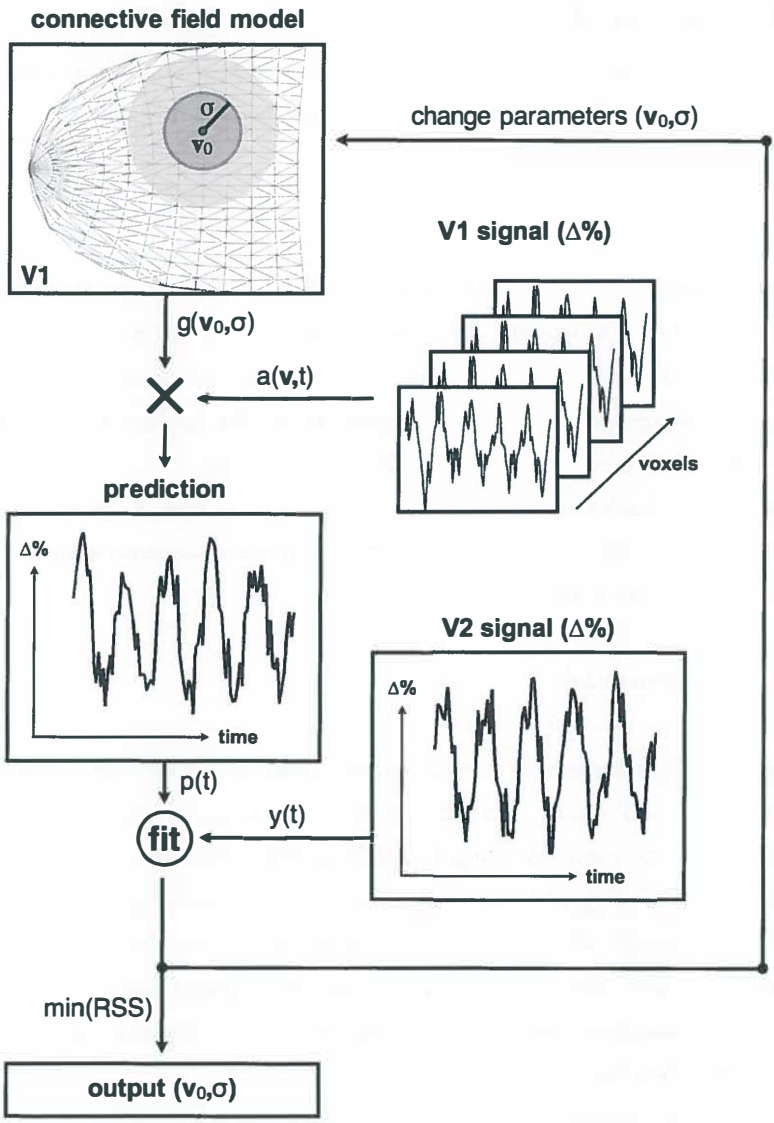

Figure 2. Estimating the V1 ► ►V2 connective field for a V2 voxel. Assuming a linear relationship between the blood-oxygenation levels and the fMRI signals, the observed blood-oxygenation level-dependent (BOLD) time course, $y(t)$, can be described in terms of the predicted BOLD signal, $p(t)$. The prediction, $p(t)$, is calculated using a parametrized model of the connective field. The parameters of the connective field model are its center location, v_0, in voxel coordinates, and the Gaussian spread, σ, laid out across the folded cortical surface in millimeters cortex. The definition of this circular symmetric Gaussian model is achieved by its projection on a three-dimensional mesh representation of the boundary between the gray and white matter of the brain. The predicted BOLD time course, $p(t)$, for a V2 voxel is then obtained by calculating the overlap between the connective field, $g(v_0,\sigma)$, and the fMRI signals in V1, $a(v,t)$. Finally, the optimal connective field model parameters are found by minimizing the residual sum of squares (RSS) between the prediction, $p(t)$, and the observed time series, $y(t)$.

5.2.6. Connective field modeling

As in the population receptive field analysis, the connective field parameters were estimated from the time-series data using a linear spatiotemporal model of the fMRI response:

$$y(t) = p(t)\beta + \varepsilon \quad (1)$$

where $p(t)$ is the predicted fMRI signal, β is a scaling factor that accounts for the unknown units of the fMRI signal, and ε accounts for measurement noise. In the present analysis, $p(t)$ is calculated using a parametrized model of the underlying neuronal population and the spatial distribution of its inputs laid out across the cortical surface. The model is estimated by finding the parameters that best predict the observed fMRI time course $y(t)$.

The current implementation of the analysis uses a circular symmetric Gaussian connective field model. The two-dimensional circular symmetric Gaussian connective field of voxel v, $g(v)$, is defined by two parameters: v_0 and σ:

$$g(v) = \exp-[d(v,v_0)^2/2\sigma^2] \quad (2)$$

where $d(v,v_0)$ is the shortest three-dimensional distance along the cortical manifold between voxel v and the connective field center v_0, and σ is the Gaussian spread (mm) across the cortical surface. The distance $d(v,v_0)$ was computed using Dijkstra's algorithm (Dijkstra, 1959) on a triangular mesh representation of the gray/white matter border. The calculation of $g(v)$ is done for each gray-matter voxel v directly adjacent to the white-matter in a predefined region-of-interest; V1 for example. Distances were calculated separately for each hemisphere: hence, a connective field model solution for any given voxel comprised voxels either in the ipsilateral hemisphere or the contralateral hemisphere, but not both.

The neuronal population inputs, $a(v,t)$, are defined as the percent BOLD signal change time course for voxels v (Δ%). Low-frequency signals were removed from these time-courses using a discrete cosine transform (DCT) high-pass filter. The time-series prediction is then obtained by calculating the overlap between the connective field and the neuronal population inputs (note that there is no need to do a convolution with the hemodynamic response function):

$$p(t) = \Sigma v\,[a(v,t) \cdot g(v)] \quad (3)$$

Finally, the optimal connective field parameters were found by minimizing the residual sum of squares (RSS) between the prediction, $p(t)$, and the observed time-series, $y(t)$. To do this, we generated various different fMRI time-series predictions by varying the connective field parameters $\mathbf{v}_0$, and σ, across all existing voxel positions on the V1 surface (both hemispheres) and 50 sigma values ranging from 0 to 25 mm. Neither spatial smoothing nor interpolation was performed; all connective field models were fitted to the observed time-series. Best models were retained if the explained variance in the fMRI time-series exceeded 15%.

5.2.7. Computing the V1 sampling extent

We obtained the V1 sampling extent by first finding the linear relationship between the pRF laterality index (λ), which indicates the extent to which a pRF overlaps with the ipsilateral visual field (0 represents no overlap, 0.5 represents 50% overlap), and the connective field size (σ):

$$\sigma(v) = m \cdot \lambda(v) + b \tag{4}$$

where m is the slope of the line and b is the intercept. We then computed the V1 sampling extent, r, for each voxel v using the following formula:

$$r(v) = \sigma(v) + [2 \cdot \lambda(v) \cdot b] \tag{5}$$

5.2.8. Statistical analyses

We derived the percent variance explained to specify how well the pRF and connective field models fit the fMRI time series. These r^2 values were calculated from the total sum of squares of the observed time series and the residual sum of squares of the predicted versus observed time series. Given that the time series consisted of 240 samples, the 15% variance explained threshold that was applied to all further analyzes corresponds to $p < 0.001$, corrected for testing ~100.000 different models per voxel (Bandettini et al., 1993). Furthermore, the correlation coefficients that were derived to quantify the agreement between the polar angle maps were circular–circular correlation coefficients to appropriately assess the association between these two angular variables (Behrens, 2009 and Jammalamadaka and Sengupta, 2001). Finally, all ranges reported in text represent 95% confidence intervals for the bootstrapped weighted means (N = 1000) using Student's t-distribution. Where appropriate, Bonferroni correction was applied to the confidence intervals — as reported in both the text and in the figures.

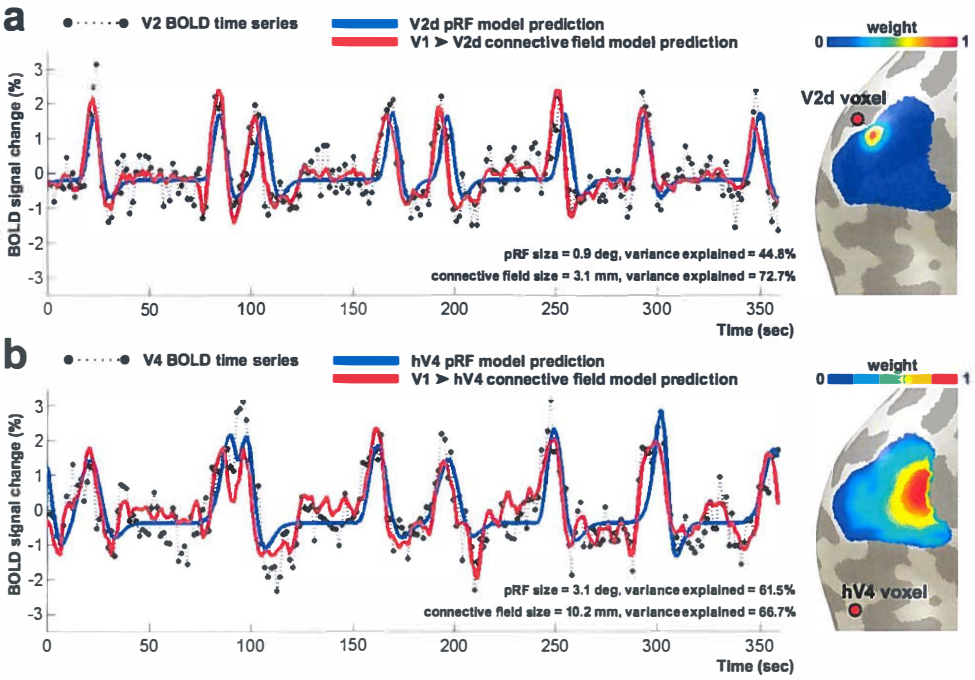

Figure 3. Examples of the connective field model fit to the BOLD time-series at voxels in V2 and V4. The BOLD time-series are indicated by the dotted lines. The conventional pRF model predictions are indicated by the solid blue lines. The connective field model predictions are indicated by the solid red lines. The connective field models are shown on an inflated portion of the left occipital lobe (medial view) on the right. (**a**) The V1 ► V2 connective field model fits the BOLD time-series very well, explaining 72.2% of the variance. For this particular V2 voxel the best-fitting connective field radius is 3.1 mm. (**b**) The best-fitting V1 ► V4 connective field model yields a radius of 10.2 mm. The BOLD time series variance explained by this model is 66.7%. Also note that the pRF model captures the peaks quite well (when the stimulus passes through the receptive field) but that it misses some of the ripples that occur when the stimulus is not directly on the receptive field. The connective field model, by contrast, does capture some of these fluctuations, which is one of the differences between the connective field model and the pRF model: the pRF model will never make accurate predictions when there is no stimulus.

5.3. Results

We first employed the conventional model-based pRF method (Dumoulin and Wandell, 2008) to derive estimates of the population receptive field for each voxel in visual cortex. These pRF estimates were used to delineate visual maps V1, V2, V3, and hV4 (Amano et al., 2009, Brewer et al., 2005, Dougherty et al., 2003, Dumoulin and Wandell, 2008, Harvey and Dumoulin, 2011, Wandell and Winawer, 2011, Wandell et al., 2007, Winawer et al., 2010 and Zuiderbaan et al., 2012). We then employed the new analysis (figure 2) to derive several inter-areal connective field

models for each voxel within the delineated visual areas. For the sake of brevity, we refer to these models in a compact manner; a connective field model m for voxel v can be specified by S ► R ("S projects on R"), if m has been defined on cortical surface S, and v falls in cortical region R (note that if S represents the visual field, the same notation can also be used to describe conventional population receptive fields). In this notation, we derived the following connective field models: V1 ► {V2, V3, hV4}. Across the two subjects and the three resolution sets, the best-fitting models explained on average 76%, 66%, and 46% of the time-series variance in V2, V3, and hV4, respectively.

Figure 3 further shows two examples of the connective field model fit to the fMRI time-series. A comparison of the connective field model prediction with the conventional pRF model prediction suggests that the connective field model captures more of the time-series variance than the pRF model. Indeed, across subjects and voxel sizes, we found an average difference (connective field - pRF) of ~23%, ~14% and ~10% in variance explained for visual areas V2, V3 and hV4 respectively. This improvement is particularly evident during the mean luminance periods when there was no stimulus. During the mean luminance periods, the conventional pRF predicts a uniform signal: in contrast, the connective field model can capture some of the time-varying signals. Note, however, that the standard pRF prediction could be improved by adding extra model parameters. For example, one could add a second Gaussian spread parameter to model the pRF's suppressive surround and explain more of the negative trenches around the peaks (Zuiderbaan et al., 2012). In addition, some of the time-series variance during the mean luminance periods could be non-neuronal physiological noise (although the time series were averaged across runs).

Connective field modeling links a voxel in one brain region to many voxels in another region. The voxels in the two regions should respond to overlapping regions of visual space (i.e., they should have similar pRFs). This is because voxels that have similar patterns of stimulus-evoked responses will also have similar time-series. Hence, once the connective fields are known it should be possible to derive the visual field map in one area from the visual field map in another area. Qualitatively, figure 4 shows that this is indeed the case. Panels a and b depict the eccentricity and polar angle maps for visual areas V1-hV4 derived with conventional pRF mapping. In the same figure, panels d and e show the result of deriving the V2-hV4 maps from V1 using the connective field models. To quantify the agreement between the conventional (pRF based) and derived (connective field based) visual field maps in these areas, we computed the correlation between the visual field positions of the V2-hV4 voxels' standard pRFs, and the pRF locations of the V1 voxels corresponding to the V2-hV4 voxels' connective field centers. The

visual field map estimates of the pRF and connective field methods are highly correlated. For S1, we found significant ($p < 0.0001$) correlations of $r = 0.96$, $r = 0.93$, and $r = 0.83$ for the eccentricity maps in V2, V3, and hV4, respectively. The corresponding values for the eccentricity maps in S2 were: $r = 0.89$, $r = 0.81$, and $r = 0.68$. Similar values were also found for the polar angle maps using a circular correlation coefficient: $r = 0.93$, $r = 0.89$, and $r = 0.82$ for S1, and $r = 0.92$, $r = 0.91$, and $r = 0.73$ for S2. The high correlation between the two methods indicates that the connective field method is capable of tracing with high accuracy the receptive field coupling between visual areas.

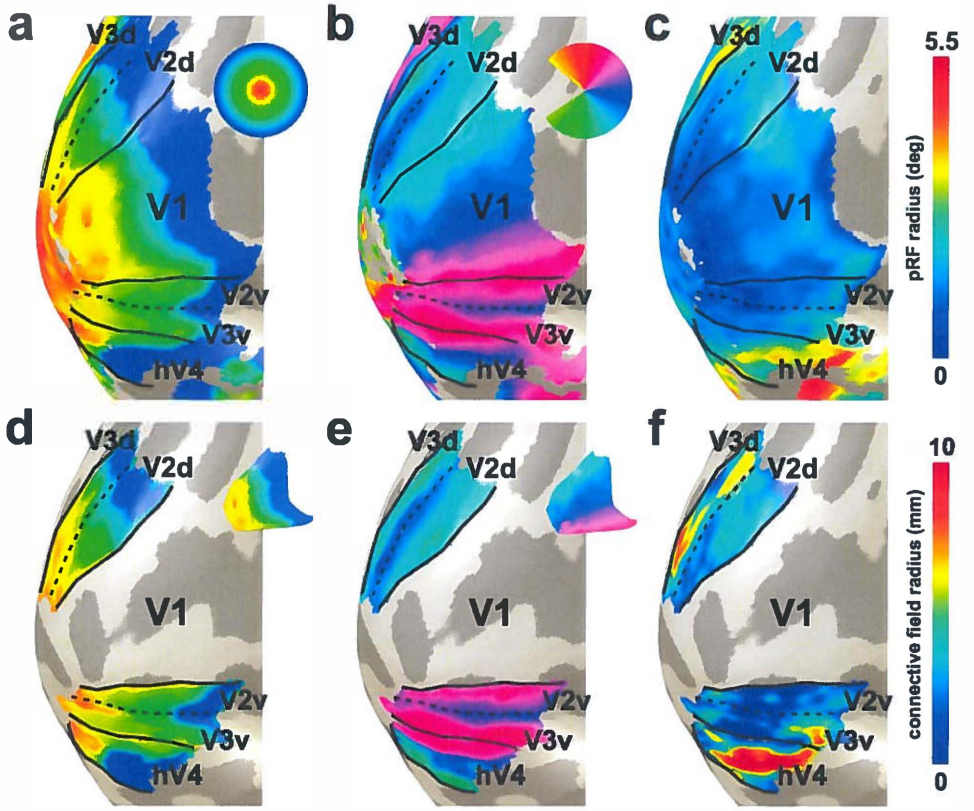

Figure 4. Stimulus- and neural-referred maps on the posterior medial surface of the occipital lobe of the left cerebral hemisphere at 7 Tesla. (**a**, **b**) Stimulus-referred eccentricity and polar angle maps revealed using conventional pRF modeling. The pRF eccentricity and pRF polar angle were used to delineate visual areas V1-hV4. Insets indicate the color maps that define the visual field locations. (**c**) The stimulus-referred pRF size estimates, as indicated by the colors shown in the color bar. The pRF size increases with eccentricity for all visual areas shown. (**d**, **e**) Neural-referred eccentricity and polar angle maps derived from the best-fitting V1 ▸ {V2, V3, hV4} connective field models in visual areas V2-hV4. The insets indicate the color maps that define the cortical locations, which are the V1 maps shown panels **a** and **b**. (**f**) The neural-referred connective field size, as indicated by the colors shown in the color bar.

There are several lines of evidence suggesting that the eccentricity-dependent receptive field scaling from V1 to higher visual areas corresponds to a constant sized sampling from the retinotopic map laid out across the cortical V1 surface (Harvey and Dumoulin, 2011, Kumano and Uka, 2010, Motter, 2009, Pelli, 2008, Pelli and Tillman, 2008 and Schwarzkopf et al., 2011). This leads to the prediction that within extra-striate cortical regions, the size of the V1 ► {V2, V3, hV4} connective field stays constant with eccentricity (unlike the size of the conventional stimulus-referred receptive field). However, figure 5a shows that the V1 ► {V2, V3, hV4} sizes increases significantly as a function of pRF eccentricity (depicted data are combined across subjects and scan resolutions). What could explain this dependency? Figure 5b shows that the connective field size of a voxel does not only depend on the voxel's position in the eccentricity map, but also on the extent to which its pRF overlaps with the ipsilateral visual hemifield (pRF laterality). This feature is expected on the basis that beyond V1, neurons close to the vertical meridian receive part of their inputs from the opposite cerebral hemisphere (Gattass et al., 1981, Gattass et al., 1988, Salin and Bullier, 1995 and Tootell et al., 1998). For the current implementation of the analysis we chose not to draw connective fields across the two V1 hemifield maps in each of the two cerebral hemispheres because this would require seaming the two V1 surfaces together. As such the present analysis is expected to underestimate the true connective field size of voxels close to the vertical meridian by an amount proportional to the amount by which their pRFs overlap with the ipsilateral visual field. To assess the effect of eccentricity on connective field size without the influence of laterality effects, we plotted the connective field size as a function of pRF eccentricity after adjusting the connective field size for pRF laterality (figure 5c; see methods). Both qualitatively and numerically, this plot agrees very well with figure 5 in a recent report by Harvey and Dumoulin (Harvey and Dumoulin, 2011). These authors derived the V1 sampling extent theoretically, using the conventional pRF estimate and an estimate of the cortical magnification factor, and also found a constant V1 sampling extent across eccentricity. Thus, in agreement with several past studies, the results are consistent with the idea that cortical magnification in extrastriate cortical areas (V2-hV4) is inherited from V1, and that there is no further magnification in the pooling of signals from V1.

From figure 5 it is also clear that the connective field size increases systematically between different visual field maps. This feature is expected on the basis that visual information converges up the visual processing hierarchy. If the connective field size corresponds to the radius of sampling from V1, then the sampling area is ~30 mm^2 for V2, ~90 mm^2 for V3, and ~300 mm^2 for hV4. These values correspond to approximately 1/100, 1/25 and 1/8 of the total V1 hemispheric surface area (Andrews et al., 1997).

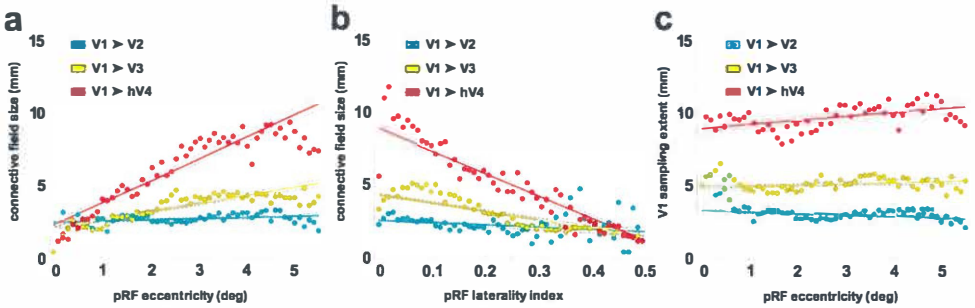

Figure 5. The relationship between eccentricity and V1-referred connective field size in visual areas V2-hV4, grouped from both participants and all voxel sizes. (**a**) The connective field size increases up the visual processing hierarchy and is dependent on eccentricity. (**b**) The connective field size decreases as a function of the pRF laterality index, which indicates the extent to which a pRF overlaps with the ipsilateral visual field (0 represents no overlap, 0.5 represents 50% overlap). (**c**) Adjusting the graph in a for pRF laterality yields the V1 sampling extent, which appears roughly constant across eccentricities. Colored lines represent a linear fit to the bins (dots). The bins were bootstrapped and linear fits repeated to give the 95% confidence intervals (dashed gray lines).

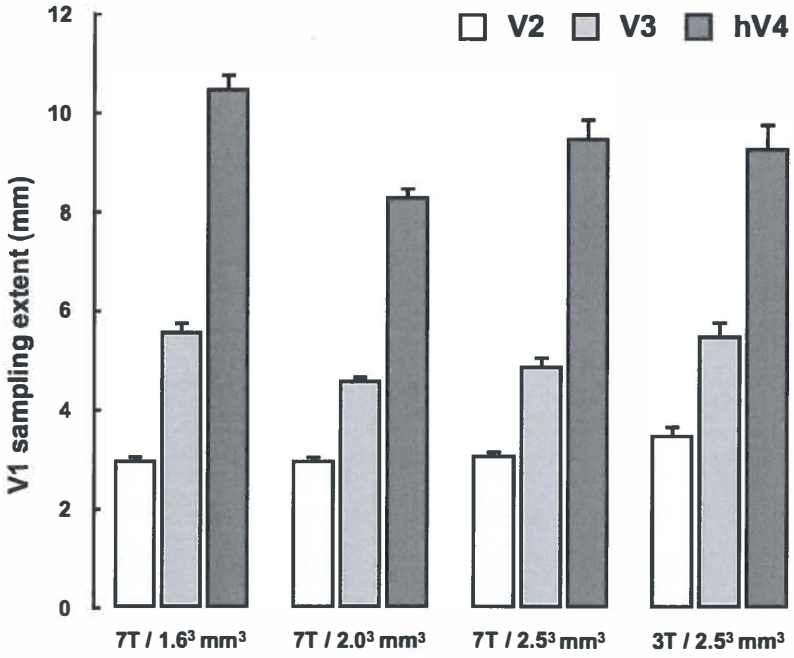

Figure 6. Estimates of the V1 sampling extent for three different voxel sizes and two different field-strengths for visual areas V2-hV4 in subject S1. Increasing the voxel size from 1.6^3 mm^3 to 2.5^3 mm^3 and then decreasing the magnetic field-strength from 7T to 3T reveals that the connective field modeling method is robust to changing these instrumental parameters; there is noise but no bias. Error-bars indicate the 95% bootstrapped confidence intervals.

	7T / 1.6³ mm³		7T / 2.0³ mm³		7T / 2.5³ mm³		3T / 2.5³ mm³	
	r	*θ*	*r*	*θ*	*r*	*θ*	*r*	*θ*
V2	0.96	0.93	0.95	0.96	0.92	0.96	0.95	0.98
V3	0.93	0.89	0.92	0.93	0.87	0.96	0.90	0.92
hV4	0.83	0.82	0.82	0.86	0.78	0.84	0.85	0.64

Table 1. Correlation between the visual field maps derived using pRF and connective field modeling. The correlation coefficients compares the eccentricity (*r*) and polar-angle (*θ*) maps in V2-hV4 for subject S1 derived using conventional pRF modeling to those derived using the connective field method. The correlation coefficients were computed for all voxels in the regions-of-interest for which the best-fitting connective field models explained more than 15% of the time-series variance. Columns indicate different combinations of magnetic field-strength and the voxels size. All correlation coefficients were highly significant ($p < 0.0001$).

Finally, there are two important instrument-related factors that could influence the spatial specificity of the connective field estimate. The first reflects the fact that coarser fMRI resolutions result in a poorer ability to estimate small changes in the connective field position and size. The second captures the feature that data from lower magnetic fields normally have a lower spatial specificity due to the increased intra-vascular contribution of draining veins (Logothetis, 2008 and Ogawa et al., 1998). Therefore, we asked whether the connective field method is robust to changing these two parameters. Table 1 summarizes the effect of changing the resolution and field-strength on the correlation between the visual field maps derived using conventional pRF modeling and the connective field method. It is clear that increasing the voxel size from ~4 mm³ to ~16 mm³ and then decreasing the magnetic field strength from 7 to 3 Tesla does not systematically influence the accuracy by which the connective field method accurately links voxels with overlapping receptive fields. Figure 6 further summarizes the effect of changing these two instrument-related features on the estimates of the V1 sampling extent. This figure indicates that the connective field size estimate is also robust to increasing the voxel size and decreasing the magnetic field-strength. These results show that the connective field method yields similar quantitative estimates from 3T and 7T data using a wide range of fMRI resolutions.

5.4. Discussion

Just as the receptive field of a visual neuron describes its response as a function of visual field position, the connective field of a neuron predicts its response as a function of activity in another part of the brain. Here, we have shown how fMRI can be used to estimate the

connective field of a population of neurons. The analysis is based on a model of neuronal responses, accurately traces the fine-grained topographic connectivity between visual areas, and provides a quantitative estimate of the connective field size. The method is non-invasive and robust to changes in fMRI resolution as well as field-strength.

Connective field modeling represents a fundamental departure from the existing approaches to estimating fMRI connectivity in the human brain. One reason is that it emphasizes the spatial profile of the functional connectivity between brain areas: connective field modeling harnesses the core strengths of fMRI — a large field of view and high spatial resolution — to make inferences about the spatial coupling among brain areas. While some of the existing methods such as seed-voxel correlation mapping (Biswal et al., 1995) and independent component analysis (Arfanakis et al., 2000) are capable of producing spatial connectivity maps, these methods have not yet provided the level of spatial detail associated with connective field modeling. Another important aspect that is unique to connective field modeling is that it informs about the direction of information flow in terms of converging versus divergent connections. For example, if the connective field size for V1 ► V2 is larger than for V2 ► V1, this would indicate that visual information converges from V1 to V2. To the best of our knowledge, existing methods for fMRI connectivity analysis only deal with the question of directionality by framing cortical information processing in terms of temporal causation (Buchel and Friston, 1997, Friston et al., 1995, Friston et al., 1997, Friston et al., 2003, Goebel et al., 2003 and Harrison et al., 2003), which is not a trivial thing to do with fMRI due to its poor temporal resolution.

The connective field modeling method depends on some but not all of the unwanted factors that also influence the conventional pRF estimate (Dumoulin and Wandell, 2008 and Smith et al., 2004). Common factors include eye and head movements, brain pulsations, and BOLD spread. These factors create a bias towards larger connective field size estimates, and add noise but no bias towards the connective field location estimates (Levin et al., 2010). Also like the pRF estimate, the connective field estimate is a statistical summary of the neuronal properties within the sampled voxel. Therefore, the connective field model parameters depend on the size and intrinsic properties of the sampled neuronal population. Different neuronal populations, for example in different cortical layers, will likely have different connective fields (Ress et al., 2007). Finally, pRF fits extending outside the maximum stimulus radius get noisy because they are based on less information than the fits that lie entirely within the stimulus area. The same is true of connective fields. If connective fields extended beyond the stimulated area of V1, then part of the connective field would be determined by the activity of the unstimulated part of V1. This unstimulated part will have lower amplitude responses than the stimulated area, so estimates here

will be noisier; connective field model solutions will generally not be great for voxels near the edge of the stimulus representation.

In the present implementation of the analysis, we used a single circular symmetric, two-dimensional Gaussian connective field model. This model provides a compact description of the connective field using only two parameters. Other models, however, may also be used. The single isotropic Gaussian connective field model could be readily replaced with sums and differences of Gaussians, an anisotropic Gaussian, or any other type of mathematical function to describe the connective field. Such models may be suitable to examine connective fields in other topographically organized cortices. In addition, determining what connective field forms best explain the fMRI time-series in the different visual areas could be a very fruitful approach for understanding the different types of computation across the visual pathways.

While different stimuli may alter the connective field estimate, an important feature of connective field modeling is that the analysis itself is stimulus-independent. Consequently, the connective field models also capture some of the spontaneous signal fluctuations during periods when there is no stimulus. Using connective field modeling, therefore, it should also be possible to extract the intrinsic properties of sensory information processing based on resting-state fMRI. This idea is supported by Heinzle and colleagues' work, who showed that "non-invasive imaging techniques such as fMRI are applicable to study detailed spatial interactions between topographically organized cortical regions in humans even in the absence of inputs driving the system under investigation" (Heinzle et al., 2011). It should be noted, however, that if connective field modeling were applied to resting-state rather than task-evoked responses, it would be important to adopt a physiological noise removal strategy, such as for example, global signal regression (Birn et al., 2006), retroicor (Glover et al., 2000), or drifter (Sarkka et al., 2012).

In conclusion, we have described and validated connective field modeling, a new model-based fMRI data-analysis that can be used to make inferences about how the spatial coupling among retinotopically organized brain regions is influenced by changes in experimental context, development, ageing, and disease. An important methodological difference between this and previous work is the use of a two-dimensional circular symmetric Gaussian connective field model. This is a valuable improvement because it is more interpretable biologically, and it allows for calculations on straightforward parameters such as the connective field size, a measure of spatial integration. Because the method is stimulus-agnostic, it should also be possible to employ the method to non-visual topographically organized brain regions as well as resting-state responses.

Acknowledgments

KVH and FWC were supported by a grant from Stichting Nederlands Oogheelkundig Onderzoek (SNOO) and European Union grants #043157 (Syntex) and #043261 (Percept). KVH was also supported by the Groningen Research School for Behavioral and Cognitive Neurosciences (BCN) and The Netherlands Society for Biophysics and Biomedical Engineering (VVB-BMT). FWC and SOD were supported by The Netherlands Organization for Scientific Research (NWO grant #433-09-251). JW was supported by National Institutes of Health grant EY022116. BAW was supported by National Eye Institute grant EY03164. The software is freely available and will be distributed as part of the VISTASOFT software package for functional MRI data analysis (http://white.stanford.edu/software).

References

Amano K, Wandell BA, Dumoulin SO. 2009. Visual field maps, population receptive field sizes, and visual field coverage in the human MT+ complex. Journal of Neurophysiology 102(5):2704-2718.

Andrews TJ, Halpern SD, Purves D. 1997. Correlated size variations in human visual cortex, lateral geniculate nucleus, and optic tract. The Journal of Neuroscience : The Official Journal of the Society for Neuroscience 17(8):2859-2868.

Angelucci A, Levitt JB, Walton EJ, Hupe JM, Bullier J, Lund JS. 2002. Circuits for local and global signal integration in primary visual cortex. The Journal of Neuroscience : The Official Journal of the Society for Neuroscience 22(19):8633-8646.

Arfanakis K, Cordes D, Haughton VM, Moritz CH, Quigley MA, Meyerand ME. 2000. Combining independent component analysis and correlation analysis to probe interregional connectivity in fMRI task activation datasets. Magnetic Resonance Imaging 18(8):921-930.

Bandettini PA, Jesmanowicz A, Wong EC, Hyde JS. 1993. Processing strategies for time-course data sets in functional MRI of the human brain. Magnetic Resonance in Medicine : Official Journal of the Society of Magnetic Resonance in Medicine / Society of Magnetic Resonance in Medicine 30(2):161-173.

Baseler HA, Gouws A, Haak KV, Racey C, Crossland MD, Tufail A, Rubin GS, Cornelissen FW, Morland AB. 2011. Large-scale remapping of visual cortex is absent in adult humans with macular degeneration. Nature Neuroscience 14(5):649-655.

Behrens P. 2009. CircStat: A MATLAB toolbox for circular statistics. Journal of Statistical Software 31(10):1-21.

Birn RM, Diamond JB, Smith MA, Bandettini PA. 2006. Separating respiratory-variation-related fluctuations from neuronal-activity-related fluctuations in fMRI. NeuroImage 31(4):1536-1548.

Biswal B, Yetkin FZ, Haughton VM, Hyde JS. 1995. Functional connectivity in the motor cortex of resting human brain using echo-planar MRI. Magnetic Resonance in Medicine : Official Journal of the Society of Magnetic Resonance in Medicine / Society of Magnetic Resonance in Medicine 34(4):537-541.

Brainard DH. 1997. The psychophysics toolbox. Spatial Vision 10(4):433-436.

Brewer AA, Liu J, Wade AR, Wandell BA. 2005. Visual field maps and stimulus selectivity in human ventral occipital cortex. Nature Neuroscience 8(8):1102-1109.

Buchel C and Friston KJ. 1997. Modulation of connectivity in visual pathways by attention: Cortical interactions evaluated with structural equation modelling and fMRI. Cerebral Cortex (New York, N.Y.: 1991) 7(8):768-778.

Dijkstra EW. 1959. A note on two problems in connexion with graphs. Numerische Mathematik 1(1):269-271.

Dougherty RF, Koch VM, Brewer AA, Fischer B, Modersitzki J, Wandell BA. 2003. Visual field representations and locations of visual areas V1/2/3 in human visual cortex. Journal of Vision 3(10):586-598.

Dumoulin SO and Wandell BA. 2008. Population receptive field estimates in human visual cortex. NeuroImage 39(2):647-660.

Fletcher R and Powell MJD. 1963. A rapidly convergent descent method for minimization. The Computer Journal 6(2):163-168.

Friston KJ, Harrison L, Penny W. 2003. Dynamic causal modelling. NeuroImage 19(4):1273-1302.

Friston KJ, Ungerleider LG, Jezzard P, Turner R. 1995. Characterizing modulatory interactions between V1 and V2 in human cortex with fMRI. Human Brain Mapping 2:211-224.

Friston KJ, Buechel C, Fink GR, Morris J, Rolls E, Dolan RJ. 1997. Psychophysiological and modulatory interactions in neuroimaging. NeuroImage 6(3):218-229.

Gattass R, Sousa AP, Gross CG. 1988. Visuotopic organization and extent of V3 and V4 of the macaque. The Journal of Neuroscience : The Official Journal of the Society for Neuroscience 8(6):1831-1845.

Gattass R, Gross CG, Sandell JH. 1981. Visual topography of V2 in the macaque. The Journal of Comparative Neurology 201(4):519-539.

Glover GH, Li TQ, Ress D. 2000. Image-based method for retrospective correction of physiological motion effects in fMRI: RETROICOR. Magnetic Resonance in Medicine : Official Journal of the Society of Magnetic Resonance in Medicine / Society of Magnetic Resonance in Medicine 44(1):162-167.

Goebel R, Roebroeck A, Kim DS, Formisano E. 2003. Investigating directed cortical interactions in time-resolved fMRI data using vector autoregressive modeling and granger causality mapping. Magnetic Resonance Imaging 21(10):1251-1261.

Haak KV, Cornelissen FW, Morland AB. 2012. Population receptive field dynamics in human visual cortex. PloS One 7(5):e37686.

Harrison L, Penny WD, Friston K. 2003. Multivariate autoregressive modeling of fMRI time series. NeuroImage 19(4):1477-1491.

Harvey BM and Dumoulin SO. 2011. The relationship between cortical magnification factor and population receptive field size in human visual cortex: Constancies in cortical architecture. The Journal of Neuroscience : The Official Journal of the Society for Neuroscience 31(38):13604-13612.

Heinzle J, Kahnt T, Haynes JD. 2011. Topographically specific functional connectivity between visual field maps in the human brain. NeuroImage 56(3):1426-1436.

Jammalamadaka, S.R. and Sengupta, A. 2001. Topics in circular statistics. World Scientific.

Kumano H and Uka T. 2010. The spatial profile of macaque MT neurons is consistent with gaussian sampling of logarithmically coordinated visual representation. Journal of Neurophysiology 104(1):61-75.

Lehky SR and Sejnowski TJ. 1988. Network model of shape-from-shading: Neural function arises from both receptive and projective fields. Nature 333(6172):452-454.

Levin N, Dumoulin SO, Winawer J, Dougherty RF, Wandell BA. 2010. Cortical maps and white matter tracts following long period of visual deprivation and retinal image restoration. Neuron 65(1):21-31.

Logothetis NK. 2008. What we can do and what we cannot do with fMRI. Nature 453(7197):869-878.

Motter BC. 2009. Central V4 receptive fields are scaled by the V1 cortical magnification and correspond to a constant-sized sampling of the V1 surface. The Journal of Neuroscience : The Official Journal of the Society for Neuroscience 29(18):5749-5757.

Nestares O and Heeger DJ. 2000. Robust multiresolution alignment of MRI brain volumes. Magnetic Resonance in Medicine : Official Journal of the Society of Magnetic Resonance in Medicine / Society of Magnetic Resonance in Medicine 43(5):705-715.

Ogawa S, Menon RS, Kim SG, Ugurbil K. 1998. On the characteristics of functional magnetic resonance imaging of the brain. Annual Review of Biophysics and Biomolecular Structure 27:447-474.

Pelli DG. 2008. Crowding: A cortical constraint on object recognition. Current Opinion in Neurobiology 18(4):445-451.

Pelli DG. 1997. The VideoToolbox software for visual psychophysics: Transforming numbers into movies. Spatial Vision 10(4):437-442.

Pelli DG and Tillman KA. 2008. The uncrowded window of object recognition. Nature Neuroscience 11(10):1129-1135.

Ress D, Glover GH, Liu J, Wandell B. 2007. Laminar profiles of functional activity in the human brain. NeuroImage 34(1):74-84.

Salin PA and Bullier J. 1995. Corticocortical connections in the visual system: Structure and function. Physiological Reviews 75(1):107-154.

Sarkka S, Solin A, Nummenmaa A, Vehtari A, Auranen T, Vanni S, Lin FH. 2012. Dynamic retrospective filtering of physiological noise in BOLD fMRI: DRIFTER. NeuroImage 60(2):1517-1527.

Schwarzkopf DS, Song C, Rees G. 2011. The surface area of human V1 predicts the subjective experience of object size. Nature Neuroscience 14(1):28-30.

Sholl DA. 1953. Dendritic organization in the neurons of the visual and motor cortices of the cat. Journal of Anatomy 87(4):387-406.

Smith SM, Jenkinson M, Woolrich MW, Beckmann CF, Behrens TE, Johansen-Berg H, Bannister PR, De Luca M, Drobnjak I, Flitney DE, and others. 2004. Advances in functional and structural MR image analysis and implementation as FSL. NeuroImage 23 Suppl 1:S208-19.

Teo PC, Sapiro G, Wandell BA. 1997. Creating connected representations of cortical gray matter for functional MRI visualization. IEEE Transactions on Medical Imaging 16(6):852-863.

Tootell RB, Mendola JD, Hadjikhani NK, Liu AK, Dale AM. 1998. The representation of the ipsilateral visual field in human cerebral cortex. Proceedings of the National Academy of Sciences of the United States of America 95(3):818-824.

Wandell BA and Winawer J. 2011. Imaging retinotopic maps in the human brain. Vision Research 51(7):718-737.

Wandell BA, Dumoulin SO, Brewer AA. 2007. Visual field maps in human cortex. Neuron 56(2):366-383.

Wandell BA, Chial S, Backus BT. 2000. Visualization and measurement of the cortical surface.

Journal of Cognitive Neuroscience 12(5):739-752.

Winawer J, Horiguchi H, Sayres RA, Amano K, Wandell BA. 2010. Mapping hV4 and ventral occipital cortex: The venous eclipse. Journal of Vision 10(5):1.

Zuiderbaan W, Harvey BM, Dumoulin SO. 2012. Modeling center-surround configurations in population receptive fields using fMRI. Journal of Vision 12(3):10.

Assessing visual dysfunction with fMRI

Based on: Haak KV, Clatworthy P, Morland AB (2011) Assessing visual dysfunction with fMRI. **Advances in Clinical Neuroscience and Rehabilitation** 11(3): 20-21.

6.1 Introduction

Functional magnetic resonance imaging (fMRI) is a well-established technique in visual neuroscience, but is not widely used in ophthalmology or neuro-ophthalmology practice, despite the information it can provide about neural function and dysfunction in patients. Here, we review some of the ways that have been used fMRI to characterize visual dysfunction, and discuss fMRI generally as a candidate for assessing visual function clinically. The studies described largely take advantage of the fact that visual cortex is arranged retinotopically, as Holmes revealed almost a century ago [1]. Selectively stimulating different regions of the visual field allows multiple visual field mappings to be identified reliably in individuals with fMRI (as shown in Figure 1, see also refs 2,3). This ability to produce informative data from a single individual is vital for a clinically viable tool and sets this method apart from many other fMRI methods. The retinotopic mapping procedures have been used to characterize visual dysfunction that arises from a number of different causes, at different stages in the human visual system.

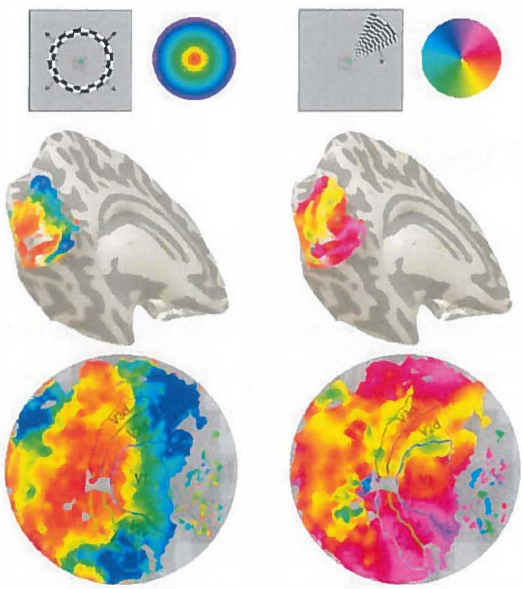

Figure 1. Retinotopic maps in a normally sighted individual. Top: the two stimuli that systematically move through eccentricity (left) and polar angle (right). Such stimuli elicit a traveling wave of activity in cortical retinotopic representations. The location in the visual field that elicits activity is colour coded (as indicated in the key to the right of the stimuli). When this colour coding of activity is presented on 3-D (middle row) and flattened (bottom row) surface reconstructions of the cortex, multiple visual maps in the occipital lobe can be identified. To the left and right data are given for activity elicited by rings and wedges, revealing maps of eccentricity and polar angle, respectively. On the flattened reconstructions the early visual areas, V1, V2 and V3, are outlined, demarcated by the representations of the vertical and horizontal meridians, visible on the polar angle maps (right).

6.2. Retinal lesions

Recently, we assessed cortical signals in patients with retinal lesions. We were motivated by neuroscientific questions concerning reorganization of cortical maps, something previously reported in patients who are born without functioning foveal photoreceptors [4]. We tested a relatively large number of patients with macular degeneration (those with Stargardt's disease and the more common age-related form), finding that the cortex does not remap visual information in these patients [5]. This allows for the intriguing possibility that assessing cortical signals might helpfully determine retinal sensitivity in ophthalmological disease; the activity at a particular spatial location within the map should predict visual sensitivity. This might be used in a number of ways. We are currently assessing the effectiveness of anti-angiogenic treatment for age-related macular degeneration, and changes in activity in the calcarine map largely reflect the changes in conventional visual measures of acuity and perimetry [6]. One of the advantages of measuring cortical signals is that the map is fixed, so no matter where the eyes are pointing, if the retina is stimulated (with a Ganzfeld stimulus for instance) activity in the cortex must reflect intact retinal processing. This is helpful in patients who find it hard to fixate for perimetry measurements.

6.3. Cortical lesions

Visual maps were also derived in the early visual areas of a patient, GY, who exhibits residual visual capacities in his right, "blind" visual field following a lesion to the calcarine cortex in the left hemisphere [7]. This patient displayed maps in early visual areas that largely reflected his scotoma, but subtle differences in the mapping of extrastriate regions were also evident when only the regions of the scotoma were stimulated. This modified mapping in the early visual cortex could be explained on the basis of changes in local connections, indicative of reorganization. Reorganization in this case may not come as a surprise given that the patient was tested over 30 years after a lesion sustained at the age of 8. Interestingly, recent evidence from diffusion tensor imaging also seems to indicate reorganization of the visual pathways in this patient [8]. Over recent years some of us have been consulted by neurosurgeons, keen to evaluate the potential visual effects of removing lesions close to the visual representations of the brain. In one such case a mass was located in a lateral area of the occipital pole. Although the location of visual maps is broadly consistent across individuals, the specific location of the representation of the central visual field varies considerably. The visual field mapping procedures showed that the mass was proximate to representations of the fovea in early visual areas allowing the surgeon to gauge the potential impact of the procedure on visual function. In addition to the primary visual

cortex more than twenty extrastriate visual maps can be identified. Many of these have specific roles in visual perception, with localized lesions giving rise to specific visual deficits such as cerebral achromatopsia [9, 10]. Knowing the spatial relationship between a potential site for surgery and a patient's extrastriate visual maps allows the impact of surgery on perception to be predicted.

6.4. Afferent visual pathways

Some developmental disorders can give rise to abnormal routing of visual information from the eye to the brain, which would escape detection with anatomical imaging. In individuals with albinism the decussation of the optic nerve at the optic chiasm is abnormal with a larger number of fibers originating from the temporal retina crossing to the hemisphere contralateral to the eye. This gives rise to abnormal lateralization and mapping of signals in the visual cortex. It was found that in humans the cortical map of the abnormal retinal input coexists with the map of the normal retinal input such that a region of primary visual cortex will respond to equal but opposite locations in the ipsilateral and contralateral visual fields [11]. When it was evaluated how fMRI might be used to detect the presence of albinism [12, 13] it was found that fMRI is very effective for detecting the abnormal lateralization of visual signals. Indeed it was equal to if not better than current electrophysiological methods used clinically [13]. Detecting albinism can be a challenge because pigmentation alone is not diagnostic.

When lesions occur in white matter, visual field defects are less straightforward to predict on the basis of anatomical imaging alone. We described how the brain signals we measured in response to visual stimuli could be used to generate a map of visual locations to which the brain responded in one such patient [14] In other words, we could use the brain activity to predict where the patient could see. The individual in question had undergone surgery to remove a left hemisphere parietal-occipital mass. The medial occipital cortex was intact following surgery, but the patient complained of difficulty reading and initial perimetry measurements pointed only to a questionable central field defect. Our fMRI mapping experiments indicated that left calcarine cortex no longer responded to a central (<3 deg) region of the lower right quadrant. Following up on this finding, finer perimetry measures of central visual field revealed a scotoma in the predicted location. It was likely therefore that the surgery resulted in a lesion of the optic radiation.

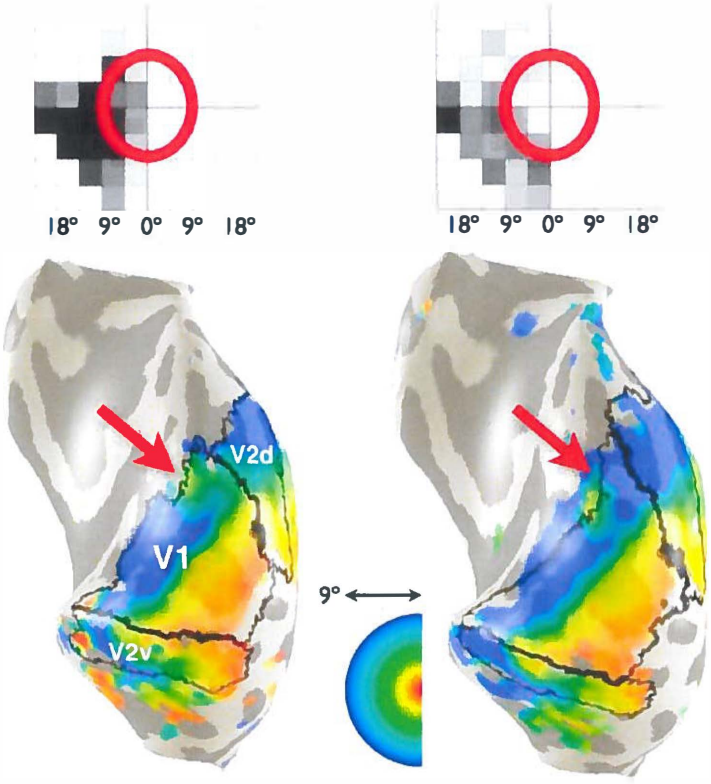

Figure 2. Visual fields as assessed behaviorally, left, and with fMRI, right. Data are given for two exams (first – left; second – right) separated by 12 weeks. At first the scotoma is dense in the lower left quadrant, but becomes less so by the second exam. This change is mirrored by a change in the cortical map in primary visual cortex, V1 (arrows). The map originally represents central locations but not peripheral (coded blue). Later the more peripheral locations are mapped.

In more recent work we have looked at a series of patients with known optic radiation lesions due to stroke. We followed one case over time and here we report on the changes in the patient's visual sensitivity and cortical activity. Figure 2 shows that the visual field recovers, particularly within the red circled region. The visual field maps represented on the surface reconstructions of the occipital lobe also exhibit a change between the examinations. Specifically, the part of dorsal primary visual cortex (V1) that would normally represent the visual field defect exhibits a disrupted map that later becomes largely normal, reflecting the change in visual sensitivity. As with the previously discussed case, the cortex initially fails to respond strongly to the region of the field deficit, but in this case as visual sensitivity recovers, so too do the cortical signals. It is noteworthy that the cortical representation of the field deficit is not silenced, but instead responds to a different field location. This could be interpreted as reorganization, but the alternative explanation, which we favor, is that the normal receptive field properties of neurons could lead to the signals we record (see refs 4,5).

6.5. Visual testing with fMRI

What issues have been and need to be overcome to allow fMRI to be translated into clinical assessments of vision? First, reliable information must be obtainable from a single individual. This has been largely overcome, however it still remains to document carefully the reliability of signals within an individual from session to session and within sessions. Second, and related to reliability, the time it takes to gather sufficient data to reliably characterize an individual's visual capacity has not been systematically explored. While our early research used examination times of 30 minutes, we have more recently gathered data over longer repeated examination periods. Clearly, a clinical application would need to minimize examination time and a suitable trade-off between examination duration and data quality needs to be established. Third, validation against other measures is required. This has been done to some extent, but further work is required. Fourth, as for other measures, norms need to be established, a process that is time consuming and may require separate values for each site at which measurements are taken. Fifth, fMRI yields large data sets that need to be processed and then assessed by experts. This process is time consuming compared to the examination time. More work is required on automated procedures to process data. Finally, fMRI is expensive, and cost will always be a consideration and perhaps the determining factor. However, if examination durations can be made short and added to an already required anatomical examination, and if much of the analysis can be automated, then costs will be reduced substantially. While there are clearly factors holding fMRI back from clinical application, techniques continue to benefit from rapid technological advances that will likely feed through to clinical imaging systems. For example, increasing field strength and the number of coil channels on scanners has increased signal quality. Developments of this type have not hit a ceiling, so much more can be expected in the future. Moreover, recent research has shown that novel contrast agents could yield enormous increases in signal over noise [15]. Taken together such technological advances will improve the efficiency of fMRI data acquisition, which in turn could lead to faster, cheaper visual testing with fMRI.

References

[1] Holmes G. Disturbances of vision caused by cerebral lesions. British Journal of Ophthalmology 1918; 2: 353-384.

[2] Sereno MI, Dale AM, Reppas JB, et al. Borders of multiple visual areas in humans revealed by functional magnetic resonance imaging. Science 1995; 268: 889-893.

[3] Engel SA, Glover GH, Wandell BA. Retinotopic organization in human visual cortex and the spatial precision of functional MRI. Cerebral Cortex 1997; 7: 181-192.

[4] Baseler HA, Brewer AA, Sharpe LT, et al. Reorganization of human cortical maps caused by inherited photoreceptor abnormalities. Nature Neuroscience 2002; 5: 364-370.

[5] Baseler HA, Gouws A, Haak KV, et al. Large-scale remapping of visual cortex is absent in adult humans with macular degeneration. Nature Neuroscience 2011; 14: 649-655.

[6] Baseler HA, Gouws A, Crossland MD, et al. Objective visual assessment of anti-angiogenic treatment for wet AMD. Optometry and Vision Science 2011; In press.

[7] Baseler HA, Morland AB, Wandell BA. Topographic organization of human visual areas in the absence of input from primary cortex. Journal of Neuroscience 1999; 19: 2619-2627.

[8] Bridge H, Thomas O, Jbabdi S et al. Changes in connectivity after visual cortical brain damage underlie altered visual function. Brain 2008; 131: 1433-1444.

[9] Meadows JC. Disturbed perception of colors associated with localized cerebral lesions. Brain 1974; 97: 615-632.

[10] Kennard C, Lawden M, Morland AB et al. Color identification and color constancy are Impaired in a patient with incomplete achromatopsia associated with prestriate cortical lesions. Proceedings of the Royal Society of London Series B-Biological Sciences 1995; 260: 169-175.

[11] Hoffmann MB, Tolhurst DJ, Moore AT et al. Organization of the visual cortex in human albinism. Journal of Neuroscience 2003; 23: 8921-8930.

[12] Morland AB, Hoffmann MB, Neveu M et al. Abnormal visual projection in a human albino studied with function magnetic resonance imaging and visually evoked potentials. Journal of Neurology Neurosurgery and Psychiatry 2002; 72: 523-526.

[13] Von dem Hagen EA, Hoffmann MB et al. Identifying human albinism: a comparison of VEP and fMRI. Investigative Ophthalmology and Visual Science 2008; 49: 238-249.

[14] Morland AB, Baseler HA, Hoffmann MB et al. Abnormal retinotopic representations in human visual cortex revealed by fMRI. Acta Psychologia 2001; 107: 229-247.

[15] Adams RW, Aguilar JA, Atkinson KD, et al. Reversible interactions with para-hydrogen enhance NMR sensitivity by polarization transfer. Science 2009; 323: 1708-1711.

General discussion

7.1 Summary

This thesis describes a number of studies in which we have evaluated the plasticity of the human visual cortex. By focusing on the receptive field properties of the visual neurons in the brain, we have provided a strong challenge to the view that the human visual brain is capable of modifying its retinotopic organization in the face of visual field defects. We have also contributed to the effort of understanding human visual cortical plasticity by providing a new fMRI data-analysis method, connective field modeling, to characterize the fine-grained functional connectivity between the visual field maps. Of final note is that the methods in this thesis could be translated into a set of clinically viable tools for assessing visual dysfunction clinically. The following paragraphs briefly review these results to arrive at a final conclusion.

Cortical reorganization is absent in adults with macular degeneration

The second chapter of this thesis describes an fMRI study on the consequences of the eye disease macular degeneration for the functional organization of the primary visual cortex in a relatively large group of patients (previous studies examined only a few patients). This study not only shows that there is no large-scale remapping of visual cortex following the retinal damage caused by macular degeneration. It also shows that, while it is possible to detect, as in animals, a change in the average receptive field, these changes are similar for the patients and a group of healthy controls in which the effect of the retinal damage was simulated. This latter result raises the strong suspicion that the primary "evidence" of visual cortical reorganization – changes in the receptive fields of visual brain cells – is indeed the result of biased sampling before and after damaging the retina.

Ectopic receptive fields are not a diagnostic feature of cortical reorganization

The third chapter of this thesis is a follow-up study, which was aimed at assessing the receptive field changes in more detail to determine what neural mechanisms could cause the effect. As in the first study, retinal lesions were simulated in a group of healthy control participants. This time, however, the size of the simulated retinal lesion was also varied. It turns out that the simulated lesions were actually much too large to explain, on the basis of biased sampling alone, the amount by which the receptive fields changed due to a simulated lesion. It also appears to be the case that larger simulated lesions do not necessarily yield a greater receptive field expansion. When these results are interpreted within the context of what is currently known about human visual cortex, it is concluded that the receptive field changes may not only be due to a biased sampling, but could also be due to a feedback mechanism, which transfers visual information back from higher visual areas to the primary visual cortex.

Large-scale cortical remapping appears to occur only in congenital visual disorders

The first two chapters of this thesis suggest that there actually little strong evidence for cortical reorganization due to retinal damage. This raises the question of whether the absence of cortical reorganization generalizes to visual disorders that do not cause retinal damage but deprive the brain of visual information in other ways. Chapter four addresses this issue in a literature review. In addition, new data is provided on the functional organization of visual cortex after one of the two cerebral hemispheres has been removed at age three. The conclusion is that there is indeed little convincing evidence of cortical reorganization on a large scale, and that large-scale cortical reorganization, if it occurs, only appears to occur in congenital visual disorders. Even in the case of a complete hemispherectomy at preschool age, the functional organization of the primary visual areas remains completely unchanged. And although an abnormal functional organization could be found in higher order visual brain areas, this abnormal organization is more likely explained on the simple basis that half the brain is missing and that development of these cortical structures has likely been arrested since the surgery.

Connective field modeling opens up new directions in cortical plasticity research

While studying the gross properties of the visually impaired brain has yielded much knowledge about visual cortical reorganization, information is still missing about a number of cerebral characteristics that may prove to be crucial for understanding how the brain responds to visual field loss. The information, which includes the information about the fine-grained functional connectivity between the visual brain areas, is missing because there is a lack of appropriate methodology to measure it. Chapter five of this thesis therefore describes how the method to estimate the receptive field properties of visual brain cells can be extended to a method – connective field modeling – that maps the functional connections between visual brain areas with an unprecedented level of detail. In principle, the functional connections can be determined with fMRI on the basis of induced as well as spontaneous brain activity, which provides interesting options for further research. On the basis of spontaneous brain activity, for example, it might be possible to trace the functional connections from the retinal lesion projection zone in the brain, which is impossible on the basis of stimulus-evoked brain activity. In the near future, therefore, the new method should allow us to capture for the first time the functional connectivity between the occipital brain areas in individuals with severe visual impairments and perhaps even in blind people.

Functional MRI may become a viable method for assessing visual dysfunction clinically

The absence of large-scale cortical reorganization makes it possible to determine, on the basis of

fMRI measurements, whether a visual condition deprives the brain from visual information. This opens up the possibility for fMRI to be used as a clinically viable method for detecting the presence or monitoring the progression of eye disease. The sixth chapter of this thesis considers the pros and cons to translating some of the fMRI experiments in this thesis into a clinically useful way of assessing the visual qualities of patients. We find that there are still several factors holding fMRI back from clinical application and that more work is needed to establish the reliability of the techniques. However, the type of fMRI experiments such as presented in this thesis continue to benefit from rapid technological advances. These advances could improve the efficiency of fMRI data acquisition, which in turn could lead to faster, cheaper visual testing with fMRI.

7.2. Future directions in research

The results in this thesis indicate several future directions of research. For example, chapters two and three indicate that subtle receptive field changes can be captured with fMRI. It is likely that previous work in animals mistook these changes for cortical reorganization. Future animal studies should therefore attempt to replicate the older findings and try to rule out alternative explanations such as receptive field scatter and feedback signaling. As such better theoretical models of healthy visual cortical responses will also have to be developed. Furthermore, as discussed in chapter three, the receptive field changes may also be a neural marker for perceptual phenomena such as color, brightness, texture, and motion filling-in. In addition, perceptual distortions such as those that are seen in patients with damage to the optic radiations following stroke may be explained by a change of the neuronal population receptive field. Therefore, it would be worth to test whether the receptive field dynamics identified in this thesis are also present under conditions in which these perceptual distortions occur. Finally, it has been observed in adult animals that the receptive fields that were initially displaced and enlarged due to induced retinal lesions, subsequently reduced in size towards the completion of the cortical reorganization process. It is clear from chapter two that only receptive field expansions can be seen in adult human patients with retinal lesions. Perhaps, therefore, the receptive field dynamics form a basis for long-term cortical reorganization, which follows through in humans with congenital visual impairments, but not in human adulthood. It would also be worth, therefore, to determine the receptive field characteristics of human individuals with congenital retinal lesions.

7.3. Conclusion

In conclusion, the results presented in this thesis indicate that there is little evidence for the existence of visual cortical plasticity in human patients with retinal damage. The classic idea, that the human visual cortex would be capable of large-scale reorganization in response to visual field loss, will therefore have to be revised. This may sound bad, but is in fact good news for patients with retinal damage. New treatments that are aimed at restoring the retina appear to be justified in assuming that the lesion projection zone within the visual cortex remains unchanged. That there is no significant cortical reorganization is reassuring because no remapping needs to be undone. It remains to be seen, however, whether the structural integrity of lesion projection zone is still good enough to process the visual input once it is restored. This issue may be addressed with the new fMRI data-analysis presented in chapter five, since this analysis could in principle be used to infer the functional organization of brain regions that are not (directly) visually stimulated. The absence of visual cortical plasticity is also good news because it opens up the possibility for the present fMRI experiments to be translated into a clinically useful way of detecting the presence and monitoring the progression of eye disease as well as assessing the effect of treatment. Here, the newly developed analysis method may also find application, as well as for future studies on the effects of visual field loss on the brain.

Nederlandse samenvatting

Een groot aantal oogziekten, zoals maculadegeneratie, glaucoom, retinis pigmentosa en amblyopie, heeft gezichtsvelduitval of anderszins een vermindering van de visuele vermogens tot gevolg. Ook is het zo dat wanneer een deel van het netvlies in beide ogen beschadigd is, een deel van de hersenen niet meer gestimuleerd zal worden. Dit roept de belangrijke vraag op wat er met dit deel van de hersenen gebeurt. Verdwijnt het of verandert de functionele organisatiestructuur van dit deel van de hersenen? Beide opties kunnen de mogelijkheden en het toepassen van behandeling beïnvloeden. Dit is vooral zo wanneer het gaat om toekomstige moderne behandeltechnieken met stamcellen of retinale prothesen, maar ook wanneer het gaat om revalidatie (training). Een belangrijke aanname bij deze behandeltechnieken is namelijk dat het visuele systeem intact en onveranderd blijft. Maar of dit werkelijk het geval is, is nog lang niet zeker. Bij revalidatie, met name bij bepaalde zeer intensieve trainingsvormen die gericht zijn op gezichtsveldherstel, gaat men er juist van uit dat het visueel systeem zich aanpast. Maar ook dat is niet helemaal zeker. De vraag die centraal staat in dit proefschrift is dan ook: hoe stabiel is de functionele organisatie van visuele hersengebieden; blijft deze intact wanneer er sprake is van een netvliesbeschadiging?

Wanneer de globale functionele organisatie van de menselijke visuele cortex in kaart wordt gebracht, gebeurt dit veelal door bepaalde delen van het visuele veld systematisch te stimuleren, terwijl met functionele magnetische resonantie beeldvorming (fMRI) de hersenactiviteit als gevolg van deze stimuli gemeten wordt. Omdat de visuele cortex op een topografische manier georganiseerd is, is het vervolgens mogelijk om verschillende functionele visuele hersengebieden aan te wijzen. Recentelijk is ook aangetoond dat het mogelijk is om, door middel van fMRI en systematische stimulatie van bepaalde delen van het visuele veld, de eigenschappen van zogenaamde receptieve velden van visuele hersencellen te schatten. Het receptieve veld van een visuele hersencel kan worden gezien als een wiskundig model dat beschrijft hoe sterk een hersencel reageert wanneer bepaalde posities in het visuele veld gestimuleerd worden. De mogelijkheid om deze receptieve velden te schatten met fMRI is belangrijk omdat het ons in staat stelt om zeer precies te bepalen op welke manier de menselijke visuele hersencellen reageren op een gebrek aan visuele stimulatie, zoals dat het geval is bij een netvliesbeschadiging.

De receptieve velden van visuele hersencellen spelen een zeer belangrijke rol binnen het onderzoek naar visuele corticale reorganisatie. In dieren zoals apen, katten en muizen lijkt men namelijk gevonden te hebben dat het aanbrengen van een netvliesbeschadiging de positie en/of de grootte van visuele receptieve velden verandert. Wanneer deze veranderingen veelvuldig

plaatsvinden heeft dit ook een gevolg voor de globale functionele organisatie van de visuele cortex. Gezamenlijk vormen de receptieve velden van visuele hersencellen namelijk de eerdergenoemde topografische organisatiestructuur, welke daarmee noodzakelijkerwijs meeverandert. Recentelijk is er echter enige controverse ontstaan over of de ogenschijnlijk veranderende receptieve velden in de bovengenoemde studies wel echt veranderden. Omdat het namelijk niet mogelijk was om dezelfde hersencellen te volgen van voor tot na het aanbrengen van de netvliesbeschadiging, bestaat het 'bewijs' niet uit de observatie dat een enkele hersencel een ander receptieve veld gekregen heeft, maar uit de observatie dat het gemiddelde receptieve veld van een groot aantal hersencellen samen veranderd is. Hierdoor bestaat de mogelijkheid dat een verandering van het gemiddelde receptieve veld eigenlijk komt doordat een specifieke groep hersencellen niet meer geactiveerd wordt, juist vanwege de netvliesbeschadiging.

Het tweede hoofdstuk van dit proefschrift beschrijft een fMRI studie naar de gevolgen van de oogziekte maculadegeneratie voor de functionele organisatie van de primaire visuele cortex in een relatief grote groep patiënten (eerdere studies onderzochten hooguit een paar patiënten). Uit deze studie blijkt niet alleen dat de globale functionele organisatie van de visuele cortex grotendeels onveranderd blijft ten gevolge van een netvliesbeschadiging door maculadegeneratie, en ook dat het weliswaar mogelijk is om, net als in apen, katten en muizen, een verandering van het gemiddelde receptieve veld van sommige hersencellen te detecteren, maar dat deze veranderdingen ook te vinden zijn in gezonde proefpersonen waarin een vergelijkbare netvliesbeschadiging gesimuleerd werd. Dit laatste wekt het sterke vermoeden dat het primaire "bewijs" voor visuele corticale reorganisatie, veranderde receptieve velden, inderdaad een gevolg is van een oneerlijke steekproef voor en na het aanbrengen van netvliesbeschadiging.

Het derde hoofdstuk van dit proefschrift beschrijft daarom een vervolg studie, waarin getracht wordt om deze receptieve veld veranderingen beter in kaart te brengen en daarmee te achterhalen welke corticale mechanismen het effect zouden kunnen veroorzaken. Net als in de eerste studie werden netvliesbeschadigingen gesimuleerd in gezonde proefpersonen. Ditmaal werd er echter een variatie aangebracht in de grootte van de gesimuleerde netvliesbeschadiging. Het blijkt zo te zijn dat de gesimuleerde netvliesbeschadigingen eigenlijk veel te groot zijn om de mate waarin de gemiddelde receptieve velden veranderen uitsluitend door middel van het argument van een oneerlijke steekproef te verklaren. Ook blijkt het zo te zijn dat een grotere netvliesbeschadiging niet per se een grotere vergroting van het receptieve veld oplevert maar juist een kleinere vergroting. Wanneer deze resultaten geïnterpreteerd worden binnen wat er op dit moment bekend is van de visuele cortex, is de conclusie dat de vroegere observaties van veranderende receptieve velden niet alleen zouden kunnen liggen aan een oneerlijke steekproef, maar ook aan een zogenoemd feedbackmechanisme dat visuele informatie via andere, hogere

orde, visuele gebieden terugvoert naar de primaire visuele cortex.

De eerste twee hoofstukken van dit proefschrift suggereren dat er eigenlijk helemaal niet zoveel bewijs is voor een veranderde corticale organisatiestructuur ten gevolge van een netvliesbeschadiging door maculadegeneratie. Maar hoe zit dat bij andere visuele aandoeningen die niet zozeer een netvliesbeschadiging veroorzaken, maar op een andere manier de hersenen visuele informatie ontnemen, of aandoeningen waarbij er verstoorde visuele informatie wordt doorgegeven? En hoe zit het met de studies die juist lijken aan te geven dat er op grote schaal corticale reorganisatie plaatsvind? Kloppen die studies wel? In het derde hoofdstuk van dit proefschrift worden deze vragen behandeld door middel van een literatuurstudie met daaraan gekoppeld een casus studie naar de gevolgen voor de functionele organisatie van de visuele cortex wanneer de helft van de hersenen op zeer jonge leeftijd is weggenomen. De conclusie is dat er inderdaad weinig overtuigend bewijs is voor corticale reorganisatie op grote schaal, en dat deze, wanneer deze voorkomt, uitsluitend lijkt voor te komen bij aangeboren visuele aandoeningen. Zelfs in het geval waarin een complete hersenhelft op zeer jonge leeftijd werd weggenomen lijken de primaire visuele gebieden zich niet te hebben gereorganiseerd. En hoewel er wel een abnormale functionele organisatiestructuur gevonden kan worden in bepaalde hogere orde visuele hersengebieden, lijkt deze abnormale organisatiestructuur eerder het gevolg van de afwezigheid van een hersenhelft op zichzelf, of een abrupt afgebroken ontwikkeling van deze hersengebieden.

Dat de functionele organisatie van de menselijke visuele cortex onveranderd blijft na een gezichtsveldverlies zou goed nieuws kunnen betekenen voor de patiënten omdat een aantal toekomstige behandelmethoden, zoals retinale inplanten of stamceltherapie, eenvoudiger toegepast kunnen worden dan voorheen werd aangenomen. Ook is het zo dat de afwezigheid van grootschalige corticale reorganisatie het mogelijk maakt om op basis van fMRI-metingen te achterhalen of een visuele aandoening ervoor zorgt dat de informatie van het oog de hersenen niet meer kan bereiken, hetgeen de mogelijkheid opent om fMRI te gebruiken als een klinisch toepasbare diagnostische methode of om de progressie van een visuele aandoening te volgen. Het vijfde hoofdstuk van dit proefschrift beschouwt daarom de voor- en nadelen om fMRI-experimenten te vertalen naar een klinisch toepasbare manier om de visuele kwaliteiten van een patiënt te beoordelen.

Hoewel het bestuderen van de grove cerebrale eigenschappen van het slechtziende brein veel kennis heeft opgeleverd, mist er nog belangrijke informatie over een aantal cerebrale eigenschappen omdat deze op dit moment nog niet in kaart konden worden gebracht. Het gaat hier bijvoorbeeld om de functionele verbindingen tussen de verschillende visuele hersengebieden. In hoofdstuk zes van dit proefschrift wordt daarom beschreven hoe de hierboven beschreven

methode, die wordt gebruikt om de eigenschappen van receptieve velden van visuele hersencellen te schatten, kan worden uitgebreid naar een methode die op een ongekend gedetailleerd niveau de functionele verbindingen tussen de visuele hersencellen in kaart kan brengen. Deze functionele verbindingen kunnen bepaald worden op basis van zowel opgewekte als spontane activiteit in de hersenen. Deze opties leveren een aantal zeer interessante mogelijkheden voor verder onderzoek op. Zo kan op basis van de spontane activiteit worden nagegaan hoe de verbindingen lopen vanuit de laesie projectie zone in de hersenen. Op basis van, door (externe) visuele stimulatie, opgewekte hersenactiviteit is dit uiteraard niet mogelijk. Dit levert de bijzondere mogelijkheid op om in de nabije toekomst bij zeer slechtzienden en zelfs blinde personen functionele hersenverbindingen in kaart te brengen.

Ter conclusie: er zijn maar weinig sterke aanwijzingen voor het bestaan van visuele corticale plasticiteit in patiënten met netvliesbeschadigingen. Het oude idee dat de visuele cortex in staat zou zijn om zich op grote schaal te reorganiseren in reactie op een dergelijke aandoening zal daarom moeten worden herzien. Dit klinkt slecht, maar is eigenlijk goed nieuws voor patiënten met een visuele beperking door netvliesbeschadigingen. Nieuwe behandelmethodes die gebaseerd zijn op het herstellen van het netvlies lijken namelijk terecht aan te nemen dat de functionele organisatie visuele cortex, welke essentieel is om de herstelde visuele beelden correct te interpreteren, onveranderd blijft. De afwezigheid van visuele corticale plasticiteit is ook goed nieuws omdat het de mogelijkheid opent om de technieken van dit proefschrift te vertalen naar een nieuwe techniek waarmee oogziekten misschien eerder geconstateerd of beter gevolgd kunnen worden. De nieuw ontwikkelde analysemethode zou hier mogelijk ook een toepassing kunnen vinden, maar zal in de eerste plaats een belangrijk stuk gereedschap kunnen worden binnen toekomstig onderzoek naar de gevolgen van een gezichtsveldbeperking voor de hersenen.